Airborne-radar and ice-core observations of snow accumulation in West Antarctica

Brooke Medley

A dissertation

submitted in partial fulfillment of the

requirements for the degree of

Doctor of Philosophy

University of Washington

2013

Reading Committee:

Ian R. Joughin, Chair

Howard B. Conway

Eric J. Steig

Program Authorized to Offer Degree:

Earth and Space Sciences

University of Washington

Abstract

Airborne-radar and ice-core observations of snow accumulation in West Antarctica

Brooke Medley

Chair of the Supervisory Committee:

Dr. Ian R. Joughin
Applied Physics Laboratory

The world's ice sheets store enough water to raise global eustatic sea level by several tens of meters, and therefore, any fluctuations in their size will cause sea level to rise or fall. The net mass exchanged with the ocean – defined as the mass balance – determines the glacial contribution to sea level and is the difference in snow accumulated in the interior and ice discharged into the ocean at the ice sheet periphery. While new techniques in remotely acquired surface velocities lead to improved discharge measurements, snow accumulation remains unmeasured over much of the of the ice sheet.

This work aims to improve our understanding of snow accumulation over two of the most rapidly evolving glaciers in Antarctica: Pine Island and Thwaites. Specifically, we use two airborne radar systems to image and track the near-surface internal stratigraphy to measure snow accumulation rates over both glaciers. This method allows for investigation of the spatial and temporal variations in accumulation at the catchment-scale, which is essential for determining glacier mass balance.

Examination of the radar-derived accumulation rates over Pine Island and Thwaites glaciers revealed several results including: (1) accumulation exhibited no significant trend

between 1980 and 2009, (2) the sea-level contribution from Pine Island and Thwaites tripled from +0.09 mm yr^{-1} in the mid-1990s to +0.27 mm yr^{-1} by 2010, (3) a shift towards higher accumulation occurred between 1944–1984 and 1985–2009, observed in both ice core and radar records, and (4) atmospheric models are an adequate replacement for accumulation measurements in areas with few observations.

These findings indicate that accumulation is not concurrently compensating the enhanced ice discharge from the region, and as a result, the sea-level contribution from these glaciers is increasing. Furthermore, a recent shift towards higher mean accumulation suggests these glaciers might have been out of balance earlier than originally thought.

TABLE OF CONTENTS

LIST OF FIGURES

LIST OF TABLES

ACKNOWLEDGEMENTS

I would like to thank my advisor, Dr. Ian Joughin, for the patience, guidance, and support he provided me the entire six years I spent at the University of Washington. I sincerely enjoyed my time working with Ian, whether it was spent sorting through problems in our Friday meetings or digging snow pits in Antarctica. While he is a true intellectual, Ian is equally down-to-earth and quite witty, and I am very fortunate to have had the opportunity to work with him.

I would also like to thank my committee members, Dr. Howard Conway and Dr. Eric Steig, for their friendly discussions and suggestions and their helpful guidance. Similarly, I would like to thank Dr. Ben Smith, Dr. Sarah Das, Alison Criscitiello, Dr. Prasad Gogineni, Dr. Joe McConnell, Dr. Michiel van den Broeke, Dr. Jan Lenaerts, Dr. David Bromwich, Julien Nicolas, Cameron Lewis, and Dr. Carl Leschen for their work on one or more of the chapters presented and their valuable edits. I would also like acknowledge the helpful hands in the field, Luke Trusel and Lou Albershardt.

Finally, I would be remiss if I did not acknowledge the many graduate students that made my pursuit possible. I would like to especially thank T. J. Fudge and Kristin Poinar for their irreplaceable collegiality and friendship. Most importantly, I would like to thank Adam Barker for his endless support over the past few years, during which he never once refused to listen to me practice a talk…even if it was for the fifth time.

Chapter 1: An Introduction to Ice-Sheet Snow Accumulation and Mass Balance

The Antarctic Ice Sheets gain ice mass every year through snowfall in the cold interior and primarily lose mass by ice flow into the ocean along the periphery. If these mass exchanges do not equal one another, the ice sheet will grow or shrink in response. Because the mass is ultimately exchanged with the ocean, the ice mass imbalance – whether negative or positive – is not only a metric for glacier health but also the determinant of the ice-sheet contribution to sea-level change. While the contribution from mountain glaciers is expected to dominate over the next century [*Meier et al.,* 2007] , the contribution from the Greenland and Antarctic ice sheets remains a large source of uncertainty in future sea-level projections [*Alley et al.,* 2005] . Therefore, measurements of the ice-sheet mass exchanges will not only improve our understanding of the current glacial contribution to sea-level rise but also provide insight into the controlling mechanisms of ice loss, which will improve future projections.

1.1 The mass balance of the Antarctic Ice Sheet

At the regional scale, ice-sheet mass exchanges at the surface include snowfall and its redistribution by the wind, meltwater runoff, sublimation and vapor deposition [*Vaughan et al.,* 1999] . While surface melt is a substantial component of the surface mass balance of the Greenland Ice Sheet, in Antarctica, where even summer temperatures do not rise above freezing [*Comiso,* 2000] , melt is a minor component. Furthermore, most melt refreezes nearby and as a result, does not influence the Antarctic mass balance [*Liston and Winther,*

2005] . Measuring each exchange would prove quite difficult, however, the net surface accumulation, defined as the combination of all surface exchanges, is more easily measured. Another component of the glacier mass balance is ice loss resulting from ice flow into the ocean, which is the primary process by which mass is lost to the ocean from the Antarctic Ice Sheet [*Rignot and Thomas,* 2002] . The ice entering the ocean might become part of a floating ice shelf, but once buoyant, the ice has contributed to sea-level rise and is considered here as mass lost. Therefore, the mass balance of the Antarctic Ice Sheet is measured by the difference in mass gain through accumulation in the interior and mass loss through ice discharge to the ocean. If the ice sheet is out of balance, it will grow or shrink accordingly, resulting in either sea-level fall or rise.

1.2 Measuring ice-sheet mass balance

There are essentially three methods to determine ice-sheet mass balance. Direct measurements of mass input and output make up the mass-budget method. The mass balance can also be inferred indirectly from measurements of surface elevation and gravity changes. The mass-budget method, also known as the flux-gate or input-output method, relies on measurements of the mass input through snow accumulation and the mass output by discharge into the ocean. Accumulation is derived from ice-core measurements [*Rignot and Thomas,* 2002] and more recently from climate models [*Rignot et al.,* 2008; *Rignot et al.,* 2011; *Shepherd et al.,* 2012] while ice discharge is measured by combining surface velocity and ice thickness at or near the grounding line. Measurements of surface elevation change reflect volume change once the fluctuations in basal elevation, mainly resulting from isostatic rebound, and the accumulation rate are considered [*Wingham et al.,* 2006; *Shepherd and Wingham,* 2007; *Pritchard et al.,* 2009; *Shepherd et al.,* 2012] . Finally, ice volume

change has been assessed by evaluating changes in gravitational attraction [*Velicogna and Wahr,* 2006; *Ramillien et al.,* 2006; *Velicogna,* 2009; *Rignot et al.,* 2011] , however, the mass change due to crustal rebound must be removed from the observed total mass change. While determining mass change through interpretation of surface elevation or gravity changes can be done remotely over majority of the ice sheet, the only direct method to assess ice-sheet mass balance is through measurements of mass input and output (the mass-budget method).

One considerable weakness of the mass-budget method is the difficulty in estimating mass exchanges over the entire ice sheet. Calculating surface velocities using interferometry [*Rignot,* 2001; *Joughin,* 2002] , however, has greatly improved our ability to determine ice loss to the ocean [*Rignot et al.,* 2008] . On the other hand, measuring the total snow accumulation over the entire ice sheet remains difficult, mainly because it is highly variable in space and time. Accumulation measured from ice-core analysis [*Kaspari et al.,* 2004; *Thomas et al.,* 2008; *Banta et al.,* 2008] provides an excellent record of the temporal variability yet only at a single location. Stake-farm measurements provide a clearer picture of the spatial variability in accumulation [*Frezzotti et al.,* 2005; *Kameda et al.,* 2008] , but they are difficult to recover on a year-to-year basis and are not a feasible method at the ice-sheet scale. Radar-derived accumulation measurements [*Rotschky et al.,* 2004; *Spikes et al.,* 2004; *Urbini et al.,* 2008] show potential for mass balance studies because they generate spatially and temporally variable measurements along the survey tracks with minimal interpretation.

1.3 Catchment mass balance using the mass-budget method

Using the mass-budget method, we can evaluate the mass balance of individual catchment areas within an ice sheet to investigate regional contributors to sea-level change. The catchment delimits the drainage area for a given ice stream. Thus, the catchment mass balance is the difference between the total snow accumulation within the drainage area and the ice stream discharge to the ocean [*Joughin and Tulaczyk,* 2002; *Rignot,* 2008] . Particular to this work, we focus on two ice streams: Pine Island and Thwaites. We refer to the ice streams and their respective catchment areas as Pine Island and Thwaites glaciers.

1.4 The Amundsen Coast glaciers

The Pine Island and Thwaites glaciers, located along the Amundsen Coast of West Antarctica, are experiencing substantial mass loss and likely are the two largest contributors to sea-level rise from Antarctica [*Rignot et al.,* 2008; *Shepherd et al.,* 2012] . Here, we briefly summarize the results from previous studies investigating mass input and output from this region.

1.4.1 Ice discharge

Early velocity and surface elevation observations from the main trunk of Pine Island glacier indicated the glacier was retreating and thinning during the mid- to late-90s, increasing the glacier's total discharge to the ocean [*Rignot,* 1998; *Shepherd et al.,* 2001] . Subsequently, Joughin et al. [2003] found two intervals of glacier acceleration, 1974 to 1987 and 1994 to 2000, separated by an interval of stagnation. More recently, Wingham et al. [2009] discovered that the glacier thinning has accelerated and spread further inland between 1995 and 2006. Discharge from Thwaites glacier has increased recently due to a widening,

rather than acceleration, of the fast-slowing trunk [*Rignot et al.,* 2002] . Thinning rates from the mid-90s [*Rignot,* 2001] had accelerated by the early 2000s [*Thomas et al.,* 2004] . Finally, Rignot [2008] determined that ice discharge from Pine Island and Thwaites glaciers has increased by 75% and 36%, respectively, between 1974 and 2007. The rapid changes in glacier dynamics are the consequence of warm ocean currents melting and thus thinning buttressing ice shelves, an effect observed over much of West Antarctica [*Shepherd et al.,* 2004; *Joughin et al.,* 2012; *Pritchard et al.,* 2012] . Based on the observed changes in dynamics, the contributions to sea-level rise from these two glaciers are most likely increasing; however, to precisely determine the actual magnitude, we must first look at changes in the snow accumulation over the same time interval.

1.4.2 Snow Accumulation

Snowfall over Pine Island and Thwaites is relatively high for Antarctic glaciers due to the intrusion of warm marine air onto the continent, attributable to winter cyclonic activity generated by a persistent low-pressure system over the Amundsen Sea [*Bromwich,* 1988] . The gradual coastal slopes of these glaciers allows the moisture-rich air to penetrate deeper into the interior than, for example, in East Antarctica where steep coastal slopes act as a barrier [*Nicolas and Bromwich,* 2011] . Accumulation measurements from this sector are relatively few with most derived from ice-core analysis. Kaspari et al. [2004] presented thirteen annually resolved accumulation records from West Antarctica and found that the three records within Pine Island and Thwaites exhibited higher recent accumulation rates (1970–2000) than the long-term average. Additional ice-core records from the West Antarctic Ice Sheet (WAIS) divide site, located near the Thwaites divide, indicated no significant trend in accumulation [*Banta et al.,* 2008] . Five records from nearby shallow

cores both within Thwaites and also beyond its divide into the Ross drainage, however, all show statistically significant decreasing accumulation trends between 1975 and 2010. Therefore, records from the eastern sector of the Pine Island-Thwaites drainage area show a recent increase in accumulation, and those from the western sector show either no trend or large negative trends. While this pattern is potentially the result of a shift in low-pressure systems within the Amundsen Sea, the limited number of measurements makes any interpretation open to debate.

The spatial pattern of accumulation over these glaciers is, perhaps, just as equally uncertain as the temporal variability and trends. In order to determine the total mass input over these glaciers for mass balance assessment, understanding of the spatial variations in accumulation is crucial for accurate determination of the spatial mean [*Richardson et al.,* 1997] . Three continent-wide accumulation climatologies, both model-derived and observation-based, provide varying catchment accumulation rates for these glaciers, ranging between 129 and 182 Gt yr^{-1} [*van de Berg et al.,* 2005; *Arthern et al.,* 2006; *Monaghan et al.,* 2006] . Atmospheric model outputs are increasingly being used in place of measurements [*Rignot et al.,* 2008; *Rignot et al.,* 2011] , however, the skill of these products has not been rigorously tested, especially temporally, due to a lack of spatiotemporal accumulation measurements. Therefore, precise estimation of these glaciers' sea-level contributions is not possible without additional spatiotemporal accumulation measurements.

1.5 Improving accumulation measurements

Because of recent technological advances, our understanding of Antarctic surface velocities and ice discharge has improved substantially; however, difficulty in measuring the spatiotemporal accumulation rate over an entire catchment limits our ability to determine

glacier mass balance using the mass-budget method. Uncertainty in catchment accumulation translates directly into uncertainty in mass balance. Improved spatial coverage of measurements is needed in order to accurately determine the spatial mean, which is crucial for mass balance studies. At the same time, measurements of the temporal evolution of accumulation will improve our understanding of the mass balance history of these glaciers. In addition to improving mass-budget balance measurements, spatiotemporal accumulation measurements are important for the indirect methods: mass balance estimates from surface elevation or gravity changes must account for accumulation variability and trends. Traditional accumulation measurements cannot reasonably cover an entire catchment area because (1) they typically sample one dimension with the near exclusion of the other and (2) they require field work to recover.

Here, we aim to improve our understanding of spatiotemporal accumulation over Pine Island and Thwaites glaciers by combining traditional measurements (i.e., ice cores) with airborne radar imaging of internal horizons. Tracking internal horizons along the radar survey paths allows us to determine the spatial variations in accumulation, while tracking multiple horizons with depth provides a look at temporal variations. The main goal of this work is to use the radar-derived accumulation rates to precisely determine the mass balance of Pine Island and Thwaites glaciers. We also use the radar-derived measurements to investigate the short- and long-term changes in accumulation in order to explore the mass balance evolution. Finally, we use these new measurements to test the skill of various atmospheric models in this region, which will allow for discrimination between models based on their ability and user need.

1.6 Summary

In order to assess the glacial contribution to sea-level rise, it is important that we examine the spatial and temporal variations in snow accumulation. Of particular interest are the Pine Island and Thwaites glaciers in West Antarctica, which are the largest contributors to sea-level rise from Antarctica. While recent observations indicate the ice discharge from these glaciers has increased over the past few decades, few accumulation observations make estimation of the total accumulation input and its temporal evolution difficult to assess. Here, we use new radar observations of the near-surface internal stratigraphy to improve our understanding of accumulation over these glaciers. In Chapter 2, we investigate the recent temporal variability and trend in accumulation and assess the skill of several atmospheric models over Thwaites glacier. In Chapter 3, we present a spatially complete accumulation map and combine it with measurements of ice discharge to determine the mass balance of both Pine Island and Thwaites glaciers over the past two decades. In Chapter 4, we use both ice-core records and radar-derived measurements to examine long-term accumulation changes and determine the spatial extent of the changes. Finally, Chapter 5 contains a summary of the main results from the work presented in Chapters 2-4 and a discussion of the need for future work.

Chapter 2: Recent Snow Accumulation Variability and Trend

Chapter 2, in full, is a reprint of "Airborne-Radar and ice-core observations of annual snow accumulation over Thwaites Glacier, West Antarctica confirm the spatiotemporal variability of global and regional atmospheric models" authored by B. Medley, I. Joughin, S.B. Das, E.J. Steig, H. Conway, S. Gogineni, A.S. Criscitiello, J.R. McConnell, B.E. Smith, M.R. van den Broeke, J.T.M. Lenaerts, D.H. Bromwich, and J.P. Nicolas as it appears in *Geophysical Research Letters* 2013. The dissertation author was the primary investigator and author of this paper.

2.1 Abstract

We use an airborne-radar method, verified with ice-core accumulation records, to determine the spatio-temporal variations of snow accumulation over Thwaites Glacier, West Antarctica between 1980 and 2009. We also present a regional evaluation of modeled accumulation in Antarctica. Comparisons between radar-derived measurements and model outputs show that three global models capture the interannual variability well ($r > 0.9$), but a high-resolution regional model (RACMO2) has better absolute accuracy and captures the observed spatial variability ($r = 0.86$). Neither the measured nor modeled accumulation records over Thwaites Glacier show any trend since 1980. Although an increase in accumulation may potentially accompany the observed warming in the region, the projected trend is too small to detect over the 30-year record.

2.2 Introduction

In Antarctica, where snowmelt and runoff are small, the competing processes of mass gain through snow accumulation and loss through ice discharge to the ocean control the ice

sheet's net mass balance and thus its contribution to sea level. Here we use accumulation interchangeably with surface mass balance (SMB), which is defined as snowfall minus sublimation and meltwater runoff and includes drifting snow processes. Basin-wide accumulation is a large source of uncertainty in regional mass loss estimates. For example, both observation- and model-based basin-wide accumulation climatologies [*van de Berg et al.,* 2005; *Monaghan et al.,* 2006; *Arthern et al.,* 2006] over Pine Island and Thwaites Glaciers vary from 129 to 182 Gt yr^{-1}, a range that is comparable to the net mass loss [*Rignot et al.,* 2008] . The mass balance of the Amundsen Coast region is of particular interest because recent accelerated ice discharge from Pine Island and Thwaites Glaciers to the ocean makes the region one of the largest Antarctic contributors to current sea-level rise [*Shepherd et al.,* 2012; *Rignot et al.,* 2008] .

Under a warming climate, the associated increase in atmospheric moisture content is expected to increase ice-sheet snow accumulation [*Genthon et al.,* 2009] , but modeling studies [*Monaghan et al.,* 2006; *Lenaerts et al.,* 2012] do not show this trend, despite significant warming in West Antarctica over recent decades [*Steig et al.,* 2009; *Orsi et al.,* 2012; *Bromwich et al.,* 2013] . Although ice cores provide long-term accumulation records, their sparse distribution undersamples the spatial variability. In West Antarctica, only a few high-elevation (> 1200 m asl) annually resolved ice-core accumulation records exist: several from ITASE in the early 2000s [*Kaspari et al.,* 2004] and three cores (PIG2010, DIV2010, THW2010) recovered in 2010/11 (Figure 2.1). None are from low-elevation coastal sites where accumulation is the highest. Furthermore, substantial small-scale accumulation variability suggests that individual cores do not adequately represent regional accumulation [*Banta et al.,* 2008] .

This work uses a newly developed airborne radar system, referred to as the "snow radar" [*Panzer et al.,* 2010; *Panzer et al.,* 2013] , with bandwidth sufficient to resolve near-surface stratigraphy continuously over hundreds of kilometers along aircraft flight paths (Figure 2.2). This radar is a frequency-modulated continuous wave system developed by the Center for Remote Sensing of Ice Sheets (CReSIS) and flown on NASA's Operation IceBridge campaign [*Leuschen,* 2010, updated 2011] . During the 2009 campaign, the system operated over the 4-6 GHz frequency range (vertical resolution ~10 cm); in 2010 and 2011, it operated over the 2-6.5 GHz frequency range (vertical resolution ~5 cm). We stacked traces to a horizontal resolution of ~55 m. The radar documentation and data are available at ftp://data.cresis.ku.edu/data/snow. The radar reflection horizons (Figure 2.2) represent contrasts in the material's dielectric permittivity, attributed to isochronous buried sequences of hoar layers and associated ice crusts [*Arcone et al.,* 2004, 2005a, 2005b; *Spikes et al.,* 2004] . The roughly annual occurrence of such sequences and the fine vertical radar resolution indicate that these horizons can be dated. Using these data with a regional firn depth-density model, we derive annual accumulation records from 1980 to 2009 along each radar profile [c.f. *Kanagaratnam et al.,* 2004] over most of the Thwaites basin (~182 Mkm^2).

2.3 Methods

Calculating spatio-temporal accumulation rates using airborne radar requires three data sets: (1) a firn depth-density profile, (2) radar-profiled isochrones, and (3) a depth-age profile to determine isochrone ages. The water-equivalent accumulation rate (m w.e. yr^{-1}) between two mapped isochrones (i.e., over a discrete time period) is

$$\dot{b}(x) = \Delta CM\,(x) / (\Delta t \cdot \rho_w) \qquad (2.1)$$

where x is location along the flight path, ΔCM is the cumulative mass per unit area (kg m^{-2}) between two isochrones that differ Δt in age, and ρ_w is the density of water (1000 kg m^{-3}). The mapped horizons are assumed to be annual isochrones, and thus Δt is independent of x and equal to 1 year. Although we employ a single cumulative mass profile for the entire region, ΔCM varies along the flight path because the isochrones vary in depth.

2.3.1 Firn density profile

A firn depth-density profile is needed to convert radar measurements of two-way travel time τ to depth d and to calculate a cumulative mass profile. Although firn densification varies with temperature and accumulation rate, here we use a single profile for the entire basin. We fit a steady state density model [*Herron and Langway*, 1980] to the mean of nine firn-core density profiles from the region (Figure A.1). We use a mixture model [*Looyenga*, 1965] to calculate the dielectric permittivity ε_d of the firn and calculate depth from the measured two-way travel time: $d = 0.5c\tau\varepsilon_d^{-0.5}$, where c is the wavespeed in a vacuum (3×10^8 m s^{-1}). The d-τ profile is calculated at 1-cm intervals to account for the depth variations of density and dielectric permittivity. The cumulative mass profile is calculated by integrating the modeled density profile.

2.3.2 Snow-radar accumulation rate error estimation

The radar-derived accumulation rate error estimates account for the regional variation in the firn density profile and the uncertainty in the horizon time interval Δt (see Appendix). The error resulting from density variation is based on the model fits to the $\pm 1\sigma$ variation in density profile from the mean (Figure A.1). We also assume an error in Δt of ± 1 month, as the time of creation of the isochrones likely varies. A digitization error of 1 radar sample is

included, equivalent to approximately 3 and 6 cm for the 2010/11 and 2009 flights, respectively. The typical accumulation rate measurement error is less than ±10%, except for the most recent years (i.e., layers near the surface) when errors approach ±15% (Figure A.2). Spatial averaging minimizes the impact of these errors and reduces the annual accumulation error to less than ±5%.

2.3.3 Ice-core analysis

Water isotope ratios and more than 30 elements and chemical species were measured at high depth resolution (~1 cm w.e.) using a continuous ice-core melter system [*McConnell et al.*, 2002; *McConnell et al.*, 2007; *Maselli et al.*, 2013] . While nearly all ratios exhibit pronounced annual cycles in concentration, here we used the summer maxima in hydrogen peroxide concentration, water isotope ratios, and non-sea-salt sulfur to sodium ratio to identify consistent annual layers. Well-known volcanic horizons identified by marked increases in wintertime sulfur concentration were used to verify the annual layer counting, which indicated a dating uncertainty of < 1 year.

2.3.4 Method validation

Snow-radar horizons were dated by counting horizons assumed to be annual. To verify this assumption, we compare the snow-radar accumulation record with that from the nearly co-located (~150-m separation) PIG2010 ice core (Figure 2.3). The 30-year averages (± 1 standard deviation) of 0.424 ± 0.065 m w.e. yr^{-1} from the core and 0.428 ± 0.055 m w.e. yr^{-1} from the radar are indistinguishable. Annual layer thicknesses are highly correlated (r = 0.85), validating our assumption that the radar resolves horizons with annual resolution and indicating that the snow-radar accumulation records are consistent with the ice-core records.

All calculated correlation coefficients are statistically significant at the 99% confidence level, accounting for autocorrelation. Comparisons between individual ice-core records and the radar- and model-derived records are displayed in Figures 2.4-2.7.

2.4 Results

2.4.1 Radar-derived accumulation rates

Using four radar surveys collected between 2009 and 2011 over an area of ~350 km × ~350 km, we generated 30-year accumulation records at 250-m intervals along track (Figure 2.1). The 30-year average accumulation rates vary spatially between 0.27 m w.e. yr^{-1} in the high-elevation interior and 0.67 m w.e yr^{-1} near the coast. The spatial mean is 0.457 ± 0.066 m w.e. yr^{-1} over elevations sampled ranged from 950 and 1840 m asl. Strong accumulation variability is associated with the slope-dependent effect of wind-driven snow redistribution [*Arcone et al.*, 2005b] , which is clearly visible in our data because the greatest accumulation variability corresponds with strongly varying surface slopes, as indicated by tonal variations in the basemap in Figure 2.1. Missing data along the flight paths indicate the 30-year accumulation record is incomplete (i.e., one or more of the thirty annual horizons could not be digitized). These data gaps could introduce a magnitude bias in our regional record, which is acceptable because we are not attempting to determine basin-wide accumulation and instead are interested in its variability and trend.

We created a regional accumulation record by spatially averaging all radar-derived records (Figure 2.8). Between 1980 and 2009 the average accumulation rate is 0.457 ± 0.055 m w.e. yr^{-1}, and the record shows no significant trend. We created two 3-core accumulation rate ensembles using our 2010/11 ice-core records and the ITASE records [*Kaspari et al.*,

2004] to produce independent quasi-regional records for comparison with the snow-radar record (Figure 2.8). The ensembles have slightly lower mean accumulation rates than the snow-radar record, yet correlate significantly (r = 0.80; Table 2.1). This comparison with ice-core data indicates that the snow radar provides accurate accumulation estimates.

2.4.2 Atmospheric model validation

Model-derived snow accumulation is increasingly being used in place of observations. Our data provide an opportunity to evaluate the skill of such models at a regional scale and at annual resolution. We compared our data with three global reanalysis precipitation-minus-sublimation (*P*-*S*) products [*Bromwich et al.,* 2011] of varying grid resolutions (see Table 2.1): the European Centre for Medium-Range Weather Forecasts "Interim" (ERA-Interim) [*Dee et al.,* 2011] , the NASA Modern Era Retrospective Analysis for Research and Applications (MERRA) [*Rienecker et al.,* 2011] , and the National Centers for Environmental Prediction Climate Forecast System Reanalysis (CFSR) [*Saha et al.,* 2010] . We also used SMB from the Regional Atmospheric Climate Model v.2.1 (RACMO2) [*Lenaerts et al.,* 2012] , which is forced on its lateral boundary with the ERA-Interim reanalysis. The reanalysis *P*-*S* products are nearly equivalent to SMB in this region because runoff is negligible and drifting snow processes typically amount to less than 6% of the total, based on analysis of the RACMO2 SMB components. We generated regional records of modeled accumulation (equivalent to *P*-*S*) by taking the average of grid cell records weighted by the percentage of snow-radar records within each cell. Figure 2.8 shows the regional snow radar and model-derived records as anomalies from their respective 1980–2009 means shown in Table 2.1. The RACMO2 30-year average accumulation rate of 0.434 ± 0.080 m w.e. yr^{-1} is slightly less than the snow-radar average of 0.457 ± 0.055 m w.e. yr^{-1}. The global

reanalyses have even lower averages between 0.346 ± 0.057 and 0.407 ± 0.060 m w.e. yr^{-1}. The correlation coefficients shown in Table 2.1 indicate that the global reanalyses are highly correlated temporally ($r > 0.9$) and RACMO2 is moderately correlated ($r = 0.68$) with the snow-radar record. The global reanalyses are moderately correlated spatially with correlation coefficients ranging between 0.68 and 0.75, whereas RACMO2 is highly correlated ($r = 0.86$).

The agreement between the models and the snow radar indicates that the models reasonably capture the magnitude and variability of accumulation in this sector of West Antarctica, but with notable deficiencies. RACMO2 adequately reproduces the mean annual accumulation, while the global reanalyses are biased low. The interannual accumulation variability is accurately reproduced by the reanalysis products, while RACMO2 exhibits exaggerated variability; its standard deviation is nearly 50% greater than that from the snow-radar observations.

2.4.3 Elevation-dependent accumulation gradients

To investigate spatial accumulation distributions further, we compared the relationship between elevation and accumulation for each data set (Figure 2.9). All models underestimate accumulation at the highest elevations: modeled accumulation declines more rapidly with elevation than is observed. Although the models show a slight overestimation of accumulation below 1000 m, the radar sampling at these elevations is not sufficient to confidently interpret the differences. To quantify discrepancies, elevation-dependent accumulation gradients are approximated by a linear fit to the data in Figure 2.9 and are listed in the inset table. We find RACMO2 captures much of the spatial variability in accumulation because of its finer spatial resolution but does not perform as well above 1400

m in this region as at lower elevations. The global models adequately capture the regional-scale variability in accumulation, even with their coarser spatial resolution, but the steep accumulation gradients below 1400 m indicate that not nearly enough accumulation is reaching moderate to high elevations.

2.5 Discussion

The snow-radar record, ice-core ensembles, and atmospheric models do not show any significant trend in accumulation over Thwaites basin between 1980 and 2009 indicating that the recent increase in ice discharge from the region has not been simultaneously compensated by a comparable increase in accumulation. The trends in accumulation range between -1.5 and +2.1% per decade and are all statistically insignificant (Table 2.1). The MERRA trend of +2.1% per decade is likely inflated due to data-assimilation artifacts [*Bromwich et al.,* 2011] . The lack of a significant trend does not necessarily rule out a relationship between rising temperatures in West Antarctica and changing snow accumulation, considering the length and interannual variance of the accumulation record. A recent model simulation of Antarctic precipitation predicts a ~2% per decade increase over the 21st century [*Genthon et al.,* 2009] . The 2-σ sampling error associated with the short (n = 30) snow-radar record with high annual variability (σ = 12.0%) is ±4.4% ($2\sigma n^{-0.5}$), indicating that a 2% per decade increase would not be detectable and cannot be ruled out. However, trend magnitudes greater than 5% per decade can be ruled out, which when compared to the ~11% per decade increase in Thwaites ice discharge [*Rignot et al.,* 2008] , confirms that the accumulation trend is not keeping pace with changes in ice dynamics.

Our results indicate that the snow radar provides a reliable annual signal over the Thwaites basin and provides high-quality accumulation rate measurements independent of

ice-core glaciochemical analysis. The high correlations between the radar- and core-derived annual accumulation records confirm our interpretation of a snow-radar annual signal, highlighting the potential of radar profiling for mass balance studies. Qualitative analysis of the radar data suggests that the snow radar is most suitable where average accumulation rates are between 0.3 to 0.6 m w.e. yr^{-1}. Outside these bounds, layers can still be resolved but not annually (based on data from systems operated in 2009–2011), making this method useful for estimating accumulation where independent age-depth information is available. The snow-radar method also serves as a much-needed means to improve model mass balance assessments through validation of and discrimination among the results from different models.

These radar-derived accumulation rates provide the data necessary to evaluate the temporal variability of modeled accumulation rates at a regional scale. Our results show that models of accumulation are reasonable substitutions in areas lacking measurements. Although the global models underestimate the magnitude of accumulation by as much as 24%, these models capture the interannual accumulation variability with high fidelity. The finer resolution regional model underestimates the mean accumulation by only 5% and more accurately captures the spatial accumulation variability and elevation-dependent gradient. The differences between the global and regional models are likely related to differences in observational constraints. The reanalyses are constrained with global observations, including observations within Antarctica, which help capture temporal variability in accumulation. By contrast, RACMO2 is forced by the observation-driven ERA-Interim reanalysis product far from the continent and is thus not as well constrained by observations from Antarctica, yielding greater uncertainty in temporal variation. Additional snow-radar observations in

Greenland and Antarctica through ongoing IceBridge campaigns will provide the constraints necessary for further refinement and improvement to these atmospheric models.

2.6 Conclusion

Comparison of new radar-derived observations of ice-sheet accumulation, ice-core records, and model data demonstrate that: (1) ultra-wideband microwave radars provide accurate and independent estimates of accumulation; and (2) both global and regional models reasonably account for the variability, while the global models underestimate the magnitude of accumulation in this sector of West Antarctica. We find that Thwaites Glacier has not experienced a statistically significant change in accumulation over the past three decades. Therefore, the recent increase in ice discharge from the glacier has not been balanced by a simultaneous increase in accumulation.

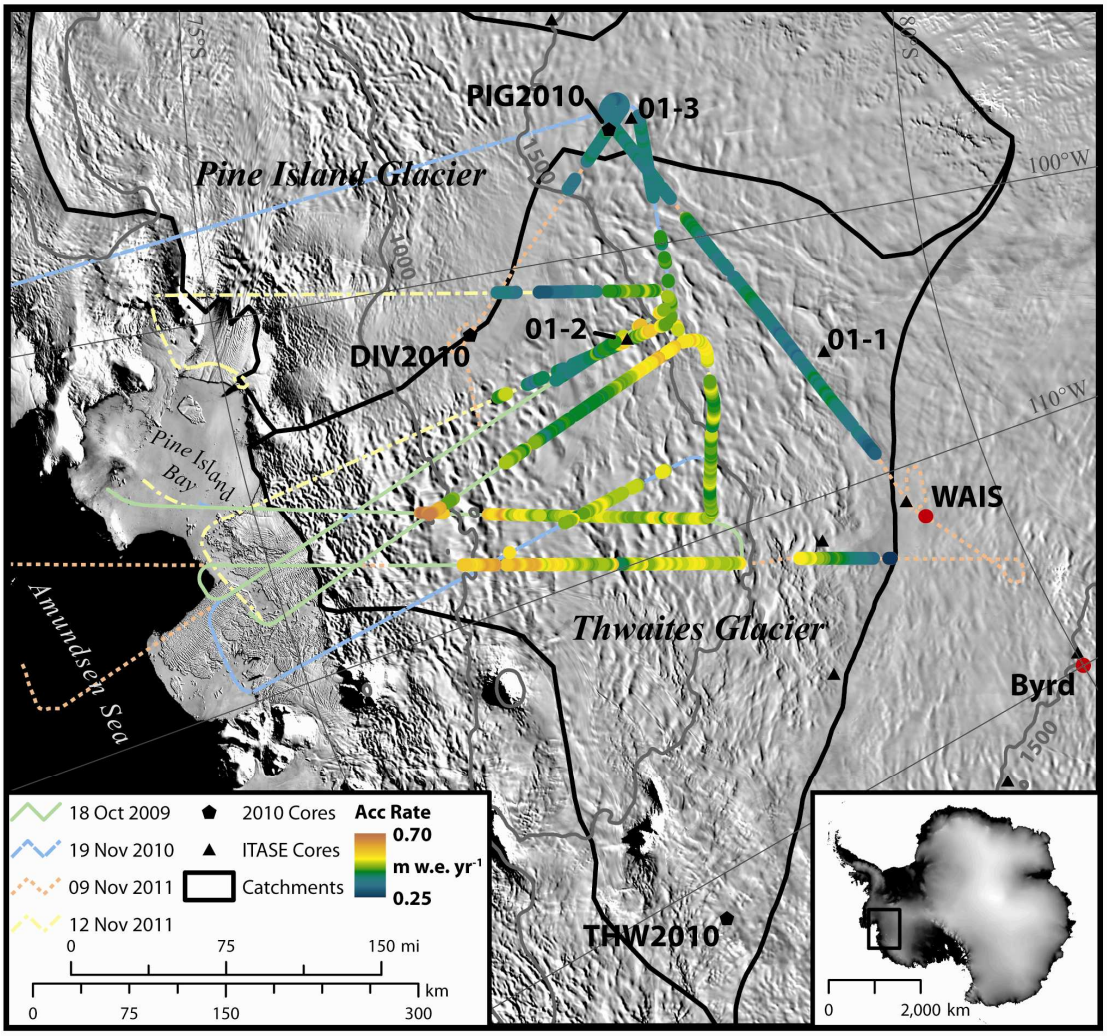

Figure 2.1 – Thirty-year average accumulation rates and select Operation IceBridge flight paths overlaid on a MODIS mosaic [*Haran et al.*, 2005, updated 2006] . The inset map outlines the study area relative to a digital elevation model of Antarctica [*Bamber et al.*, 2009] . The catchments are outlined in black. Elevation contours (m) are labeled accordingly. The ITASE cores collected between 2000 and 2001 are shown as triangles and cores collected in 2010/11 are shown as pentagons. Red circles show the major field camps.

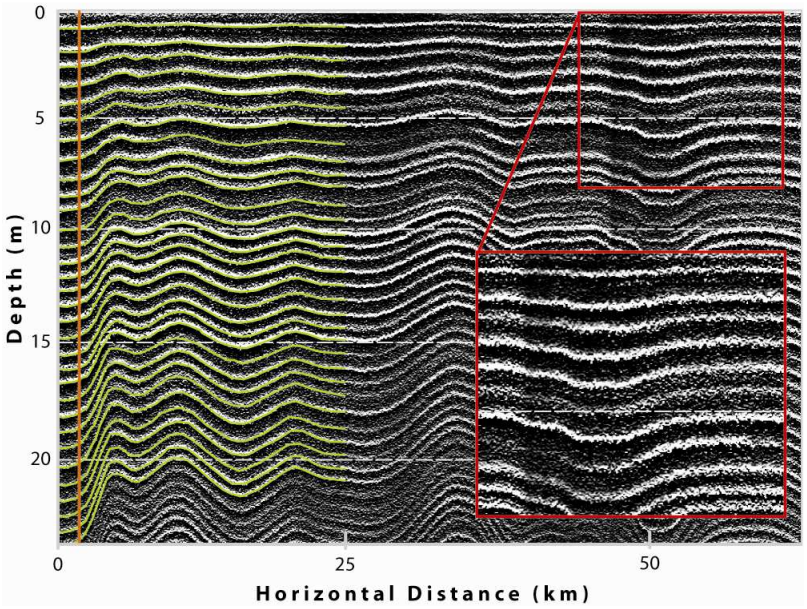

Figure 2.2 – Sample snow radargram partly overlaid by manual horizon picks. The vertical orange line shows the location of the PIG2010 ice core. These data were collected 9 November 2011 and show the consistency of horizons over large distances. Inset shows detail in the upper ~7 m outlined in red.

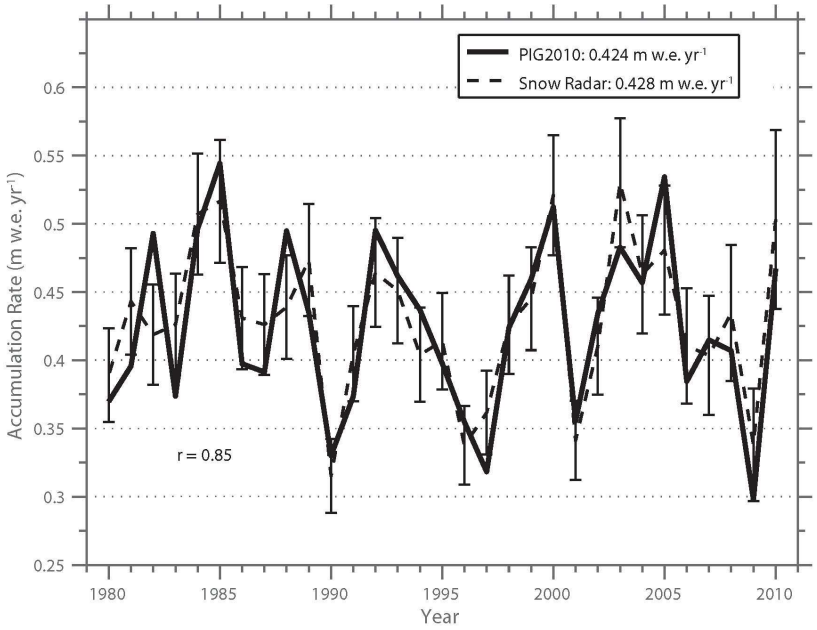

Figure 2.3 – The radar- and core-derived accumulation records at the PIG2010 core site. The records are nearly co-located (~150 m separation) and are highly correlated. The 30-year averages are listed in the legend and are statistically indistinguishable. Snow radar measurement uncertainties are shown as well.

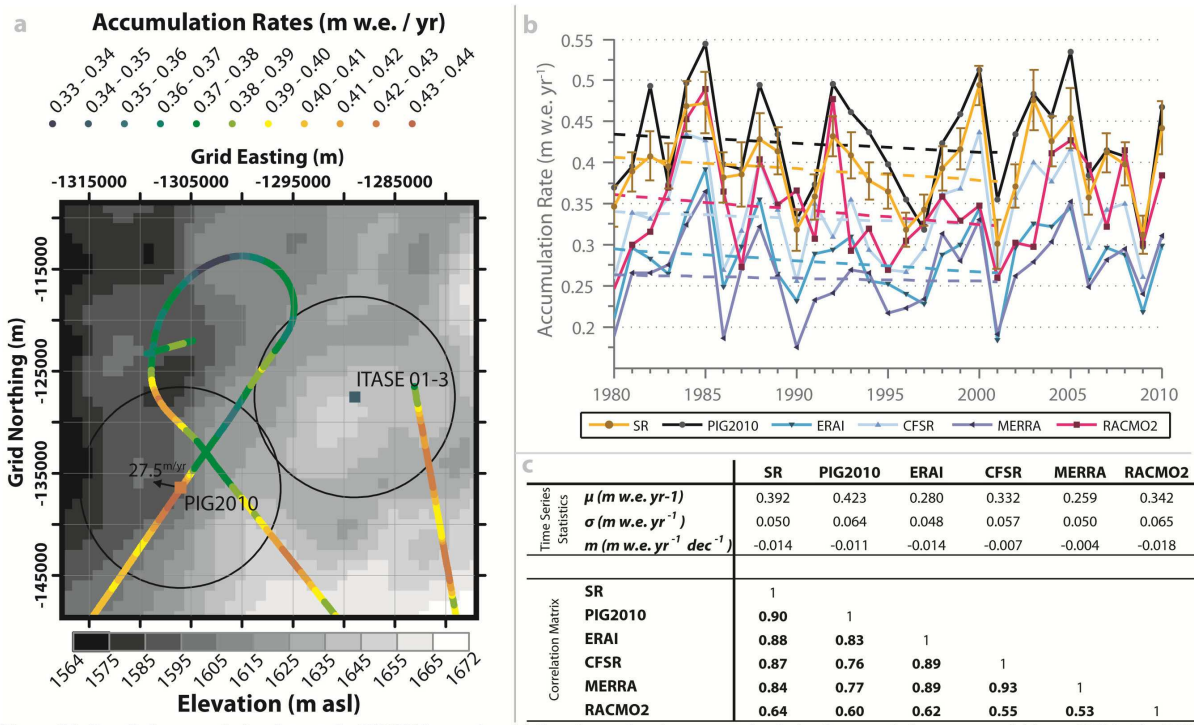

		SR	PIG2010	ERAI	CFSR	MERRA	RACMO2
Time Series Statistics	*μ (m w.e. yr-1)*	0.392	0.423	0.280	0.332	0.259	0.342
	σ (m w.e. yr^{-1})	0.050	0.064	0.048	0.057	0.050	0.065
	m (m w.e. yr^{-1} dec^{-1})	-0.014	-0.011	-0.014	-0.007	-0.004	-0.018
Correlation Matrix	SR	1					
	PIG2010	**0.90**	1				
	ERAI	**0.88**	**0.83**	1			
	CFSR	**0.87**	**0.76**	**0.89**	1		
	MERRA	**0.84**	**0.77**	**0.89**	**0.93**	1	
	RACMO2	**0.64**	**0.60**	**0.62**	**0.55**	**0.53**	1

Figure 2.4 – Detailed accumulation data at the PIG2010 core site. (a) Local map showing snow radar derived accumulation rates overlaid on a DEM. The DEM is shaded in 10 m intervals. The radar and core-derived accumulation rates are color-coded in 0.01 m w.e. yr-1 intervals. Ice cores are indicated by squares. Velocity vectors are placed where data were available. Black circles are 10 and 20-km buffers around the core sites. (b) Annual time series of accumulation rates from the PIG2010 core (black), the average of the radar-derived accumulation records within the 10-km buffer (orange) where error bars show ± 1 standard deviation of the records, model-derived accumulation rates from the closest grid cell (blues and red). The 1980-2001 trends are shown as dashed lines. (c) Table of time series statistics for each dataset plotted, including the annual mean (μ), standard deviation (σ), and trend slope (m), and correlation coefficients between each dataset from 1980-2001 where bold (italic) indicates significance at the 99% (95%) confidence level.

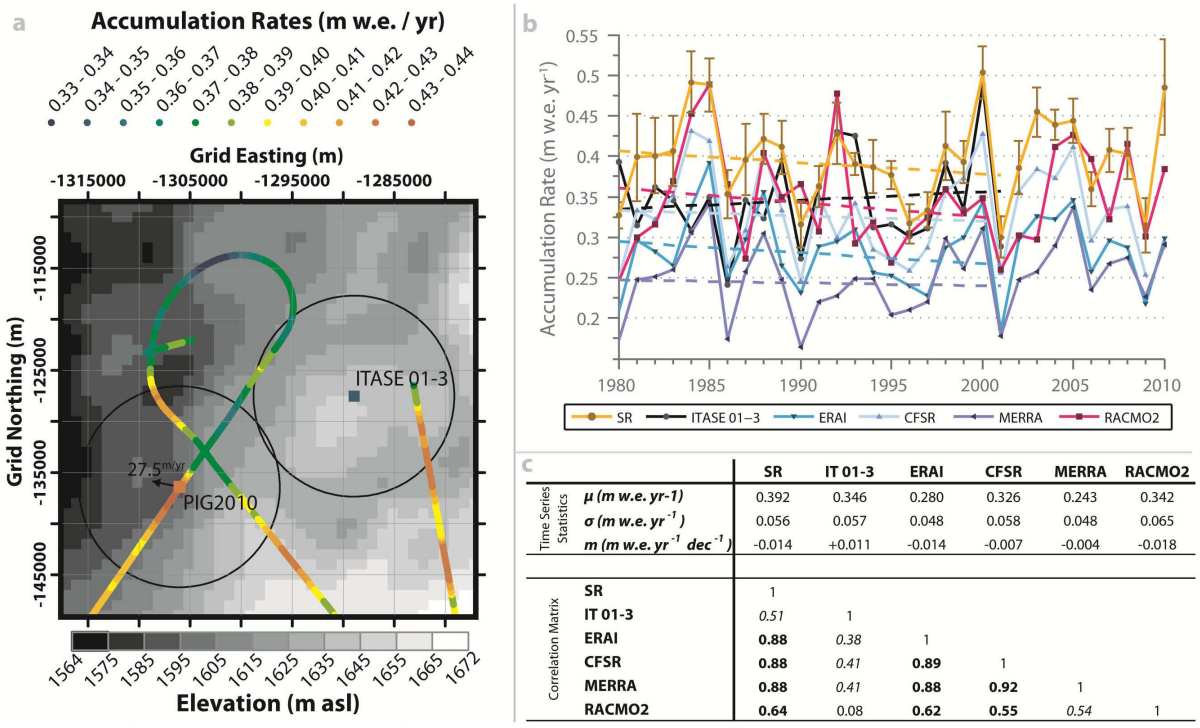

c

		SR	IT 01-3	ERAI	CFSR	MERRA	RACMO2
Time Series Statistics	μ (m w.e. yr-1)	0.392	0.346	0.280	0.326	0.243	0.342
	σ (m w.e. yr^{-1})	0.056	0.057	0.048	0.058	0.048	0.065
	m (m w.e. yr^{-1} dec^{-1})	-0.014	+0.011	-0.014	-0.007	-0.004	-0.018
Correlation Matrix	SR	1					
	IT 01-3	*0.51*	1				
	ERAI	**0.88**	*0.38*	1			
	CFSR	**0.88**	*0.41*	**0.89**	1		
	MERRA	**0.88**	*0.41*	**0.88**	**0.92**	1	
	RACMO2	**0.64**	0.08	**0.62**	**0.55**	*0.54*	1

Figure 2.5 – Detailed accumulation data at the ITASE 01-3 core site. (a) Local map showing snow radar derived accumulation rates overlaid on a DEM. The DEM is shaded in 10 m intervals. The radar and core-derived accumulation rates are color-coded in 0.01 m w.e. yr-1 intervals. Ice cores are indicated by squares. Velocity vectors are placed where data were available. Black circles are 10 and 20-km buffers around the core sites. (b) Annual time series of accumulation rates from the ITASE 01-3 core (black), the average of the radar-derived accumulation records within the 10-km buffer (orange) where error bars show ± 1 standard deviation of the records, model-derived accumulation rates from the closest grid cell (blues and red). The 1980-2001 trends are shown as dashed lines. (c) Table of time series statistics for each dataset plotted, including the annual mean (μ), standard deviation (σ), and trend slope (m), and correlation coefficients between each dataset from 1980-2001 where bold (italic) indicates significance at the 99% (95%) confidence level.

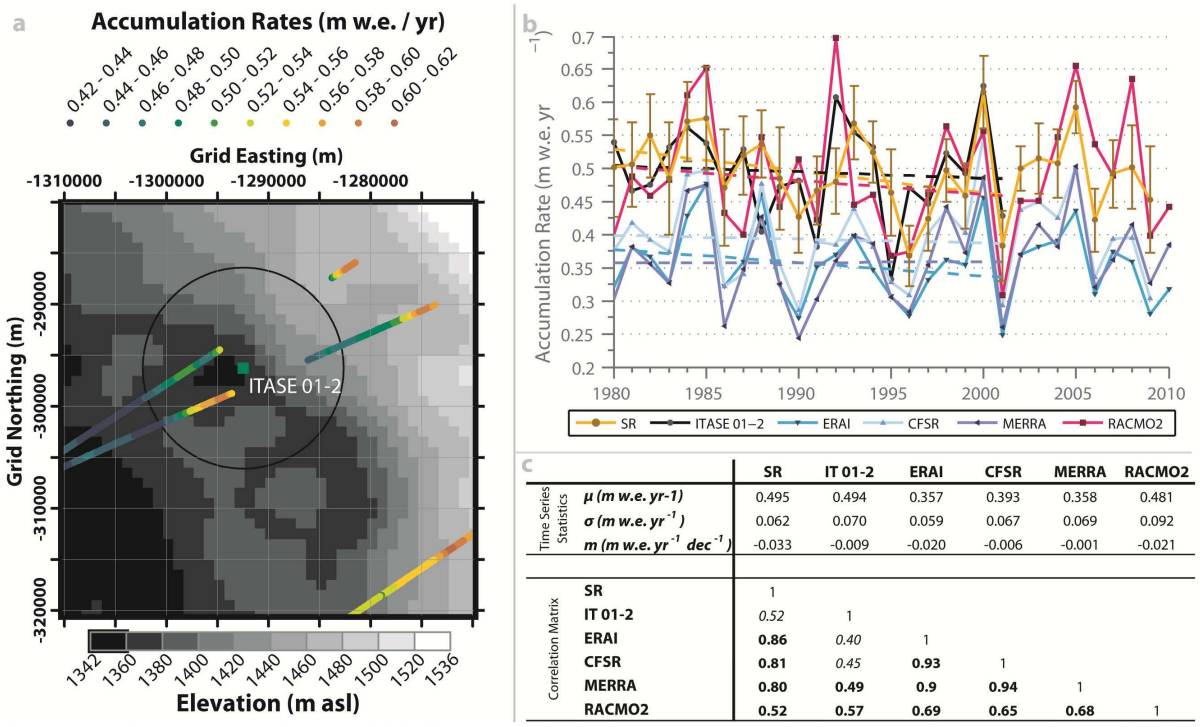

c

		SR	IT 01-2	ERAI	CFSR	MERRA	RACMO2
Time Series Statistics	*μ (m w.e. yr-1)*	0.495	0.494	0.357	0.393	0.358	0.481
	σ (m w.e. yr^{-1})	0.062	0.070	0.059	0.067	0.069	0.092
	m (m w.e. yr^{-1} dec^{-1})	-0.033	-0.009	-0.020	-0.006	-0.001	-0.021
Correlation Matrix	**SR**	1					
	IT 01-2	*0.52*	1				
	ERAI	**0.86**	*0.40*	1			
	CFSR	**0.81**	*0.45*	**0.93**	1		
	MERRA	**0.80**	**0.49**	**0.9**	**0.94**	1	
	RACMO2	**0.52**	**0.57**	**0.69**	**0.65**	**0.68**	1

Figure 2.6 – Detailed accumulation data at the ITASE 01-2 core site. (a) Local map showing snow radar derived accumulation rates overlaid on a DEM. The DEM is shaded in 20 m intervals. The radar and core-derived accumulation rates are color-coded in 0.02 m w.e. yr-1 intervals. Ice cores are indicated by squares. Velocity vectors are placed where data were available. Black circles are 10 and 20-km buffers around the core sites. (b) Annual time series of accumulation rates from the ITASE 01-2 core (black), the average of the radar-derived accumulation records within the 10-km buffer (orange) where error bars show ± 1 standard deviation of the records, model-derived accumulation rates from the closest grid cell (blues and red). The 1980-2001 trends are shown as dashed lines. (c) Table of time series statistics for each dataset plotted, including the annual mean (μ), standard deviation (σ), and trend slope (m), and correlation coefficients between each dataset from 1980-2001 where bold (italic) indicates significance at the 99% (95%) confidence level.

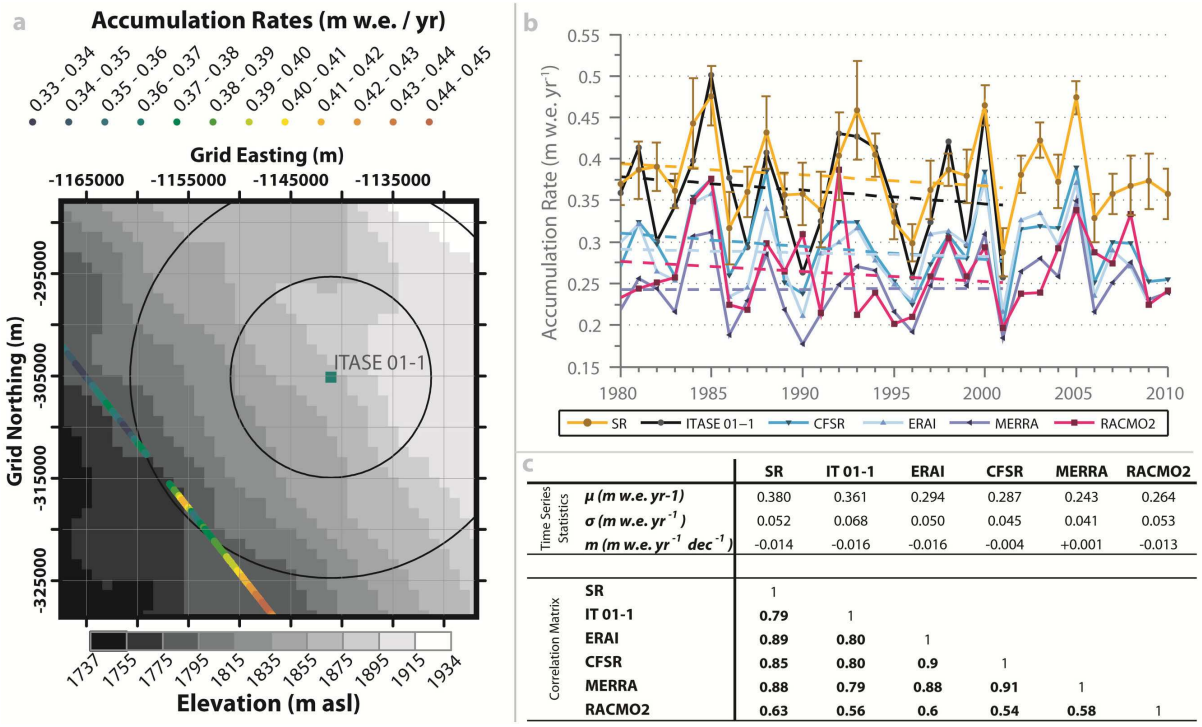

c

		SR	IT 01-1	ERAI	CFSR	MERRA	RACMO2
Time Series Statistics	*μ (m w.e. yr-1)*	0.380	0.361	0.294	0.287	0.243	0.264
	σ (m w.e. yr^{-1})	0.052	0.068	0.050	0.045	0.041	0.053
	m (m w.e. yr^{-1} dec^{-1})	-0.014	-0.016	-0.016	-0.004	+0.001	-0.013
Correlation Matrix	SR	1					
	IT 01-1	**0.79**	1				
	ERAI	**0.89**	**0.80**	1			
	CFSR	**0.85**	**0.80**	**0.9**	1		
	MERRA	**0.88**	**0.79**	**0.88**	**0.91**	1	
	RACMO2	**0.63**	**0.56**	**0.6**	**0.54**	**0.58**	1

Figure 2.6 – Detailed accumulation data at the ITASE 01-1 core site. (a) Local map showing snow radar derived accumulation rates overlaid on a DEM. The DEM is shaded in 20 m intervals. The radar and core-derived accumulation rates are color-coded in 0.01 m w.e. yr-1 intervals. Ice cores are indicated by squares. Velocity vectors are placed where data were available. Black circles are 10 and 20-km buffers around the core sites. (b) Annual time series of accumulation rates from the ITASE 01-1 core (black), the average of the radar-derived accumulation records within the 20-km buffer (orange) where error bars show ± 1 standard deviation of the records, model-derived accumulation rates from the closest grid cell (blues and red). The 1980-2001 trends are shown as dashed lines. (c) Table of time series statistics for each dataset plotted, including the annual mean (μ), standard deviation (σ), and trend slope (m), and correlation coefficients between each dataset from 1980-2001 where bold (italic) indicates significance at the 99% (95%) confidence level.

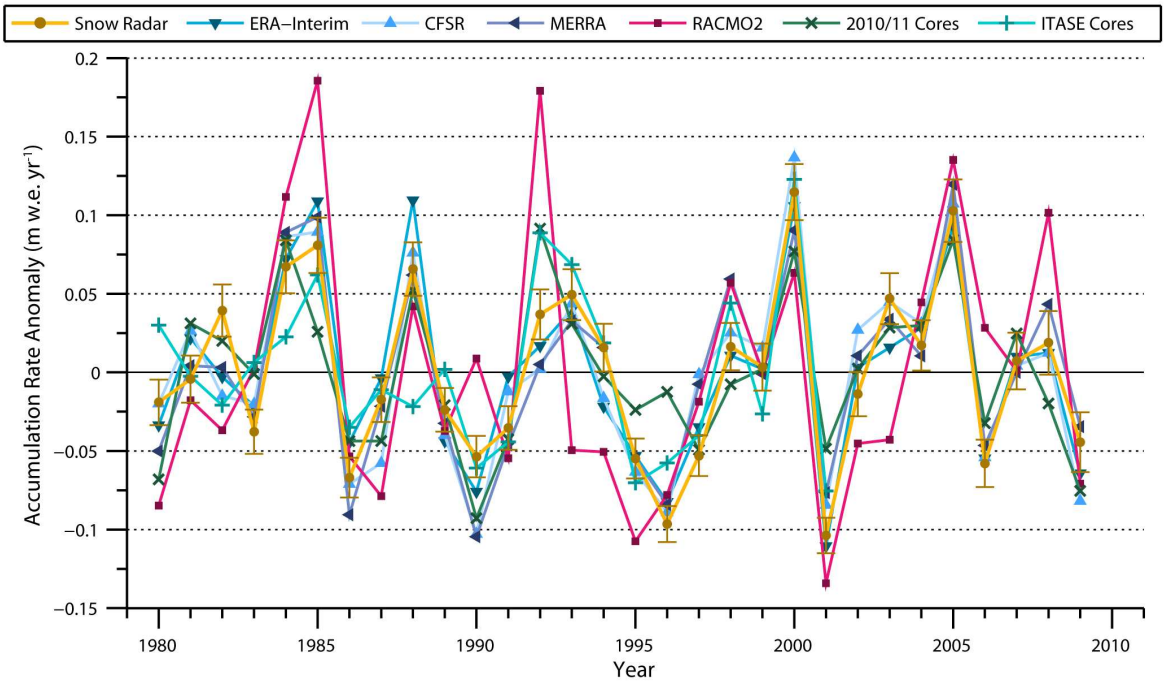

Figure 2.8 – Comparison of the accumulation rate anomalies derived from the snow radar (orange circles), the 2010/11 (green ×) and ITASE (blue-green +) core ensembles, RACMO2 (red squares), and three global reanalyses (blue triangles). The snow-radar record is the spatial average of all complete records shown in Figure 2.1 and includes 1-σ error bars. The 2010 core ensemble is the average of the PIG2010, DIV2010, and THW2010 cores, which have age uncertainties of < 1 year. The ITASE ensemble is the average of the ITASE 01-1, 01-2, and 01-3 core records, which have age uncertainties of ≤ 1 year. All anomalies were estimated by subtracting the long-term (1980–2009) mean, which are listed in Table 2.1.

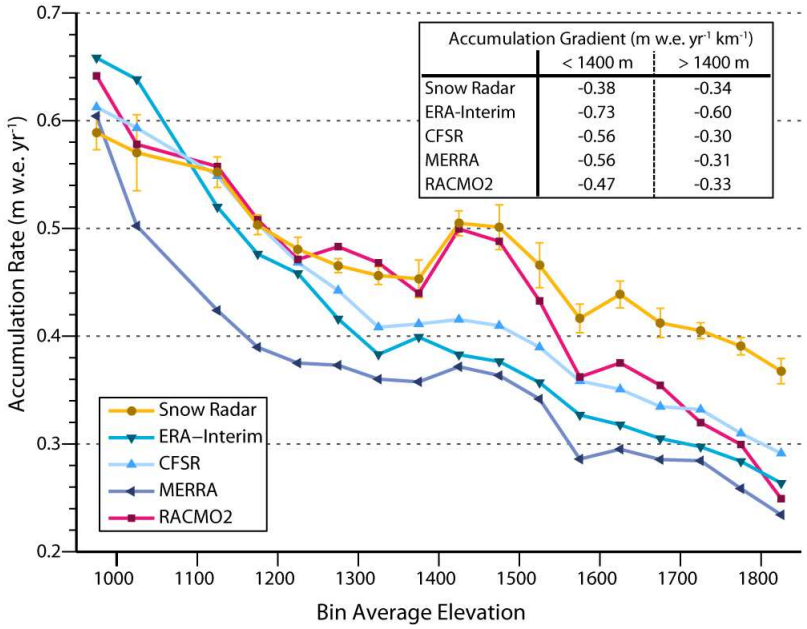

Figure 2.9 – Snow-radar (orange circle), RACMO2 (red square), and reanalysis (blue triangles) accumulation rates averaged over 50-m elevation bins. Inset table contains the accumulation gradients (linear) above and below 1400 m for each data set. Accumulation rates generally decrease with increasing elevation for all data sets. RACMO2 is the most capable of reproducing the small-scale features found in the snow-radar profile. The three global reanalyses all underestimate accumulation, with potential exceptions at the lowest elevations where there is insufficient sampling.

Table 2.1 – Time Series Statistics and Spatial and Temporal Correlation Coefficients (*r*)

		Snow Radar	RACMO2[c]	ERA-Int[c]	CFSR[c]	MERRA[c]	2010 Cores	ITASE Cores[d]
Time Series Statistics[a]	μ ± σ (m w.e. yr^{-1})	0.457 ± 0.055	0.434 ± 0.080	0.382 ± 0.056	0.407 ± 0.060	0.346 ± 0.057	0.377 ± 0.049	0.401 ± 0.053
	m (% per decade)	-0.3 ± 5.4 %	+1.1 ± 8.2 %	-1.5 ± 6.5 %	+0.5 ± 6.6 %	+2.1 ± 7.3 %	-0.1 ± 5.7 %	-1.2 ± 9.5 %
Correlation Matrix[b]	Snow Radar	--	*0.86*	*0.68*	*0.75*	*0.75*		
	RACMO2[c]	**0.68**	--	*0.78*	*0.86*	*0.86*		
	ERA-Int[c]	**0.93**	**0.69**	--	*0.91*	*0.78*		
	CFSR[c]	**0.91**	**0.64**	**0.94**	--	*0.85*		
	MERRA[c]	**0.92**	**0.69**	**0.91**	**0.93**	--		
	2010 Cores	**0.80**	**0.64**	**0.79**	**0.81**	**0.77**	--	
	ITASE Cores[d]	**0.80**	**0.64**	**0.69**	**0.73**	**0.72**	**0.66**	--

[a]The mean (μ), standard deviation(σ), and trend slope (*m*) with 95% confidence intervals during 1980-2009.

[b]Upper right italicized (lower left bolded) corner contains the spatial (temporal) correlation coefficients. All *r* are statistically significant at the 99% confidence level.

[c]Model grid resolution approximated over Thwaites Glacier: 27 km (RACMO2), ~80 km (ERA-Int), ~ 38 km (CFSR), ~55 x 20 km (MERRA).

[d]ITASE Cores 01-1, 01-2, 01-3; Statistics calculated over the period of record (1980-2001).

Chapter 3: The Mass Balance of the Amundsen Sea Glaciers

Chapter 3, in full, is currently being prepared for publication as "Constraining the recent mass balance of Pine Island and Thwaites glaciers, West Antarctica with airborne observations of snow accumulation" authored by B. Medley, I. Joughin, B.E. Smith, S.B. Das, E.J. Steig, H. Conway, S. Gogineni, C. Lewis, A.S. Criscitiello, J.R. McConnell, M.R. van den Broeke, J.T.M. Lenaerts, D.H. Bromwich, J.P. Nicolas, C. Leuschen. The dissertation author was the primary investigator and author of this paper.

3.1 Abstract

Uncertainties in mass input and output translate directly into uncertainty in glacier mass balance. While remotely sensed observations of ice velocity and thickness have improved our understanding of ice loss to the ocean, snow accumulation over large areas remains unmeasured. We show that an airborne radar system, combined with ice-core glaciochemical analysis, provide the data necessary to measure accumulation rates at the catchment-scale in the high accumulation Amundsen Sea sector of West Antarctica. Using the radar-derived accumulation measurements, we generated an accumulation grid capable of resolving moderate- to large-scale features (> 25 km) over the Pine Island-Thwaites drainage system to assess catchment-wide accumulation. We found that accumulation equivalents from atmospheric models and gridded climatologies are often underestimated in the high elevation, low accumulation interior and are likely overestimated in the low elevation, high accumulation coastal zones. Ice discharge is measured over various time intervals between 1994 and 2012, which are combined with our catchment-wide accumulation rates, allowing us to create a recent mass balance history for the sector. While Thwaites exhibited the largest mass loss in the mid-1990s, the mass loss from Pine Island increased substantially by

2006, overtaking Thwaites as the largest contributor to sea-level rise; however, the increasing discharge trend appears to have leveled off in 2008 for both glaciers.

3.2 Introduction

Pine Island (PIG) and Thwaites (THW) glaciers are two of the largest Antarctic contributors to recent sea-level rise (SLR) [*Rignot et al.,* 2008; *Shepherd et al.,* 2012] and will likely continue contributing substantially over the next century [*Joughin et al.,* 2010; *Gladstone et al.,* 2012] . Snow accumulation and ice discharge to the ocean are the predominant sources of mass input and ouput in Antarctica, and their difference defines the glacier's mass balance. While measuring these processes at the catchment-scale was once difficult, satellite observations at and around the grounding line have vastly improved estimates of ice discharge. Remotely sensed measurements of ice surface velocity over the past few decades revealed the rate of ice discharge from Pine Island and Thwaites is increasing [*Rignot,* 2001; *Joughin et al.,* 2003; *Rignot,* 2008] , resulting in extensive thinning near their margins [*Thomas et al.,* 2004; *Pritchard et al.,* 2009] . This rapid dynamical change is likely the consequence of warm ocean currents melting and thus thinning buttressing ice shelves, an effect observed over much of West Antarctica [*Shepherd et al.,* 2004; *Joughin et al.,* 2012; *Pritchard et al.,* 2012] . While our understanding of the dynamics of these glaciers has improved substantially over the past decade, snow accumulation over large areas of these glaciers has only been sparsely sampled [*van den Broeke et al.,* 2006] .

Determining catchment-wide snow accumulation is difficult because rates vary considerably in space and time, and as a result, field measurements of accumulation typically sample one dimension with exclusion of the other. For example, ice-core records of

accumulation [e.g., *Kaspari et al.,* 2004] capture the temporal signal but are sparsely distributed. Stake farm accumulation measurements [e.g., *Frezzotti et al.,* 2005; *Kameda et al.,* 2008; *Agosta et al.,* 2012] are collected over broader areas to capture the spatial variability yet typically span only a few years. These *in situ* measurements also are inadequate for mass balance studies because recovery is sometimes impossible over certain regions such as highly crevassed areas. Accumulation measurements using ground-based radar systems overcome some of the disadvantages of the traditional *in situ* measurements; they capture the spatial variability in accumulation over discrete (i.e., annual to multi-decadal) and consistent time horizons over hundreds of kilometers [*Rotschky et al.,* 2004; *Spikes et al.,* 2004] . These ground-based systems, however, remain insufficient for regional studies because of inaccessibility issues.

Here, we use data from two airborne radar systems to calculate the 1985–2009 average annual accumulation over the Pine Island-Thwaites drainage system along the Amundsen Coast of West Antarctica. The spatial coverage limitation that makes *in situ* accumulation measurements disadvantageous for regional mass balance studies is overcome by aerial survey. Using two frequency-modulated continuous-wave (FMCW) radar systems developed by the Center for Remote Sensing of Ice Sheets (CReSIS), we tracked a few near-surface horizons over hundreds of kilometers of the flight surveys. The radar-derived accumulation survey was spatially extensive, which enabled us to generate a complete map of the recent accumulation rate. Combining these basin-wide accumulation measurements with flux-gate estimates of ice discharge, we determined the recent mass balance history of the Amundsen Coast glaciers and their contribution to SLR.

3.3 Study Area

Located in West Antarctica along the Amundsen Coast, Pine Island and Thwaites glaciers cover areas of 167×10^3 km^2 and 176×10^3 km^2, which together account for nearly 3% of the grounded ice in Antarctica but ~7% of accumulation [*Lenaerts et al.,* 2012] . While Pine Island and Thwaites are the primary interest, smaller adjacent catchments are investigated as well (Figure 3.1). Although the Crary mountains in the Thwaites catchment reach over 3500 m asl, the great majority of both catchments lie below 2300 m asl (Figure 3.2).

The Amundsen Coast glaciers receive large amounts of snowfall because their low elevation coastal slopes allow for moisture-rich cyclones to penetrate well into their interiors. Until recently, few reliable measurements of snow accumulation existed from these glaciers [*van den Broeke et al.,* 2006] . Kaspari *et al.* [2004] presented several ice-core accumulation records produced by the International Trans-Antarctic Scientific Expedition (ITASE), but only four lie within the Pine Island-Thwaites drainage system. Based on three of these records (one is disregarded as it is just over 20 years in length), the authors found that recent accumulation between 1970 and 2000 increased relative to the long-term average. Radar-derived annual accumulation shows no significant trend in accumulation over Thwaites glacier between 1980 and 2009 [*Medley et al.,* 2013] .

3.4 Data and Methods

Radar imaging of both near-surface [*Sinisalo et al.,* 2003; *Rotschky et al.,* 2004; *Spikes et al.,* 2004; *Eisen et al.,* 2005; *Anschutz et al.,* 2007; *Frezzotti et al.,* 2007; *Anschutz et al.,* 2008; *Urbini et al.,* 2008] and deep [*Nereson et al.,* 2000; *Siegert and Payne,* 2004; *Waddington et al.,* 2007; *Huybrechts et al.,* 2009; *MacGregor et al.,* 2009] internal horizons

has provided the basis for calculating recent and historical spatio-temporal snow accumulation rates over Antarctica. Because radar-derived accumulation measurements capture the spatial variability better than widely spaced point measurements, they provide a more accurate representation of the spatial mean, and thus are more appropriate for mass balance studies [*Richardson et al.*, 1997] . For this study, we recovered three intermediate-depth firn cores, which are connected by an airborne radar survey network designed to capture the regional variations in snow accumulation over the entire Pine Island-Thwaites drainage system (Figure 3.1).

3.4.1 Accumulation radar

The first CReSIS radar – referred to as the "accumulation radar" – is an ultra-wideband FMCW system that operated between 550 and 900 MHz and was designed to image horizons in the upper 100–150 m of the ice sheet [*Lewis*, 2010; *Rodriguez-Morales et al.*, 2013] . These near-surface horizons represent contrasts in the material's dielectric permittivity, which are likely the result of seasonal variations in firn density [*Arcone et al.*, 2005] . The theoretical vertical range resolution in ice is 40 cm and in firn (density of 550 kg m^{-3}) is 50 cm. The vertical resolution of this system is too coarse to image annual stratigraphy, and consequently, an independent ice core depth-age scale is necessary to determine horizon ages. The radar data and full documentation are available at ftp://data.cresis.ku.edu/data/accum. We processed the echograms by (1) zeroing the ice-sheet surface under the assumption that it is represented by the strongest return from each trace; (2) stacking every 12 traces to reduce noise; (3) normalizing the range bin return relative to the average bin return from all traces in order to brighten deeper horizons; and (4) applying a horizontal Sobel edge-detection filter to enhance horizon contrast. The 2009/2010 Twin

Otter flight survey was designed to maximize spatial coverage over the Pine Island-Thwaites catchment area (Figure 3.1) with nearly 10,000 km of flight surveys covering an area of nearly 300×10^3 km^2.

We used the formula, $d = 0.5c\tau\varepsilon^{-0.5}$, for conversion between two-way travel time τ and depth d where c is the wavespeed in a vacuum (3×10^8 m s^{-1}) and the dielectric permittivity ε is calculated using a mixture model [*Looyenga,* 1965] . We fit a steady-state density model [*Herron and Langway,* 1980] to the average of nine firn core density profiles from the region for input into the mixture model (Figure 3.3a). Because ε is depth dependent, the d-τ profile is generated incrementally at 1-cm intervals through the firn column (Figure 3.3b). We integrated the regional density model to generate a cumulative mass profile (kg m^{-2}; Figure 3.3c). Use of a regional density profile means the d-τ and cumulative mass profiles do not vary spatially, and is thus a potential source of error that is discussed further below.

Because we focused on generating a spatially complete and temporally consistent map of snow accumulation, we tracked a single strong and continuous reflector (H1) over as much of the radar survey as possible (Figure 3.4). The depth of H1 ranged from 4.3 to 19.6 m. Tracking a relatively shallow, and thus young horizon means any undulations in the stratigraphy have not substantially steepened, making the horizon reasonably trackable. Using a consistent horizon over multiple flight surveys is important so that the resulting accumulation rates will cover the same time interval. In the limited areas where H1 was not traceable with confidence, we mapped other brightly visible horizons (H2-H3). All horizon tracking began at the PIG2010 site where the horizons were dated.

3.4.2 Firn cores

We collected three intermediate-depth firn cores the year following the accumulation radar survey, which allowed us to use the radar data in core site selection. The cores were collected in approximately 1-m segments (diameter: 81 mm) using the Badger-Eclipse drill provided by the U.S. Ice Drilling Program. The PIG2010 and THW2010 cores reached depths of ~60 m, while the DIV2010 core reached ~110 m (Table 3.1). Density measurements of the core segments were completed in the field for the DIV2010 and THW2010 cores and at the U.S. National Ice Core Laboratory in Denver, CO for PIG2010. Water isotope ratios and concentrations of more than 30 elements and chemical species were measured at high depth resolution (~1 cm water equivalent) using a continuous ice core melter system [*McConnell et al.,* 2002; *McConnell et al.,* 2007; *Maselli et al.,* 2013] . While nearly all ratios exhibit pronounced annual cycles in concentration, here we used the summer maxima in hydrogen-peroxide concentration, water-isotope ratios, and non-sea-salt sulfur to sodium ratio to identify consistently annual layers. Well known volcanic horizons identified by marked increases in wintertime sulfur concentration were used to verify the annual layer counting, which indicated a dating uncertainty of < 1 year. The PIG2010 core was selected to date horizons because of its optimal location: the core was drilled at the intersection of several radar surveys (Figure 3.1).

While all horizons were dated using the PIG2010 core, we evaluated the isochronal accuracy by dating H1 at the DIV2010 and THW2010 core sites. The depths of H1 at the PIG2010, DIV2010, and THW2010 cores were 19.75 ± 0.33 m, 18.95 ± 0.35 m, and 14.15 ± 0.34 m (error calculations described below), respectively, which correspond to ages of 25.4 ± 0.4 yr, 25.7 ± 0.4 yr, and 25.2 ± 0.6 yr. Although the depth errors at each core are

comparable in magnitude, the age uncertainty at the THW2010 core is larger because the site has a lower accumulation rate than the other sites. As a result, the THW2010 depth-age curve is shallower (Figure 3.4d), which translates into a larger age uncertainty. Nonetheless, the H1 ages differ by 0.5 yr, which is remarkable because THW2010 is separated from the other cores along the survey paths by more than 750 km. This comparison confirms that the horizons observed in the accumulation radar echograms are isochronous over very large distances.

3.4.3 Accumulation rate calculations

For each of the three mapped horizons, the spatial variation in the accumulation rate is solely the result of variable horizon depth. The long-term accumulation rate (between the horizon and surface) is determined by dividing the cumulative firn mass per unit area (Figure 3.3c) above the horizon by the time since horizon burial (i.e., the horizon age in years). While the horizon age does not vary spatially, the horizon depth does vary substantially, which results in variable firn mass above the horizon. Over the survey portions where we were unable to map H1, we measure accumulation using an alternate horizon (H2 or H3) and correct for the temporal bias. The bias corrections were based on accumulation measurements where both H1 and the alternate horizon were coincidently mapped. We completed a total of five robust regressions (Figure 3.5), one for each flight survey segment where an alternate horizon was used to measure accumulation (see Figure 3.1). The different relationships are the potential result of (1) different temporal biases from using two alternate horizons and (2) spatial variations in the bias. These corrected data make up only 8% of the total accumulation measurements and are entirely concentrated in the northern Pine Island catchment.

3.4.4 Radar-derived accumulation rate errors

The uncertainty in radar-derived accumulation rates stems from the uncertainties in the regional density profile and horizon age. At any location, the deviation of actual density profile from the regional mean translates into errors in the cumulative mass and d-τ profiles and ultimately the measured accumulation rate. To account for this error, we fit the aforementioned density model to the $\pm 1\sigma$ deviation of the measured density profiles from the mean (Figure 3.3a). We then calculate the error in the d-τ and cumulative mass profiles (Figure 3.3b-c) assuming the density uncertainty could bias our results, which means errors accumulate with depth. This assumption is conservative and reasonable based on evaluation of the individual core profiles relative to the regional mean. Digitization error of ± 1 range bin is included in the depth error, which is equal to ~ 30 cm in firn.

Uncertainty in the age of the horizon also introduces error into our accumulation measurements. Using the regional mean density profile and its uncertainty, we determined H1 depth and error at each of the three core sites using their measured depth-age profiles shown in Figure 3.4d (see above). While the measured age at each site falls within the error bounds of the other two sites, the range of values is large enough that we must consider its impact. We assign the error in the age of H1 at ± 1 year, which based on the evaluation of the isochronal accuracy above is likely an overestimation.

Finally, we must consider error in the bias correction for measurements based on the alternate horizons (H2-H3). These measurements are assigned errors equal to the root mean square error of the robust regression fits shown in Figure 3.5, which vary from 0.018 to 0.069 m water equivalent (w.e.) yr^{-1} depending on survey leg.

3.4.5 Snow radar

The second CReSIS radar – referred to as the "snow radar" – is another ultra-wideband FCMW system that operated over a higher frequency range (2009: 4–6 GHz; 2010/11: 2–6.5 GHz) than the accumulation radar. This system images the stratigraphy in the upper 20–30 m of the ice sheet at very high vertical resolution. Specifically, the theoretical vertical range resolution for the 2009 (2010/11) survey is 8 cm (4 cm) in ice and 10 cm (5 cm) in firn. The snow radar was flown as part of NASA's Operation IceBridge, a mission focused on areas of rapidly changing ice in and around the major outlet glaciers. While the survey was not designed with catchment coverage in mind, the data set provides additional measurements over ~2,000 km of the survey tracks primarily within the Thwaites catchment. To be temporally consistent with the accumulation radar measurements, we take the 1985–2009 mean annual accumulation derived from the snow radar and presented in [*Medley et al.*, 2013] .

3.4.6 Interpolation

While the along-track measurement interval (500 m) is relatively small, large data gaps remain between flight paths (up to 150 km; Figure 3.6a). The presence of large data gaps means the spatial resolution of any interpolated map will be substantially coarser than the along-track resolution: accumulation was not appropriately sampled to recover the high-frequency variations. To minimize the high-frequency variability in the accumulation measurements, we applied a 25-km running average filter to the profile data (Figure 3.6b). Approaching the ends of the surveys, the filtering length was tapered down to 5 km to maximize the spatial coverage for interpolation. Using the smoothed accumulation measurements, we generated a gridded map of accumulation using the geostatistical

interpolation technique of kriging [*Leuangthong et al.*, 2011] . Prior to interpolation, we used an ordinary least squares (OLS) linear regression model with northing, easting, and elevation as explanatory variables to create an accumulation rate surface (Figure 3.7a). The interpolation was then performed on the OLS model residuals. We found the best fit to the measured semivariogram was an isotropic spherical model with a range of 175 km. Sharp lines and edges in the radar survey result in unrealistic artifacts in the interpolated map. Therefore, we smoothed the 3-km grid with a 9 × 9 cell mean filter to minimize these high-frequency interpolation artifacts. Finally, the OLS surface is added to the kriged residuals to generate the final accumulation map, which is shown in Figure 3.7b.

We created an accumulation error grid that accounts for measurement and interpolation uncertainties (Figure 3.7c). The kriging standard prediction error is based on the distances to the nearest measurements (i.e., cells further from measurements have a greater error) and the spatial structure of the data as described by the semivariogram. We also investigate the impact of measurement error on the final accumulation map. Random error is added to each accumulation measurement and these perturbed values are then interpolated to a grid using the same parameters described above. The error added to each measurement point is randomly selected from a normal distribution with a mean of zero and standard deviation equal to the measurement error for that data point. This process was repeated 200 times, and the measurement error for each grid cell was taken as the standard deviation of these 200 realizations. The final accumulation error grid was generated by root-sum-square (RSS) of the interpolation and measurement grids and was smoothed using a 9 × 9 cell mean filter.

3.4.7 Surface velocities and catchment discharge

We derived surface velocities using a combination of interferometric synthetic aperture radar (InSAR) and speckle-tracking techniques [*Joughin,* 2002] . Velocities from 2000 and before were determined using data from the European Space Agency's ERS-1/2 mission and later velocities were derived from a combination of data from the Japanese ALOS and German TerraSAR-X mission [*Joughin et al.,* 2003; *Joughin et al.,* 2010] . System noise produces errors of ~10 m yr^{-1} and there are additional velocity and slope-dependent errors of ~3% [*Joughin,* 2002] .

Catchment discharge was estimated using ice-surface velocities and a time-varying estimate of ice thickness along a transect that roughly follows the grounding line. Because ice-thickness estimates are sometimes confused by the presence of basal crevasses downstream of the grounding line, and because grounding lines have retreated during the decade considered in this study, the transect was displaced 5−10 km inland to ensure that high-quality ice-thickness data were available.

We constructed a high-resolution model of the time-varying ice-surface height using ICESat satellite altimetry data [*Zwally et al.,* 2012] , and airborne scanning laser altimetry data supplied by NASA's IceBridge program [*Krabill,* 2010, updated 2013; *Blair and Hofton,* 2010, updated 2012] . These give irregular spatial and temporal coverage between the late fall of 2002 and 2012, which we integrated into an estimate of surface elevation and elevation change by fitting a DEM surface for 2010 and a series of correction surfaces giving height differences between 2002 and 2010. The solution was selected to minimize, in a least-squares sense, the difference between the model surface and the observed surface heights, while also minimizing the second derivative of the DEM surface and the second derivative of

the ice-surface change rate between any pair of years. This technique lets us estimate surface heights at any time and at any position on the grounded ice, although the accuracy of any estimate likely depends strongly on the temporal and spatial sampling of the input data. Typically surface-elevation error estimates for points within 2−4 km of a flight line are less than 10 m. Ice-surface elevations for flux estimates before 2003 are calculated by linear extrapolation of the 2003-07 elevation rate of change. This extrapolated elevation difference is assigned an error of 100%.

We combined our ice-surface height estimates with ice-thickness estimates derived from ice-penetrating radar [*Holt et al.,* 2006; *Vaughan et al.,* 2006; *Allen,* 2010, updated 2013] to form a set of bed-elevation estimates. We applied a minimum-curvature gridding technique that minimized, in a least-squares sense, the second spatial derivative of the bed elevation, while also miminizing the data misfit. The cost function on the derivatives was selected based on ice-velocity maps so that curvature in the along-ice-flow direction was penalized more heavily than the curvature in the across-flow direction, giving bed-elevation estimates that preserve channel structures while suppressing small-scale noise in the data. The RMS misfits between data and the fit surface were better than 7 m over the smooth basal topography near the grounding line. This small misfit suggests that the fit surface adequately resolves the details of the bed topography; uncertainties in the data picking and in the location of radar footprints contribute substantially larger errors to the ice thickness, which we conservatively estimate at 50 m.

We derived ice-discharge estimates using surface-height, surface-velocity, and ice-thickness estimates assuming that ice flow is almost entirely due to sliding at the bed:

$$D(t) = \rho_{ice} \int \vec{u}(x,y,t) \cdot \vec{n}\,[z_s(x,y,t) - b(x,y) - h_{air}]ds. \quad (3.1)$$

Here $\vec{u} \cdot \vec{n}$ is the component of the ice-surface velocity perpendicular to the transect, z_s is the surface height at the time the velocity was measured, b is the bed elevation, and h_{air} is the depth-integrated thickness of air contained in the firn, as estimated from a published map [*van den Broeke, M. R.*, 2008] . We evaluate the flux integral on points spaced every 50 m along the transect.

When the velocity maps contain gaps, we interpolate spatially within the same map to close gaps smaller than 4 km, and interpolate in time between temporally adjacent maps to fill larger gaps. Velocity values so interpolated are assigned an additional error component of 100 m yr^{-1} in each direction. If temporally adjacent maps do not supply a valid velocity estimate, the velocity is estimated from the mean of all available velocities for that point, and the error estimate is set to 250 m yr^{-1}, which happens only for a few points at the north edge of PIG and a few points along the Wedge.

We estimate errors in our flux estimate by propagating the measurement errors in equation 1, as if each component were independent between 50-meter grid points. We then account for spatial correlation in the errors, which we conservatively assume to be spatially correlated on 10-km scale, by multiplying these initial error estimates by $\left({}^{10\ km}/_{50\ m}\right)^{1/2}$, or about a factor of 14. Other reasonable choices of a correlation scale could cut our error estimates roughly in half, but we feel that significantly larger errors are unlikely.

3.5 Results

3.5.1 Radar-derived accumulation measurements

The 1985–2009 mean annual accumulation derived from the accumulation and snow radars are shown in Figure 3.6a, which includes the bias corrected rates. The nearly 20,000

accumulation measurements span an entire order of magnitude ranging from 0.132 to 1.374 m w.e. yr^{-1} and have a mean (± standard deviation) of 0.409 ± 0.116 m w.e. yr^{-1}. The more than 6,300 measurements within Pine Island vary from 0.177 to 1.374 m w.e. yr^{-1} with a mean of 0.431 ± 0.145 m w.e. yr^{-1}, and the 11,400 within Thwaites vary from 0.209 to 0.841 m w.e. yr^{-1} with a mean of 0.421 ± 0.080 m w.e. yr^{-1}. Rates exceeding 1.0 m w.e. yr^{-1} are found along coastal Pine Island glacier and in isolated depressions. Rates below 0.2 m w.e. yr^{-1} are found on bumps alongside the depressions as well as across the Thwaites southern divide toward WAIS and Byrd camps. The several measurements (n =1568) outside the Pine Island-Thwaites catchment area are used in the OLS regression and interpolation. The average 1σ measurement errors for Pine Island and Thwaites are 0.025 and 0.017 m w.e. yr^{-1} respectively. While the minimum error in each catchment is the same (0.007 m w.e. yr^{-1}), the maximum is much greater over Pine Island (0.171 m w.e. yr^{-1}) than over Thwaites (0.035 m w.e. yr^{-1}), which is due to the larger accumulation rates and the bias correction within Pine Island.

The radar-derived accumulation rates (± 1σ error) at the PIG2010, DIV2010, and THW2010 sites are 0.425 ± 0.019, 0.406 ± 0.019, and 0.292 ± 0.014 m w.e. yr^{-1}, respectively, which match those derived from the core records shown in Table 3.1 (0.424, 0.412, and 0.286 m w.e. yr^{-1}). The nearly identical measurements at the PIG2010 site is not surprising as the core's depth-age scale was used to determine horizon ages and its density profile was one of nine used to determine a regional profile. The only information used from the DIV2010 and THW2010 cores was their density profiles, meaning the radar-derived measurements at these cores are largely independent of the core-derived accumulation rates. At both sites, the core measurements fall within the radar-derived error interval.

3.5.2 Gridded accumulation rates

Not surprisingly, the OLS accumulation rate surface (Figure 3.7a) shows elevated accumulation at low elevations that diminish moving inland towards high elevations. While the general structure is correct, there are several moderate-scale (25 to 50 km) features that cannot be reproduced with the simple OLS model, which is clearly apparent when comparing the OLS model (Figure 3.7a) with the smoothed measurements (Figure 3.6b). The final gridded accumulation map (Figure 3.7b reproduces both the regional and moderate-scale features observed in the measurements and will provide the snow input values for our mass balance estimates.

The average (± standard deviation) gridded accumulation rates over Pine Island and Thwaites glaciers are 0.40 ± 0.13 and 0.43 ± 0.09 m w.e. yr^{-1}, values similar to those from the radar-derived measurements (Table 3.2). The accumulation grid errors range from 2.6 to 32.7% with an average of 8.6%. Nearly 90% of the cells have errors less than 15% (Figure 3.7c). Maximum errors are found over the southern Pine Island catchment where the accumulation rates are very low and the radar coverage is sparse. The lowest errors are in central Thwaites where multiple overlapping flight paths provide better spatial coverage.

We compared several core-derived accumulation rate averages from within the Pine Island-Thwaites drainage system to their coincident gridded estimate. Specifically, we used the ITASE 01-1, 01-2, 01-3, and 01-6 average rates between 1985 and 2001 and the PIG2010, DIV2010, and THW2010 average rates between 1985 and 2009. At five of the seven sites, the average rate falls within the 1σ grid error. The other two sites (ITASE 01-3 and PIG2010), which interestingly are separated by only 20 km, fall within the 2σ error. Even though the grid has been smoothed removing small-scale accumulation features, it still

matches isolated core measurements very well. Therefore, we are confident that our gridded accumulation rates and errors are reasonable.

3.5.3 Accumulation distribution by elevation

We next investigate the elevation-dependent accumulation distribution for Pine Island (Figure 3.8) and Thwaites (Figure 3.9) by binning their accumulation grids over 100 m intervals. The average accumulation rates over both glaciers decrease rather consistently with increasing elevation, but the average rate over a given elevation bin is larger for Thwaites than for Pine Island. Due hypsometric differences, the elevations that contribute the most total snow accumulation fall between 700 and 1500 m within Pine Island and between 1200 and 1900 m within Thwaites. Totals of 67.3 ± 6.1 and 75.9 ± 5.2 Gt yr^{-1} fell on average between 1985 and 2009 over Pine Island and Thwaites, respectively, and 158.5 ± 12.5 Gt yr^{-1} fell over the entire region (Table 3.3). We assumed the gridded errors were not independent, and as a result, the errors were calculated by cell-by-cell summation (not RSS) of the grid errors. Therefore, the error bounds are likely a conservative estimate.

3.5.4 Comparison with climatologies and atmospheric models

The elevation-dependent accumulation distributions for various accumulation climatologies, reanalysis products, and a regional climate model output were also analyzed and compared. The three climatologies are van de Berg et al. [2005] , Arthern et al. [2006] , and Monaghan et al. [2006] , which are henceforth referred to as VDB05, ART06, and MON06 and are representative of the long-term accumulation rate in this region. The three global reanalysis precipitation-minus-sublimation (*P*-*S*) products include the European Centre for Medium-Range Weather Forecasts “Interim” (ERA-Interim) [*Dee et al.*, 2011] ,

the NASA Modern Era Retrospective Analysis for Research and Applications (MERRA) [*Rienecker et al.,* 2011] , and the National Centers for Environmental Prediction Climate Forecast System Reanalysis (CFSR) [*Saha et al.,* 2010] . Finally, we use surface mass balance from the Regional Atmospheric Climate Model v2.1 (RACMO2) that is forced laterally with ERA-Interim (Figure 3.7d) [*Lenaerts et al.,* 2012] . Even though these products do not all estimate precisely the same variable (i.e., accumulation, SMB, or *P-S*), they are all nearly equivalent to snow accumulation in this region [*Medley et al.,* 2013] . To ensure consistency, all grids were bilinearly resampled to the same 3 km grid and were binned as explained above (Figures 3.8 & 3.9). At high elevations nearly all the accumulation products underestimate the average accumulation rate over both glaciers. For Thwaites, with the exception of ART06 all products have higher accumulation rates than our grid at low elevations. Because our grid is not based on measurements below 800 m from Thwaites, we cannot confidently determine whether the products are indeed overestimating accumulation; however, they appear to overestimate accumulation between 800 and 1200 m. For Pine Island, a range of differences does occur at the low elevations: some overestimate, some underestimate, and others fall within our grid values. In general, these accumulation products (except ART06) have steeper elevation-dependent accumulation gradients than our grid.

The largest spread in average accumulation between these products occurs at the lowest elevations (below ~ 600m), but these elevations occupy a relatively small area and thus do not contribute substantially to the spread in the cumulative accumulation rates (Figures 3.8b & 3.9b). With the exception of MON06 and MERRA, the products fall within the error range of the total cumulative accumulation rate for Pine Island, albeit towards the

low end (Figure 3.8c). Only CFSR, RACMO2, and VDB05 fall within this range for Thwaites where the spread is much larger (Figure 3.9c). Although several of these products generate values similar to our grid (Table 3.3), it is often the result of low-elevation regions of overestimation balancing high-elevation regions of underestimation, which is most apparent in Figures 3.8b and 3.9b.

3.5.5 Ice discharge

The total flux of ice lost to the ocean from this region increased from 192.7 ± 5.3 Gt yr^{-1} in the mid-1990s to 254.1 ± 4.3 Gt yr^{-1} in 2010, which is a more than 30% increase over ~15 years and is consistent with earlier estimates [*Rignot,* 2008] . Over the same interval, the discharge from Pine Island alone increased more than 50% whereas Thwaites increased just under 20%. Although between the mid-90s and mid-00s only a few data points exist, this is likely the period over which the discharge increased substantially and was followed by a period of relatively steady flow between 2008 and 2010 for Thwaites and between 2008 and 2012 for Pine Island (Table 3.4). From the mid-1990s to 2010, the Wedge only increased discharge by 9%, but Haynes increased by more than 20% and Thwaites East by 50%.

3.5.6 Mass balance

The mass imbalance of Pine Island-Thwaites drainage system nearly tripled between the mid-1990s and 2010, changing from -34.1 ± 13.6 to -96.1 ± 13.2 Gt yr-1, values which correspond to +0.09 ± 0.04 and +0.27 ± 0.04 mm SLR yr-1 (Table 3.5). During the mid-1990s, Pine Island was slightly negative (-5.7 ± 6.3 Gt yr-1) with errors large enough to suggest these values were likely not different from zero (i.e., Pine Island was at or near balance). Thwaites, Thwaites East, and Haynes showed imbalances that were all

substantially less than zero. Thwaites glacier was furthest out of balance at -17.3 ± 6.9 Gt yr-1 followed by Haynes at -8.3 ± 1.3 Gt yr-1. By 2010, Pine Island had become significantly out of balance, losing 43.0 ± 6.9 Gt yr-1 and overtaking Thwaites (-35.7 ± 5.6 Gt yr-1) as the largest contributor to SLR. Thwaites East and Haynes mass balances decreased as well, but the Wedge remained essentially in balance.

3.6 Discussion

The more than 20,000 radar-derived accumulation measurements reveal both regional and local features that were not uncovered using the existing ice-core measurements alone. The ice cores remain instrumental to our work, however, because they provide the depth-age scale necessary to date the radar horizons from the accumulation radar. Tracking the horizons over 100s of kilometers proved successful except over a few areas. Notably, horizons disappeared travelling from the PIG2010 site northward while entering the area of enhanced ice flow and rougher surface undulations around the Pine Island trunk. Additionally, we were unable to differentiate with confidence between horizons moving westward from WAIS to Byrd because the accumulation rate is substantially lower at Byrd, resulting in the merging of horizons. The areas of more extreme surface undulations, as indicated by the tonal differences in the basemap in Figure 3.1, often coincide with data gaps where the horizons could not be tracked. Nonetheless, we were able to track horizons over the majority of the Pine Island-Thwaites drainage system and over a wide range of elevations and accumulation rates. Outside of regions with large accumulation gradients, the accumulation radar likely should image continuous and discretely trackable horizons that when combined with ice cores and a well-defined survey, will provide catchment-wide accumulation measurements elsewhere in Antarctica.

Because of the smoothing of the raw accumulation measurements and grid filtering, our map contains moderate- to large-scale accumulation features with scales on the order of 25 km or greater. Smaller-scale (< 25 km) features certainly exist as evidenced in the echograms and raw accumulation measurements, but a denser survey network would be required to capture these features over the large catchment areas and was not feasible. If we consider the small-scale features as high-frequency noise, our catchment-wide accumulation measurements are not negatively impacted. Because of the moderate-scale data resolution (~25 km), we do not expect ice core accumulation measurements to match the coincident grid accumulation with high fidelity. For example, the PIG2010 core site is clearly located in a minor depression where accumulation rates are enhanced relative to the background (Figure 3.4) and is one of the cores with the greatest mismatch from our grid. At same time, majority of the cores fall within the ±1 σ grid error; thus, our final accumulation grid is a good representation of the moderate-scale accumulation rate with errors suitably large to encompass any smaller-scale features not resolved.

Beyond determining catchment-wide accumulation, our grid provides the means with which to test various climatologies, reanalyses, and climate models abilities to reproduce the accumulation rate over a large area. Rather than comparing the models to isolated point measurements of accumulation, which do not make for equal comparison with large grid cell values, our grid is of comparable data resolution (i.e., is more representative of the scales resolved by the models). A consistent feature amongst the reanalysis and climate models is the underestimation of accumulation in the high elevation, low accumulation interior. Our measurements suggest overestimation in the low elevation, high accumulation coastal areas even though we lack radar measurements below 500 m; however, for mass balance purposes

the discrepancy is not nearly as important as in the interior because the low elevations cover relatively small areas in our study area. Additional accumulation measurements from lower elevations are necessary before we can confidently quantify the models' discrepancies. Nevertheless, RACMO2 and CFSR are able to generate catchment-scale accumulation rates that fall within our grid error bounds for both Pine Island and Thwaites.

When considering the ability of the climatologies it is important to understand how each was created. ART06 was generated using field-based measurements of snow accumulation, which were gridded using remotely sensed microwave emission data to guide the interpolation. Therefore, it is not surprising that it performs poorly at the low-elevation, high-accumulation areas where few measurements exist. The fact that ART06's performance is worse over Thwaites is likely due to the presence of fewer *in situ* measurements over Thwaites than over Pine Island. The MON06 mean annual (1979−2002) simulated precipitation-minus-sublimation estimate is derived from the Polar MM5 atmospheric model. While the model long-term averages matched continent-wide ice core observations satisfactorily, the model shows overestimation relative to cores from West Antarctica [*Monaghan et al.,* 2006] , which might explain the very high accumulation rates shown here. Finally, VDB05 is the 1958−2002 mean annual simulated surface mass balance from RACMO2 forced laterally by ERA-40 with a horizontal resolution of ~55 km. Although van de Berg *et al.* [2005] explained that the model appeared to underestimate accumulation in the interior and overestimate it on the coastal slopes, we find that at least in these basins the picture is not as clear: VDB06 performs better over coastal Pine Island rather than Thwaites and over inland Thwaites rather than Pine Island. When both glaciers are combined, VDB06 performs well at all elevations.

From a catchment-wide perspective, RACMO2, CFSR, and VDB05 perform well, but this might not directly translate to other areas of the ice sheet. For example, ART06 performs well over Pine Island but poorly over Thwaites. Consideration of the catchment hypsometry could potentially aid accumulation product selection: RACMO2, CFSR, and VDB05 might perform well over catchments with similar hyspometries as Pine Island and Thwaites. Obviously, the atmospheric models might perform better or worse in areas with different atmospheric dynamics regardless of topography. The performance of the measurement-based ART06 should depend on the local density of *in situ* measurements as well.

Although accumulation varies on a year-to-year basis, because no recent (1980−2009) trend in accumulation was found by *Medley et al.* [2013] over Thwaites, our 1985–2009 mean annual accumulation should adequately represent the net snowfall input for our mass balance estimates. Ice discharge, on the other hand, shows a strong negative trend and was thus measured over multiple years. The ice discharge measurements presented here are in excellent agreement with those from *Rignot* [2008], showing a strong increase from Pine Island and a moderate increase from Thwaites between the mid-1990s and 2007. The additional values presented in this study from 2008 to 2012 indicate that the increasing trends have not continued for both glaciers and that ice discharge has, for the time being, leveled off. While Thwaites had the largest mass imbalance between 1994 and 1998, the mass loss from Pine Island overtook that from Thwaites by 2006, making Pine Island the largest contributor to SLR from the region. Haynes, a relatively small glacier, shows large mass losses, which are likely an upper bound because the accumulation rates from this sector could be biased low. Nevertheless, Haynes would still show mass losses over the entire period even if we

doubled our accumulation rates over the entire glacier. The same is true of Thwaites East but due to its small size, the imbalance is not as large. The Wedge between Pine Island and Thwaites is relatively stable and in balance, receiving some of the highest accumulation rates in the region. While Thwaites East and Haynes mass losses are dwarfed by those from Pine Island and Thwaites, their ice discharges have increased substantially since the mid-1990s (50% and 22%, respectively). If the increases continue into the future, these small glaciers are likely to have a relatively large impact on SLR.

In total, the region receives on average 158.5 ± 12.5 Gt yr^{-1} of snow accumulation at an average accumulation rate of 0.43 m w.e. yr^{-1}. Between 1994 and 1998, total ice discharge was 192.7 ± 5.3 Gt yr^{-1} resulting in a mass change of -34.1 ± 13.6 Gt yr^{-1}. By 2010, ice discharge increased substantially to 254.1 ± 4.3 Gt yr^{-1} yielding a much larger mass change of -96.1 ± 13.2 Gt yr^{-1}. These mass imbalances translate into rates of SLR of 0.09 ± 0.04 and 0.27 ± 0.04 mm yr^{-1}. To compare with the recent ice-sheet mass balance inter-comparison exercise (IMBIE) [*Shepherd et al.*, 2012] , which assessed the mass balance of Greenland and Antarctica from 1992 to 2011, we make the following assumptions about our discharge history: (1) the ice discharge from 1992 to 1998 is constant and equal to our 1994−1998 measurement; and (2) in subsequent years, the discharge steps up or down at the beginning of the next measurement interval. For example, the Thwaites discharge is set to 93.2 ± 4.6 Gt yr^{-1} from 1992 to 2005 and jumps to 104.3 ± 2.4 Gt yr^{-1} in 2006. These assumptions result in a conservatively low estimate of the 1992−2011 ice discharge because we assume all changes occur instantaneously. Subtracting the mean ice discharge over the entire record from our catchment-wide accumulation rates provides the 1992−2011 mean mass balances, which are -19.4 ± 6.1 Gt yr^{-1} and -22.0 ± 5.3 Gt yr^{-1} for Pine Island and

Thwaites respectively. These measurements match the IMBIE estimates well for Pine Island, but our estimate for Thwaites is on the more negative end of the IMBIE range. As a result, we have Thwaites more negative on average than Pine Island, which is reversed relative to the IMBIE measurements. This discrepancy could be the result of difference catchment boundaries. Our results indicate the region as a whole has contributed 3 mm to SLR over the 1992−2011 period, which amounts to 25% of the total contribution to SLR of 11.2 mm from both Greenland and Antarctica as determined by IMBIE.

3.7 Conclusions

We find that an appropriately designed accumulation radar survey combined with glaciochemical analysis of one or more ice cores provides ample means to generate catchment-wide accumulation map that resolves moderate- to large-scale features. Our results indicate that various climatologies and reanalysis and climate models underestimate accumulation in the high elevation interior while potentially overestimating it in the low elevation coastal areas. These discrepancies often balance each other, resulting in catchment-wide accumulation values similar to our grid. Between the mid-1990s and 2010, the mass balance of the region decreased from -34.1 ± 13.6 Gt yr^{-1} to -96.1 ± 13.2 Gt yr^{-1}, a near tripling of its imbalance and associated contribution to SLR. While Pine Island overtook Thwaites as the largest contributor to SLR in 2006, Thwaites showed greater mass loss on average between 1992 and 2011. Although the glaciers experienced a substantial increase in ice discharge between the mid-1990s and 2008, subsequent measurements indicate discharge from these glaciers has leveled off for the time being.

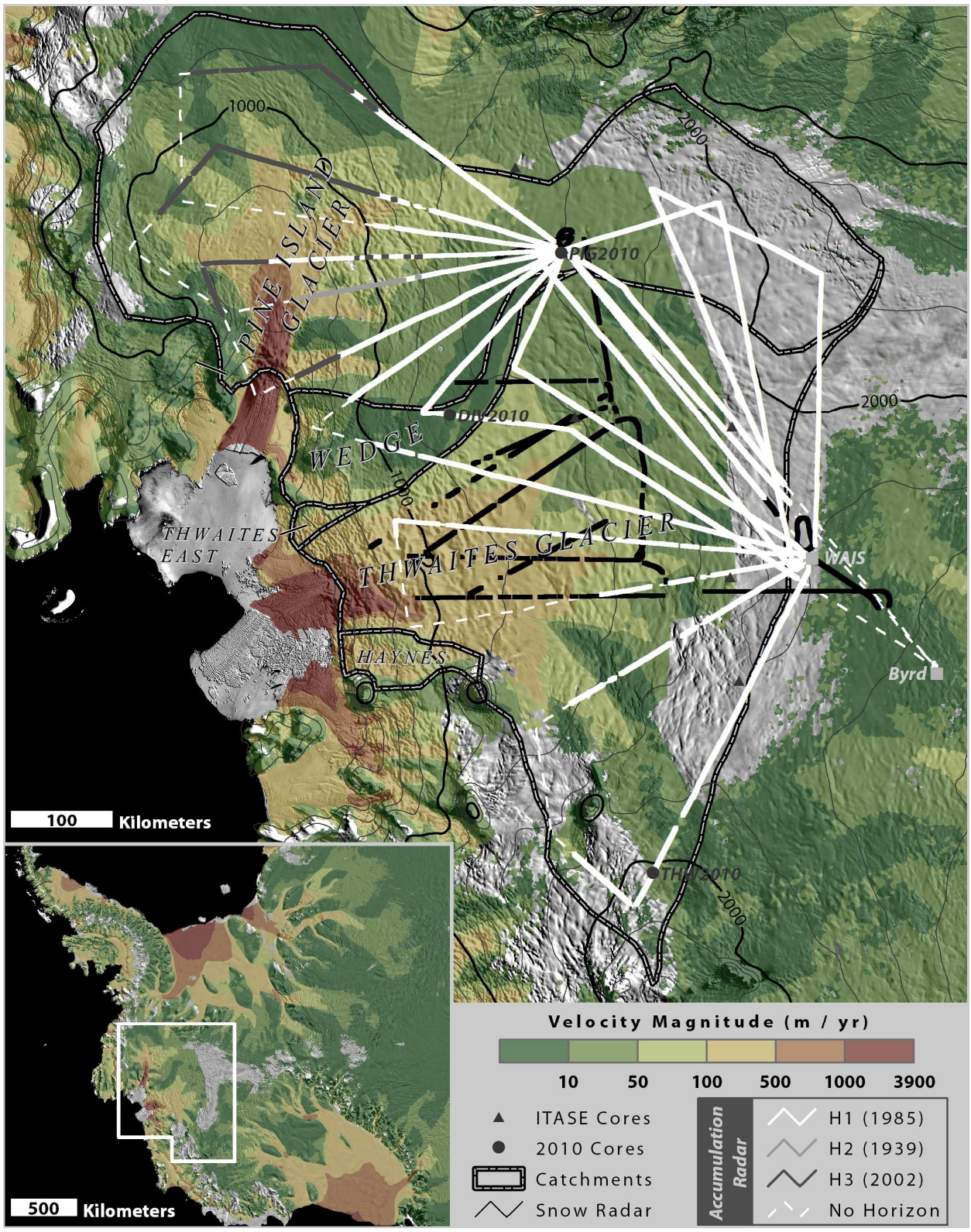
1000
2000
PIG 2010
PINE ISLAND GLACIER
DIV 2010
WEDGE
2000
THWAITES EAST
THWAITES GLACIER
WAIS
HAYNES
Byrd
100 Kilometers
THW 2010
2000
500 Kilometers
Velocity Magnitude (m / yr)
10
50
100
500
1000
3900
ITASE Cores
2010 Cores
Catchments
Snow Radar
Accumulation Radar
H1 (1985)
H2 (1939)
H3 (2002)
No Horizon

Figure 3.1 – The Amundsen Coast glaciers and locations of the radar flight surveys. Here, the MODIS mosaic is overlaid transparently by measured ice velocities from Joughin *et al.* [2010] and elevation contours (200 m intervals). The catchments are outlined and labeled. The complete accumulation radar survey consists of the white and grey lines. A dashed white line indicates no horizon was mapped, a solid white line indicates H1 was mapped, and light (dark) grey indicates that H2 (H3) was mapped. The solid black lines show where accumulation measurements were taken from Medley *et al.* [2013]. The three 2010 ice cores are labeled and indicated by a grey circle. The ITASE cores are displayed as grey triangles, and the WAIS divide and Byrd camps are labeled and indicated by light grey squares. The inset map shows the location of our study area.

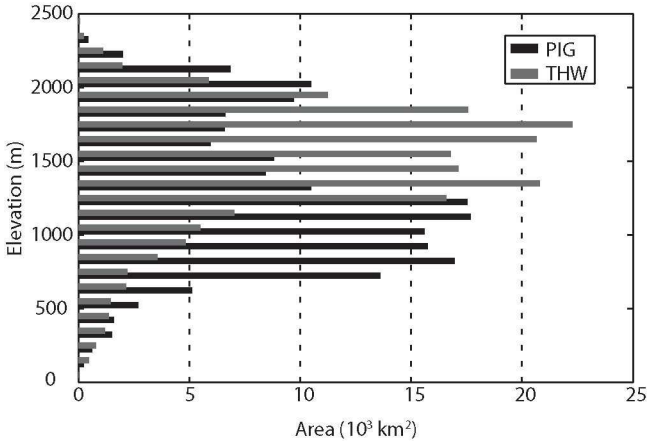

Figure 3.2 – The hypsometric distributions of the Pine Island and Thwaites catchments. The sub-basins included in PIG are Pine Island and the Wedge and in THW are Thwaites, Thwaites East, and Haynes. The median elevations within the PIG and THW are 1210 m asl and 1540 m asl, respectively.

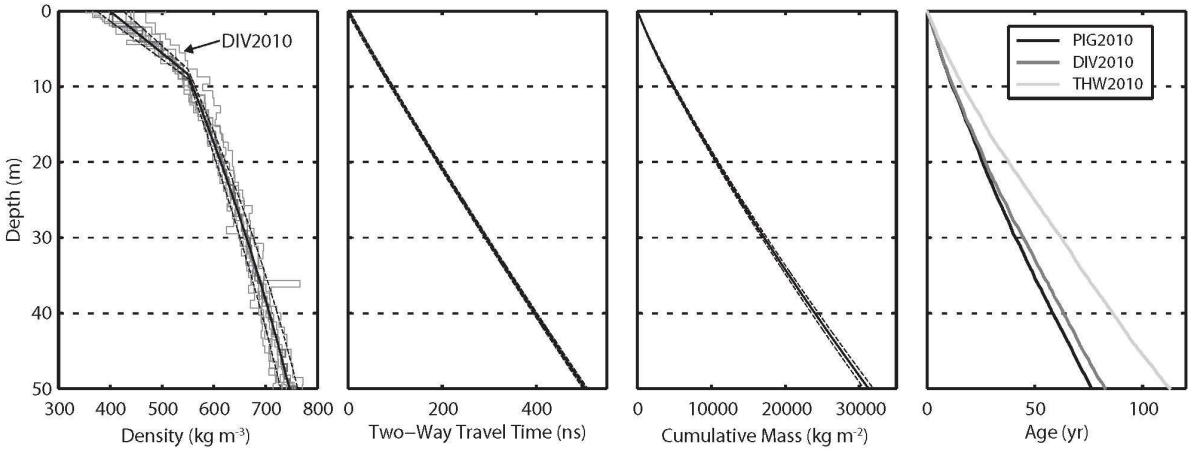

Figure 3.3 – Profiles of (a) density, (b) two-way travel time, (c) cumulative mass, and (d) age with depth. a) The density profiles from nine firn cores from the region are plotted in light grey and the model fit to their mean is shown as a solid black line. The dashed black lines show ± 1 standard deviation from the mean. b) The solid line was produced using the formula, $d = 0.5c\tau\varepsilon - 0.5$, for conversion between two-way travel time and depth using the density model in (a), and the dashed lines were generated from the deviations in (a). c) The cumulative mass profiles were created by integrating the mean (solid) density profile with depth as well as the deviations (dashed) from (a). d) The depth-age profiles for the three 2010 cores determined from glaciochemical analysis.

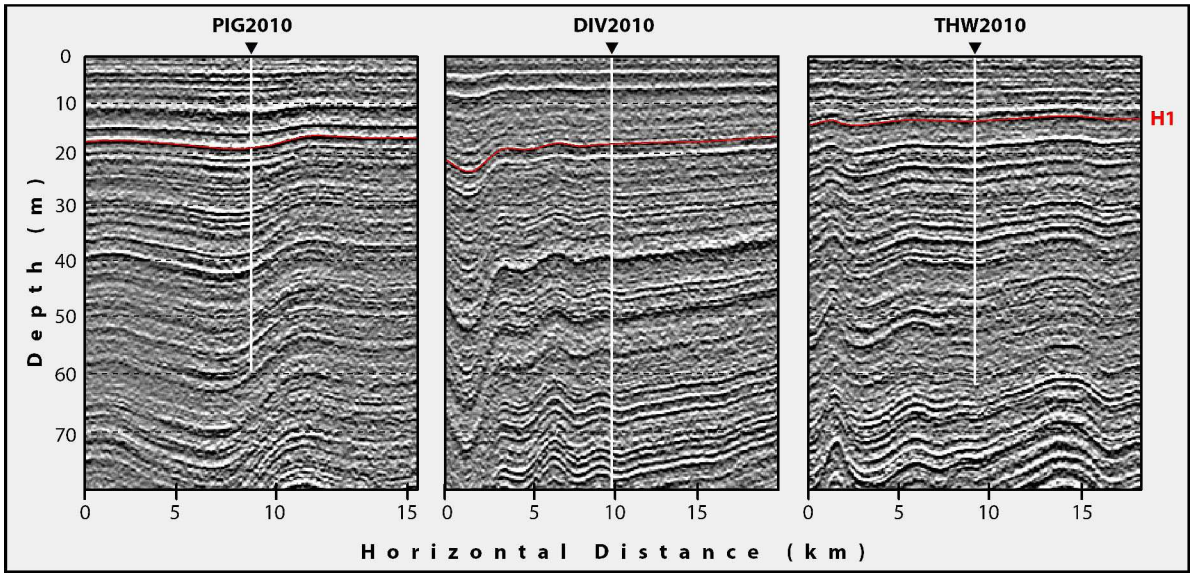

Figure 3.4 – Echograms at each 2010 core site and the tracked H1 horizon. From left to right, we display the echograms from the PIG2010, DIV2010, and THW2010 sites along with H1 mapped in red. The vertical white line shows the location closest to the each core, which extends from the surface to the actual recovery depth.

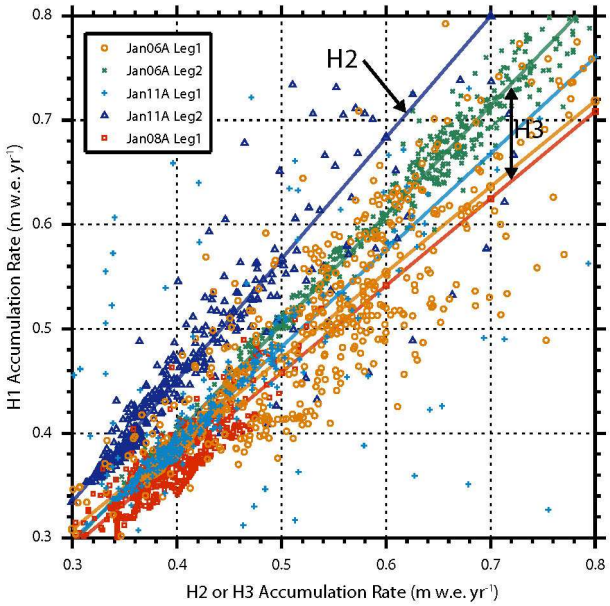

Figure 3.5 – Bias correction regression models for five survey legs where an alternate horizon was used to measure accumulation. Using a robust regression model, we correct accumulation measurements derived from the alternate horizon (either H2 or H3) to more appropriately represent its H1 measurement where both horizons were coincidently tracked. The relationship was then applied to the measurements derived from the alternate horizons where H1 was not tracked. Four of the corrections use the same alternate horizon H3, whereas one leg uses H2. Interestingly, H2 dates to 1939 and the resulting accumulation rates are found to be much lower than those from H1 (i.e., the regression model lies well above the 1:1 line). This result is consistent with ice core observations that recent accumulation has increased relative to the long-term mean. Corrections for measurements derived from H3 (2002) are much hover around the 1:1 line, especially in the areas of the majority of the measurements (0.3–0.5 m w.e. yr^{-1}).

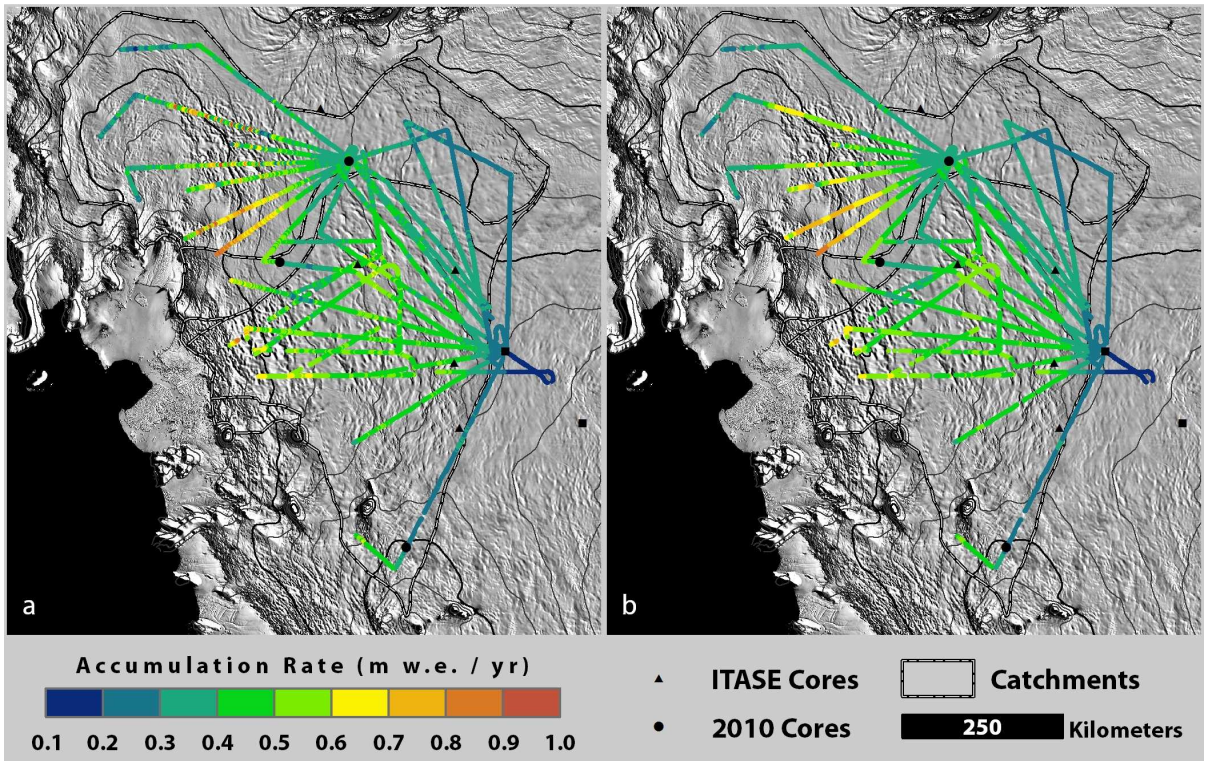

Figure 3.6 – The (a) raw and (b) smoothed radar-derived accumulation rates. a) The raw accumulation rates derived from the accumulation radar, including the bias corrected rates as well as the 1985−2009 mean annual accumulation from the snow radar. b) Same as from (a) except a 25-km (tapered to 5-km approaching the ends) running average has been applied.

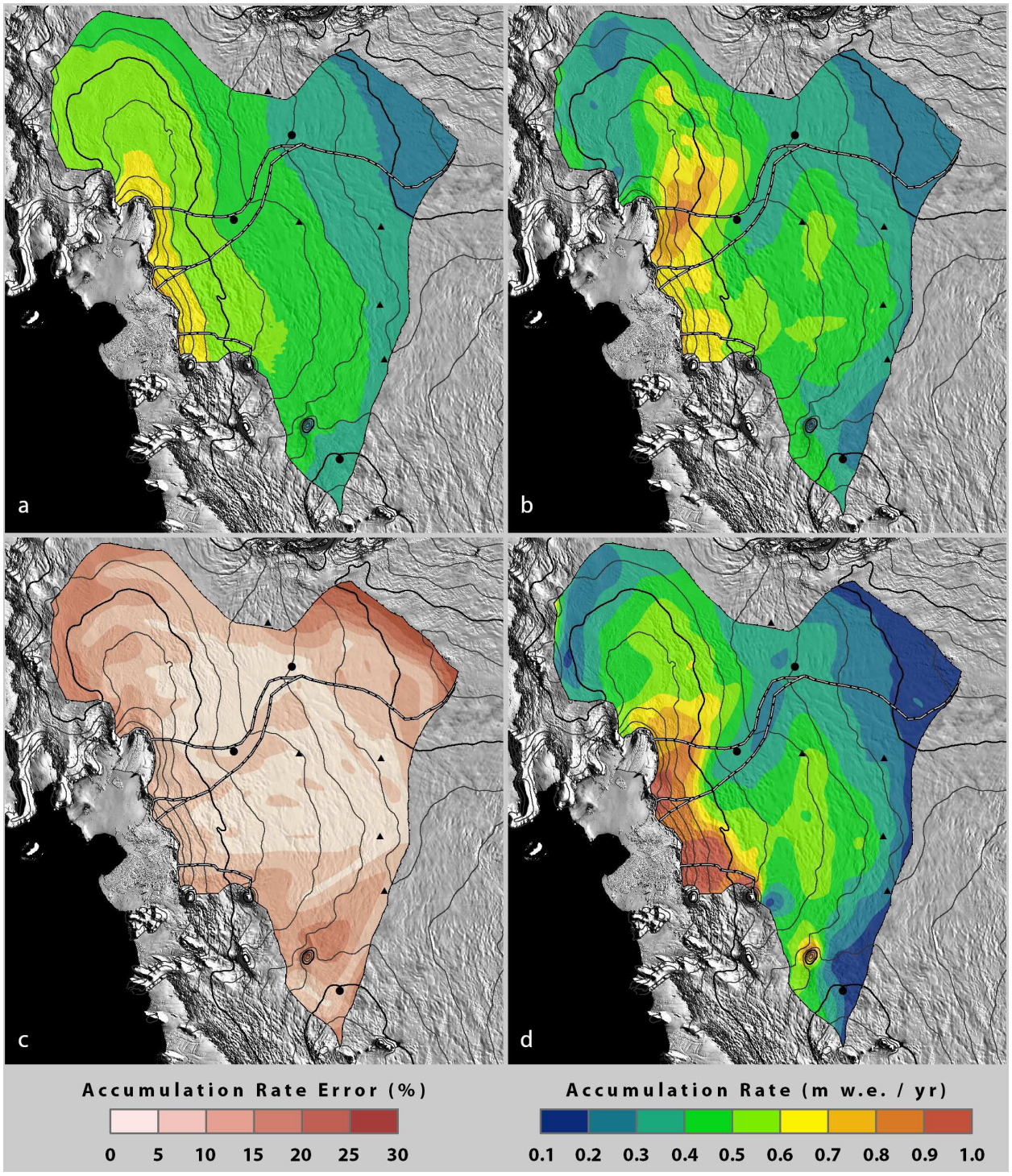
a
b
c
d
Accumulation Rate Error (%)
0 5 10 15 20 25 30
Accumulation Rate (m w.e. / yr)
0.1 0.2 0.3 0.4 0.5 0.6 0.7 0.8 0.9 1.0

Figure 3.7 – The (a) OLS linear regression model accumulation surface, (b) final accumulation grid, (c) accumulation error grid, and (d) 1985−2009 average surface mass balance from RACMO2. a) The accumulation surface derived from an OLS linear regression model with northing, easting, and elevation as dependent variables. b) Our final accumulation surface derived by adding the kriged OLS model residuals to the OLS regression surface from (a). c) The combined measurement and interpolation errors displayed as a percentage of our gridded accumulation map shown in (b). d) The 1985−2009 average surface mass balance from RACMO2, widely used in mass balance studies, is shown for comparison to our gridded map in (b).

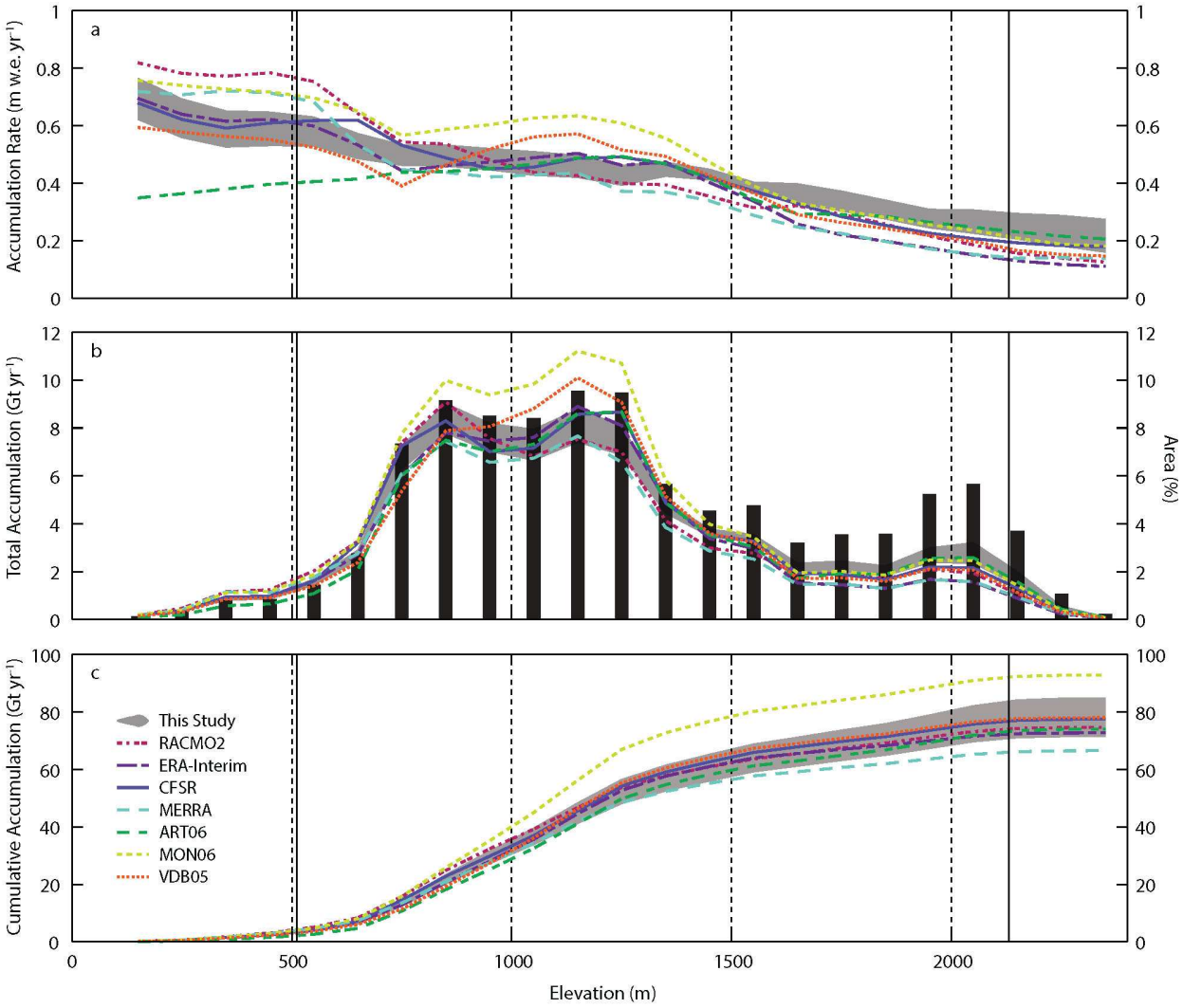
a
b
c
Accumulation Rate (m w.e. yr⁻¹)
Total Accumulation (Gt yr⁻¹)
Cumulative Accumulation (Gt yr⁻¹)
Area (%)
Elevation (m)
This Study
RACMO2
ERA-Interim
CFSR
MERRA
ART06
MON06
VDB05

Figure 3.8 – The elevation-dependent accumulation distribution for Pine Island glacier (including the Wedge) and comparison with climatologies and reanalysis and climate models. For each part, the grey shaded area shows the quantity of interest from our final accumulation grid including its $\pm 1\sigma$ deviation. The climatologies and reanalysis and climate models do not have errors because the products do not provide error grids. The three part figure shows: a) the average accumulation rates over 100 m elevation bins, b) the bin-summed accumulation rates scaled by the cell size of 9 km^2 with bars representing the bin size, and c) the cumulative bin-summed accumulation rates from (b). The solid vertical black lines on each plot display the elevation limits of our radar-derived accumulation measurements, and thus bound the area with high data integrity.

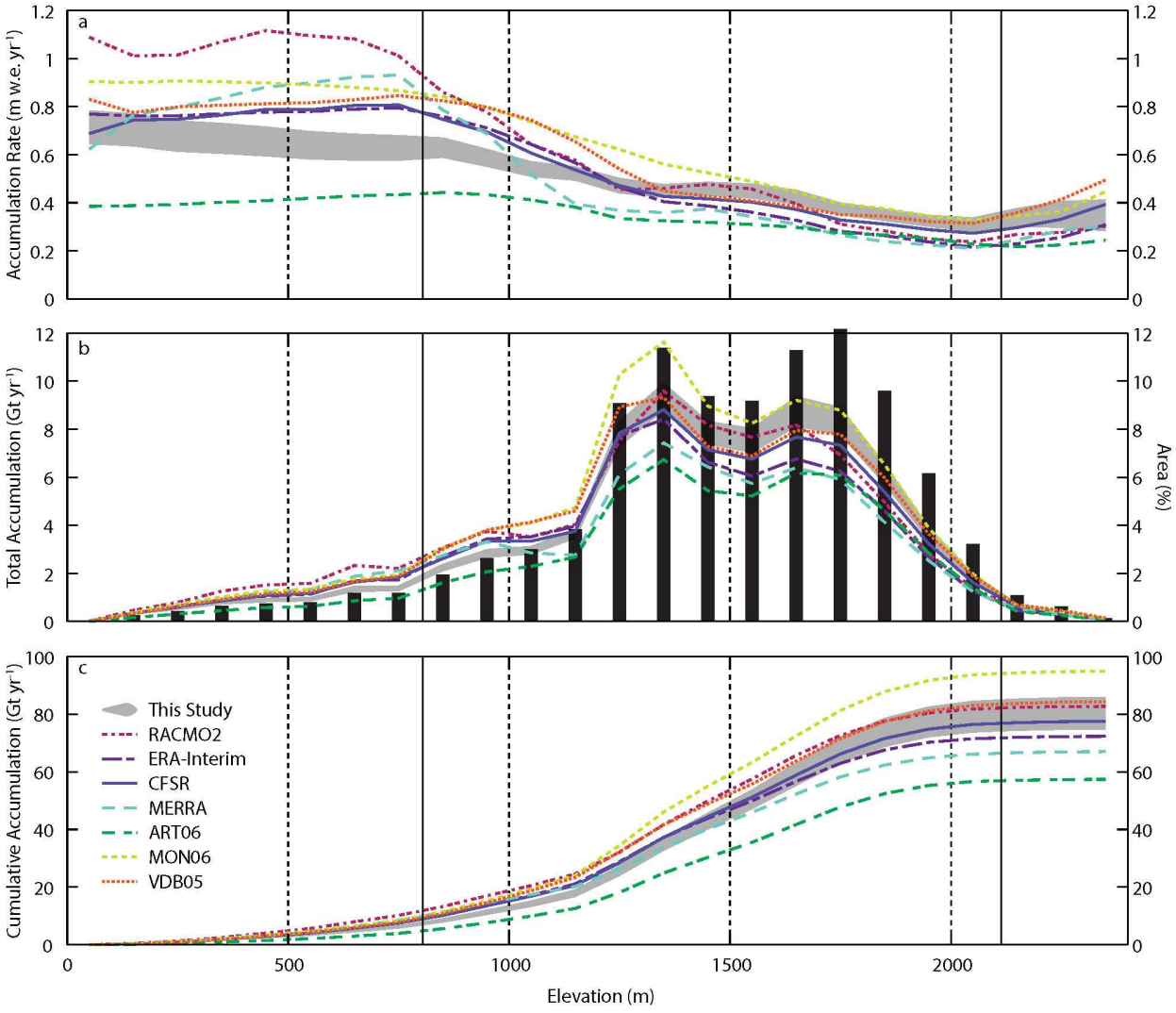

Figure 3.9 – Same as Figure 3.8 but for Thwaites glacier (including Thwaites East and Haynes).

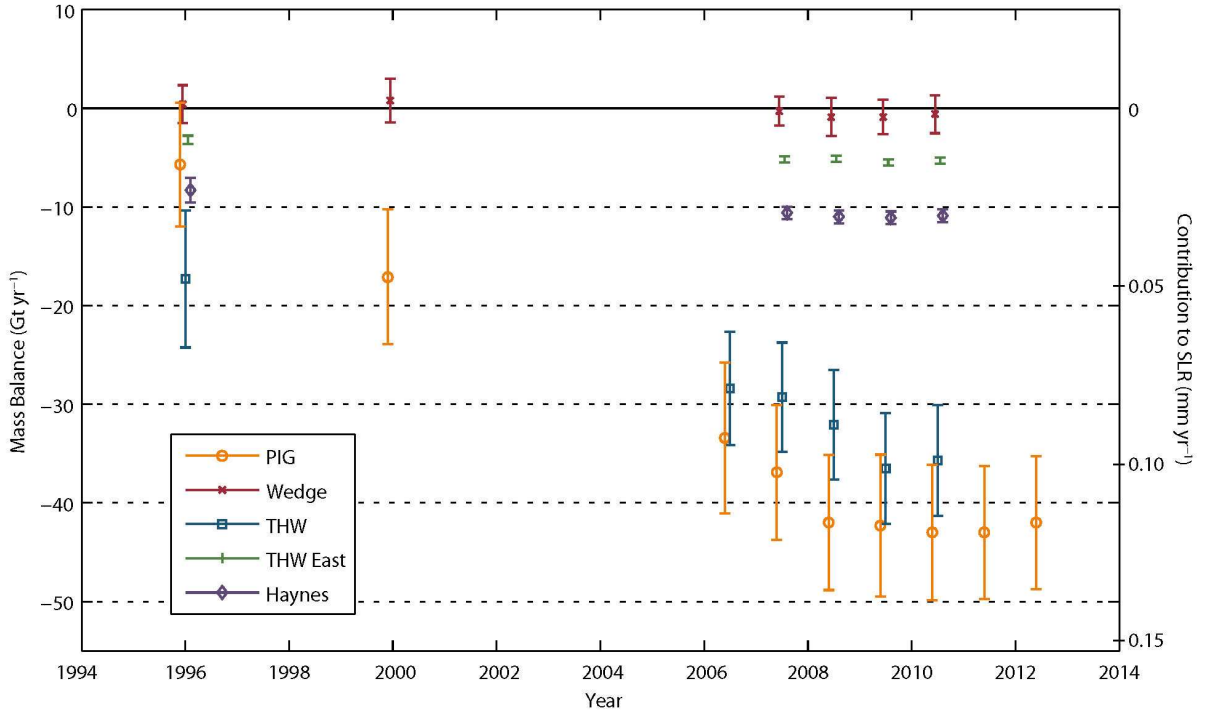

Figure 3.10 – Mass balance history from 1994 to 2012 for each catchment. The mass balance was measured by subtracting the ice discharge measurements from various time intervals from Table 3.4 from the 1985−2009 mean catchment-wide snowfall from Table 3.3. The actual mass balance values are listed in Table 3.5. The points are offset slightly for clarity and do not represent actual differences in the data collection period.

Table 3.1 – Summary of ice-core accumulation records

Name	Latitude (°)	Longitude (°)	Elevation (m)	Velocity (m / yr)	Bottom Depth (m)	Time Interval	Accumulation Rate (m w.e. / yr)[a]		
							1920-2000	1970-2000	1985-2009
PIG2010	-77.96	-95.96	1590	27.5	59.4	1917–2010	0.40 ± 0.06	0.43 ± 0.06	0.42 ± 0.07
DIV2010	-76.77	-101.74	1330	4.6	111.7	1786–2010	0.39 ± 0.07	0.41 ± 0.07	0.41 ± 0.07
THW2010	-76.95	-121.22	2020	5.5	61.8	1867–2010	0.28 ± 0.04	0.28 ± 0.05	0.29 ± 0.05

[a]Values represent the $\mu \pm 1\ \sigma$

Table 3.2 – Catchment average (μ), standard deviation (σ), minimum, and maximum gridded accumulation rates and errors

	Accumulation Rate (m w.e. yr^{-1})				Error (%)			
Glacier	μ	σ	min	max	μ	σ	min	max
Pine Island	0.40	0.13	0.21	0.84	10.4	6.1	2.6	30.0
Wedge	0.59	0.16	0.33	0.84	6.3	1.8	2.9	10.8
Thwaites	0.43	0.09	0.17	0.72	7.1	3.9	2.6	32.7
Thwaites East	0.67	0.02	0.64	0.71	9.4	0.6	7.5	10.0
Haynes	0.63	0.06	0.21	0.74	10.6	1.0	8.6	32.7
Total	0.43	0.12	0.17	0.84	8.6	5.2	2.6	32.7

Table 3.3 – Catchment-wide accumulation from this work, compared to climatologies, reanalysis products, and a regional climate model

Table 3. Catchment-wide snowfall from climatologies, reanalysis products, and a climate model compared to this study

		Snowfall (Gt yr^{-1})							
Glacier	Area (10^3 km^2)	This Study	RACM02	ERA-Interim	CFSR	MERRA	ART06	MON06	VDB05
Pine Island	166.8	67.3 ± 6.1	63.3	60.4	65.8	55.4	65.8	79.4	66.6
Wedge	18.6	11.0 ± 0.7	11.1	12.4	11.7	11.0	8.2	13.4	11.4
Thwaites	175.9	75.9 ± 5.2	74.6	66.9	71.8	61.0	54.5	89.0	78.6
Thwaites East	1.4	1.0 ± 0.1	1.3	1.1	1.1	1.1	0.6	1.3	1.1
Haynes	5.5	3.4 ± 0.4	6.3	4.4	4.6	4.9	2.2	4.6	4.7
Total	368.2	158.5 ± 12.5	156.6	145.2	155.0	133.4	131.3	187.7	162.4

Table 3.4 – Flux-gate discharge measurements and errors from 1994 to 2012

	Ice Discharge (Gt yr^{-1})								
Glacier	Jan 94 – Jan 98	Jun 99 – Jun 00	May 06 – Nov 06	Sep 07 – Dec 07	Sep 08 – Dec 08	Sep 09 – Dec 09	Sep 10 – Dec 10	Oct 11 – Nov 11	Jul 12 – Aug 12
Pine Island	73.0 ± 1.5	84.4 ± 3.1	100.7 ± 4.6	104.2 ± 3.1	109.3 ± 3.1	109.6 ± 3.8	110.3 ± 3.2	110.3 ± 2.9	109.3 ± 2.8
Wedge	10.6 ± 1.8	10.2 ± 2.1		11.3 ± 1.3	11.9 ± 1.8	11.9 ± 1.6	11.6 ± 1.8		
Thwaites	93.2 ± 4.6		104.3 ± 2.4	105.2 ± 1.9	108.0 ± 2.0	112.4 ± 2.1	111.6 ± 2.1		
Thwaites East	4.2 ± 0.4			6.2 ± 0.3	6.1 ± 0.3	6.5 ± 0.3	6.3 ± 0.3		
Haynes	11.7 ± 1.2			14.0 ± 0.5	14.4 ± 0.5	14.5 ± 0.5	14.3 ± 0.5		
Total	192.7 ± 5.3			240.9 ± 3.9	249.7 ± 4.1	254.9 ± 4.7	254.1 ± 4.3		

Table 3.5 – Mass balance measurements and errors from 1994 to 2012.

Table 5. Mass balance measurements and errors from 1994 to 2012

	Mass Balance (Gt yr^{-1})								
Glacier	Jan 94 – Jan 98	Jun 99 – Jun 00	May 06 – Nov 06	Sep 07 – Dec 07	Sep 08 – Dec 08	Sep 09 – Dec 09	Sep 10 – Dec 10	Oct 11 – Nov 11	Jul 12 – Aug 12
Pine Island	-5.7 ± 6.3	-17.1 ± 6.8	-33.4 ± 7.6	-36.9 ± 6.8	-42.0 ± 6.8	-42.3 ± 7.2	-43.0 ± 6.9	-43.0 ± 6.8	-42.0 ± 6.7
Wedge	0.4 ± 1.9	0.8 ± 2.2		-0.3 ± 1.5	-0.9 ± 1.9	-0.9 ± 1.7	-0.6 ± 1.9		
Thwaites	-17.3 ± 6.9		-28.4 ± 5.7	-29.3 ± 5.5	-32.1 ± 5.6	-36.5 ± 5.6	-35.7 ± 5.6		
Thwaites East	-3.2 ± 0.4			-5.2 ± 0.3	-5.1 ± 0.3	-5.5 ± 0.3	-5.3 ± 0.3		
Haynes	-8.3 ± 1.3			-10.6 ± 0.6	-11.0 ± 0.6	-11.1 ± 0.6	-10.9 ± 0.6		
Total	-34.1 ± 13.6			-82.3 ± 13.1	-91.1 ± 13.2	-96.3 ± 13.4	-96.1 ± 13.2		

Chapter 4: Long-term Accumulation Changes

4.1 Introduction

Ice-core accumulation records provide insight into past climate conditions and the regional mass balance history over decades to millennia. The climate and mass balance history of West Antarctica are of particular interest in part because of the recent observed thinning and acceleration of the Amundsen Coast glaciers, especially Pine Island and Thwaites [*Shepherd et al.,* 2001; *Rignot et al.,* 2002; *Joughin et al.,* 2003; *Rignot,* 2008; *Pritchard et al.,* 2009] , where the infiltration of warm ocean water has substantially thinned their buttressing ice shelves [*Shepherd et al.,* 2004; *Pritchard et al.,* 2012] . These glaciers are located in one of the most rapidly warming regions on Earth [*Steig et al.,* 2009; *Bromwich et al.,* 2013] , which could potentially affect snow accumulation rates. Warmer air temperatures increase the atmospheric moisture-holding capacity and are expected to increase snowfall; however, the majority of snow accumulation occurs in non-summer months in West Antarctica [*Bromwich,* 1988] , indicating air temperature might not be the dominant control on snowfall. Instead, non-summer cyclonic activity, combined with the relatively low-elevation terrain, allows warm marine air to penetrate deep into the interior to act as a major control on accumulation rates in this region [*Nicolas and Bromwich,* 2011] .

Previous ice-core analysis from Kaspari *et al.* [2004] showed that the 1970–2000 average accumulation rate within the Pine Island-Thwaites drainage system had increased relative to the long-term average, but that records from beyond its divide in the Ross drainage had decreased. Banta *et al.* [2008] found no significant trend in accumulation using an array of three ice cores from the West Antarctic Ice Sheet (WAIS) Divide project. At the same time, Burgener *et al.* [2013] found more recent negative accumulation trends between 1975

and 2010 from a series of shallow cores near WAIS both within Thwaites and across the divide into the Ross drainage system. A regional radar-derived annual accumulation record for Thwaites glacier, however, indicates the region experienced no significant change in accumulation between 1980 and 2009 [*Medley et al.,* 2013] . While these records reveal potential zones of accumulation increases and decreases, without additional accumulation measurements over larger areas, we cannot determine with confidence the total spatial extent of these accumulation changes. Therefore, improving the spatial coverage of the accumulation changes will aid in our understanding of the spatial extent of changes and also improve our confidence in those changes.

Here, we analyze three new ice cores recovered from the Pine Island–Thwaites catchment for recent changes in snow accumulation and place the cores in context of the previously recovered cores from the region. To determine the spatial extent of accumulation changes, we investigate the change in radar-derived accumulation rates between 1944–1984 and 1985–2009 over most of the Thwaites and a substantial portion of the Pine Island catchments. Finally, we examine several scenarios that could falsely generate an increase in the radar-derived accumulation rates to assess the validity of the changes observed.

4.2 Methods

4.2.1 Ice-core accumulation records

We recovered three intermediate-depth ice cores, referred to as PIG2010, DIV2010, and THW2010, in the austral summer of 2010–2011 using the Badger-Eclipse drill provided by the U.S. Ice Drilling Program (Figure 4.1) [*Medley et al.,* 2013] . The cores were collected in approximately 1-m long segments with a diameter of 81 mm. The core density

measurements were completed in the field for DIV2010 and THW2010 and at the U.S. National Ice Core Laboratory (NICL) in Denver, CO for PIG2010. All cores were cut at NICL and shipped to the Desert Research Institute for chemical and isotopic analysis. Water isotope ratios and more than 30 elements and chemical species were measured at high depth resolution (~1 cm water equivalent) using a continuous ice-core melter system [*McConnell et al.,* 2002; *McConnell et al.,* 2007; *Maselli et al.,* 2013] . While nearly all ratios exhibit pronounced annual cycles in concentration, here we used the summer maxima in hydrogen peroxide concentration, water isotope ratios, and non-sea-salt sulfur to sodium ratio to identify annual layers. Well known volcanic horizons identified by marked increases in wintertime sulfur concentration were used to verify the annual layer counting, which indicated a dating uncertainty of < 1 year.

The PIG2010 core site lies within the Pine Island catchment and is located approximately 20 km from the earlier ITASE core site 01-3 (Figure 4.1). The DIV2010 core site is located between the Pine Island and Thwaites catchments and is only 200 km from the coast. Finally, THW2010 is a high-elevation core located within Thwaites catchment close to the divide and yet relatively close to the coast. The PIG2010, DIV2010, and THW2010 cores reach depths of 60 m, 112 m, and 62 m, respectively, which date to 1917, 1786, and 1867 (Table 4.1). We calculated annual water-equivalent (w.e.) accumulation rates by combining the annual layer thickness with the measured density profiles.

4.2.2 Radar-derived accumulation rates

We mapped near-surface internal horizons imaged using an airborne ultra-wideband frequency-modulated continuous waveform (FMCW) radar system developed by the Center for Remote Sensing of Ice Sheets (CReSIS) to calculate accumulation rates [*Lewis,* 2010;

Rodriguez-Morales et al., 2013; *Medley et al.,* 2013] . The horizons are dated at the intersection of the radar survey with the PIG2010 core site. A regional density profile, generated from the average of several profiles from the region, is used to convert two-way travel time to depth and radar-derived thicknesses to water equivalence. We use two internal reflectors to calculate accumulation rates over two time intervals from which we estimate accumulation change. Specifically, we use a shallow internal reflector from Chapter 3 and a newly mapped deeper reflector, which were dated to 1985 and 1944, respectively. We follow the methodology presented in Chapter 3 to generate accumulation rate maps from each mapped horizon. To ensure consistency, we only used accumulation measurements where both layers were mapped. Therefore, gaps in the measurements means one or both of the layers could not be tracked with confidence. Finally, we calculated the percent change in accumulation from 1944–1984 to 1985–2009 to assess the spatial pattern of accumulation changes.

4.3 Results

4.3.1 Ice-core accumulation records

When analyzing the ice core accumulation records (Figure 4.2), we consider three different time periods: the entire length of each record, 1944−1984, and 1985−2010. The latter two periods correspond to the time intervals for the radar-derived accumulation rates, which we present later. The average accumulation rates (± 1 standard deviation) over the entire record length for PIG2010, DIV2010, and THW2010 are 0.403 ± 0.062, 0.372 ± 0.075, and 0.274 ± 0.045 m w.e. yr^{-1} (Table 4.1). To determine whether the recent period (1985−2010) has a higher average accumulation rate than the prior period (1944−1984), we

used a one-tailed two-sample student's t-test to test the null hypothesis that the distributions from each interval have equal means and the alternate hypothesis that the recent mean is greater than the prior. At the 90% confidence level, we find that the mean from the recent period is higher than the mean from the prior period for all three records.

Both the DIV2010 and PIG2010 records have statistically significant positive trends over the entire length of their records, while the THW2010 record exhibits a positive, yet statistically insignificant trend. All significance tests take into account autocorrelation. From 1786 to 2010, the DIV2010 site shows a positive accumulation trend of 0.020 ± 0.015 m w.e. yr^{-1} per century, approximately equivalent to a 5% increase per century. Between 1918 and 2010, the PIG2010 record exhibited a larger trend of 0.072 ± 0.045 m w.e. yr^{-1} per century, an approximate 18% increase per century. The THW2010 record between 1867 and 2010 has a 0.003 ± 0.018 m w.e. yr^{-1} per century trend, which is insignificant. For comparison, the DIV2010 record has a larger, yet insignificant, trend between 1918 and 2010 of 0.042 ± 0.057 m w.e. yr^{-1} per century, equivalent to ~11% per century, whereas the THW2010 trend remained essentially zero.

We next explore the temporal variability of the core records and their correspondence with one another. The coefficients of variation (CV = σ / μ) over the entire record, which in this case represents the interannual accumulation variability, are 0.20, 0.15, and 0.17 for the DIV2010, PIG2010, THW2010 cores, respectively. These values do not change substantially when considering the prior and recent time intervals. The records are highly correlated with one another when considering the time interval common to all three records (1918−2010). Specifically, the DIV2010 record is significantly correlated with PIG2010 (r = 0.39, p = 0.01) and THW2010 (r = 0.48, p = 0.01), and the PIG2010 record is moderately correlated

with THW2010 (r = 0.30, p = 0.01). We find these coefficients vary between the time intervals of interest. Between 1944 and 1984, DIV2010 and THW2010 are highly correlated (r = 0.63, p = 0.01), while PIG2010 is somewhat correlated with both the former (r = 0.34, p = 0.05) and the latter (r = 0.34, p = 0.01). From 1985 to 2010, DIV2010 and PIG2010 are highly correlated (r = 0.53, p = 0.01) and THW2010 is no longer significantly correlated with either (r = 0.26 and r = 0.30, p > 0.1).

To determine the representative footprint of each accumulation record, we correlate the records with global reanalysis precipitation-minus-sublimation (*P*-*S*) products, which accurately reproduce the temporal variability in accumulation in this area [*Medley et al.*, 2013] . The three *P*-*S* products include the European Centre for Medium-Range Weather Forecasts "Interim" (ERA-Interim) [*Dee et al.*, 2011] , the NASA Modern Era Retrospective Analysis for Research and Applications (MERRA) [*Rienecker et al.*, 2011] and the National Centers for Environmental Prediction Climate Forecast System Reanalysis (CFSR) [*Saha et al.*, 2010] . We only display correlations with ERA-Interim (Figure 4.3); however, the spatial patterns are essentially identical when compared to MERRA or CFSR. The DIV2010 record is moderately correlated (r = 0.4–0.6, p < 0.1) with nearly the entire Pine Island-Thwaites drainage area with the exception of a small sliver in northeast Pine Island. The record is highly correlated (r > 0.6, p < 0.1) closer to the coast. The spatial pattern from the PIG2010 record is very similar to the DIV2010 record; however, the correlation coefficients within in the Pine Island-Thwaites drainage area are larger for PIG2010 than DIV2010. The THW2010 record is only moderately correlated with the Thwaites drainage area and is not correlated with the Pine Island catchment. All correlation patterns show infiltration of moderate-to-high correlation coefficients towards the South Pole and curving northward

towards the Ross Sea. This pattern is similar to the regions of higher cloudiness and accumulation associated with frequent marine air intrusions [*Nicolas and Bromwich,* 2011] .

4.3.2 Radar-derived accumulation rates

We calculated the 1944−1984 and 1985−2009 average accumulation rates for more than 13,000 points spaced 500 m apart over much of the Thwaites and some of the Pine Island catchment areas. The average accumulation rates (± standard deviation) for all points are 0.368 ± 0.106 and 0.392 ± 0.109 m w.e. yr^{-1} for the prior (1944−1984) and recent (1985−2009) periods, respectively. Out of all the points, 90% show a positive change from the prior to recent period (i.e., the recent accumulation rate is greater than the prior), leaving only 10% with a negative change. The difference in the accumulation rate at a given point is considered significant if it is larger in magnitude than the root-sum-square of the accumulation rate errors for the prior and recent periods. Nearly 60% (40%) of all the points showing a positive (negative) change are significant, which means the significant positive changes outnumber the negative 14:1.

The map of accumulation change (Figure 4.4) was created by subtracting the gridded recent accumulation rates from the gridded prior rates, and the change is presented as a percentage of the prior rate. The map shows a main band of larger increases up the eastern side of Thwaites catchment area. To the west of the band is a region of insignificant change followed by another band of larger increases towards the western tip of Thwaites. The more coastal areas show a larger increase (> 14%) in accumulation, while a zone of significant accumulation decreases exists just to the east. To verify this spatial pattern, we overlaid the 1944−1984 to 1985−2009 percent change from various ice-core records. For the records that do not extend through 2009, the recent period still begins in 1985 yet extends only through

the most recent year of the record, which is 2000−2001 and 2004 for the ITASE and WAIS divide cores, respectively. Although the core spatial sampling is poor, we find that the accumulation changes found in the ice core records corroborate the changes found in the radar survey. Additionally, all of the ice-core records within the Pine Island-Thwaites drainage area showed a recent increase in accumulation (Table 4.2).

4.4 Discussion

Both the ice core and radar-derived accumulation rates indicate snow accumulation over much of Thwaites and parts of Pine Island catchments has increased from 1944−1984 to 1985−2009. A somewhat abrupt increase in accumulation between the two periods is more likely than a gradual upward trend: a transition from lower to higher accumulation occurs around 1980 in all three records (Figure 4.2). The radar data show a band of statistically significant increases up the eastern half of Thwaites with majority of the points showing increases of 6 to 10%. The pattern is clear in several different flight paths, confirming the pattern is real. The western half of Thwaites, with the exception of the westernmost tip, has experienced no significant change in snow accumulation. The portion of Pine Island, closest to Thwaites, has experienced minor to large increases as well, while the area further to the east is experiencing an accumulation decrease. This area exhibits large fluctuations in accumulation over relatively short distances, resulting from undulating topography. Any translation of the accumulation undulations will result in changes not representative of climate, but rather topography. One flight, however, does appear to show a clear decreasing signal approaching the main trunk of Pine Island glacier.

The ice-core records are significantly correlated with each other over their coincident time interval (1918−2010), but when considered over our periods of interest, an interesting

pattern emerges. During the earlier period (1944−1984), the DIV2010 record showed greater correlation with THW2010 than PIG2010. This relationship flipped in the recent period (1985−2010) when the DIV2010 and PIG2010 records correlation increased (r = 0.53, p=0.05) and THW2010 no longer was significantly correlated (r = 0.26, p > 0.1). This change could indicate changes in the common moisture pathways between the two intervals.

While the accumulation increase is spatially pervasive, we evaluate the potential impact of various assumptions made concerning our accumulation measurements to ensure that we are not falsely generating the increase. First, misinterpretation of the radar surface return could potentially bias the recent accumulation measurements. The range error, however, would have to be quite large to introduce substantial bias: thickness errors near the surface are minimized due to the low firn density. Furthermore, consistent misinterpretation of the surface return over the entire domain is unlikely. Another potential source of accumulation bias stems from errors in the horizon ages, which are determined from ice-core glaciochemical analysis. For instance, if the shallow, more recent horizon was dated too young or the deep, older horizon was dated too old, a false increase in accumulation is possible. Because the horizon ages, however, match very well at all three 2010 core sites, unless the chemical markers were consistently misinterpreted in each record, the horizons were likely correctly dated. Incorporation of a horizon age error of ± 1 year should suffice in consideration of this error. Therefore, we find that accumulation bias resulting from misinterpretation of the radar surface return and the core depth-age scale are not likely to generate a false increase in accumulation.

We also considered the potential underestimation of accumulation during the earlier period from not accounting for the thinning due to longitudinal stretching. To approximate the

thinning at depth outside of densification, we use a simple model of the vertical strain rate [*Dansgaard and Johnsen,* 1969] . Using Bedmap2 ice thicknesses [*Fretwell et al.,* 2013] and the 1944–2009 average accumulation rate, we estimated the thinning of the radar-derived thicknesses due to lateral stretching as every measurement point. The largest additional thinning experienced by the prior thickness was 2%, however, it was less than one percent for nearly 95% of all the measurements. Therefore, thinning outside of densification likely accounts for no more than 1% of the observed increase in the accumulation rate, which is not significant when compared to majority of the observed increases (Figure 4.4).

Snow accumulation from the prior interval originated further upglacier, likely at a higher elevation with a lower accumulation rate. If the accumulation gradient and surface velocity are large enough, displacement into a region of higher accumulation could result in a false increase in accumulation. Less than 5% of the radar-derived accumulation measurements are located where surface velocities exceed 100 m yr^{-1}, and are mainly found along coastal trunk of Thwaites. To determine the approximate accumulation increase resulting from displacement towards the coast, we calculated the local accumulation slope from the radar-derived measurements and the distance traveled over the 34-year interval. Because the accumulation rates are time-averaged, we consider the interval between the middle of each time period (i.e., 1964 to 1997). At 100 m yr^{-1}, the displacement between intervals is ~ 3.5 km, which results in a ~0.002 m w.e. yr^{-1} (< 1%) accumulation rate increase. At an excessive 500 m yr^{-1}, we would expect an increase of 0.011 m w.e. yr^{-1} (< 2.5 %). Because of the relatively short span between intervals and the fact that velocities are very low for majority of the points, displacement likely does not contribute to the observed increases. The recent accumulation measurements from coastal Thwaites could be elevated

by a few percent, however, that contribution is relatively small considering this region experienced a large increase (> 14%) in accumulation.

Finally, we consider the impact of spatial bias in our regional density profile, which could potentially generate a false increase in accumulation if the density is too high (low) near the surface (at depth). Spatial variation in the density profile is the result of variable climate conditions, including air temperature and the accumulation rate. Here, we consider the climate scenarios necessary to decrease near surface densities and increase densities at depth, which would act to minimize the measured accumulation increases. Colder temperatures result in lower densities near the surface, however, the densities at depth are reduced as well. An empirical model of densification [*Herron and Langway*, 1980] found near-surface densities are not dependent on the accumulation rate while densities at depth are inversely related. Therefore, decreased accumulation alone or combined with decreased temperatures would increase the densities at depth relative to the near-surface density. Our regional density profile was generated from the average of several core-measured profiles, all of which are located at moderate-to-high elevations with moderate-to-low accumulation rates. Therefore, the regional density profile is likely more representative of relatively low temperatures and accumulation rates, which indicates our profile is likely preferentially biased towards lower near-surface densities and higher densities at depth. As a result, the density bias in warmer areas off the divides and in higher accumulation zones potentially results in recent accumulation rates that are too low and prior rates that are too high. Based on the climate conditions at the core sites, we believe that the density bias favors a decrease in accumulation in the areas of warmer temperatures and higher accumulation rates and does not generate a false increase in accumulation.

Based on these considerations, we find that the accumulation increases observed over much of Thwaites and parts of Pine Island catchments area likely climatic in origin. The increase, however, cannot be definitively associated with the observed rapid increase in air temperature. While the PIG2010 and DIV2010 cores both show statistically significant increasing trends over the length of their records, the THW2010 record contains past intervals of above average accumulation of the same magnitude as the most recent increase. The increasing trend could vary spatially, however, additional records are needed to verify the pattern in long-term accumulation changes. Nevertheless, the spatial pattern of change from 1944–1984 to 1985–2009 shows regions of significant increases in accumulation, which are confirmed with several ice-core records.

This recent increase in accumulation has important implications for the mass balance history of these glaciers, glacier dynamics, and interpretation of observed surface elevation change. When estimating past glacier mass balance, using accumulation values from current climate state would erroneously minimize mass loss. For example, Rignot [2008] used recent accumulation rates to determine Thwaites' mass balance in the 1970s and found the glacier was losing an insignificant amount of mass (5 Gt yr^{-1}). Assuming a 5–10% decrease in accumulation, however, translates directly into additional mass loss, which increases to ~9–12 Gt yr^{-1}. An increase in the mean accumulation rate would affect glacier dynamics as well, increasing the total mass in the catchment, which results in higher driving stresses, velocities, and total ice discharge. Finally, a jump in the accumulation rate should increase firn column thickness, which occurs rapidly at first but can continue for decades after the initial change [*Arthern and Wingham*, 1998] . Therefore, it is possible that the firn column

over much of Thwaites has been thickening since the early 1980s, which if not properly considered could mask any underlying dynamic thinning.

4.5 Conclusions

Ice-core and radar-derived measurements indicate much of Thwaites and parts of Pine Island catchments have experienced a significant increase snow accumulation, which is in line with the findings from Kaspari *et al.* [2004]. After discounting the several scenarios in which a false increase in accumulation could be generated (e.g., substantial thinning of layers due to lateral stretching, a biased density profile), we find that the accumulation increase is most likely climatic in origin. Because the ice-core records show periods of high accumulation in the past that are similar to the most recent values, it is unclear whether the increase is associated with the observed warming in the region. Consideration of this accumulation increase is necessary to fully understand the recent mass balance history and dynamic evolution of the glacier as well as to properly interpret surface elevations changes from this region.

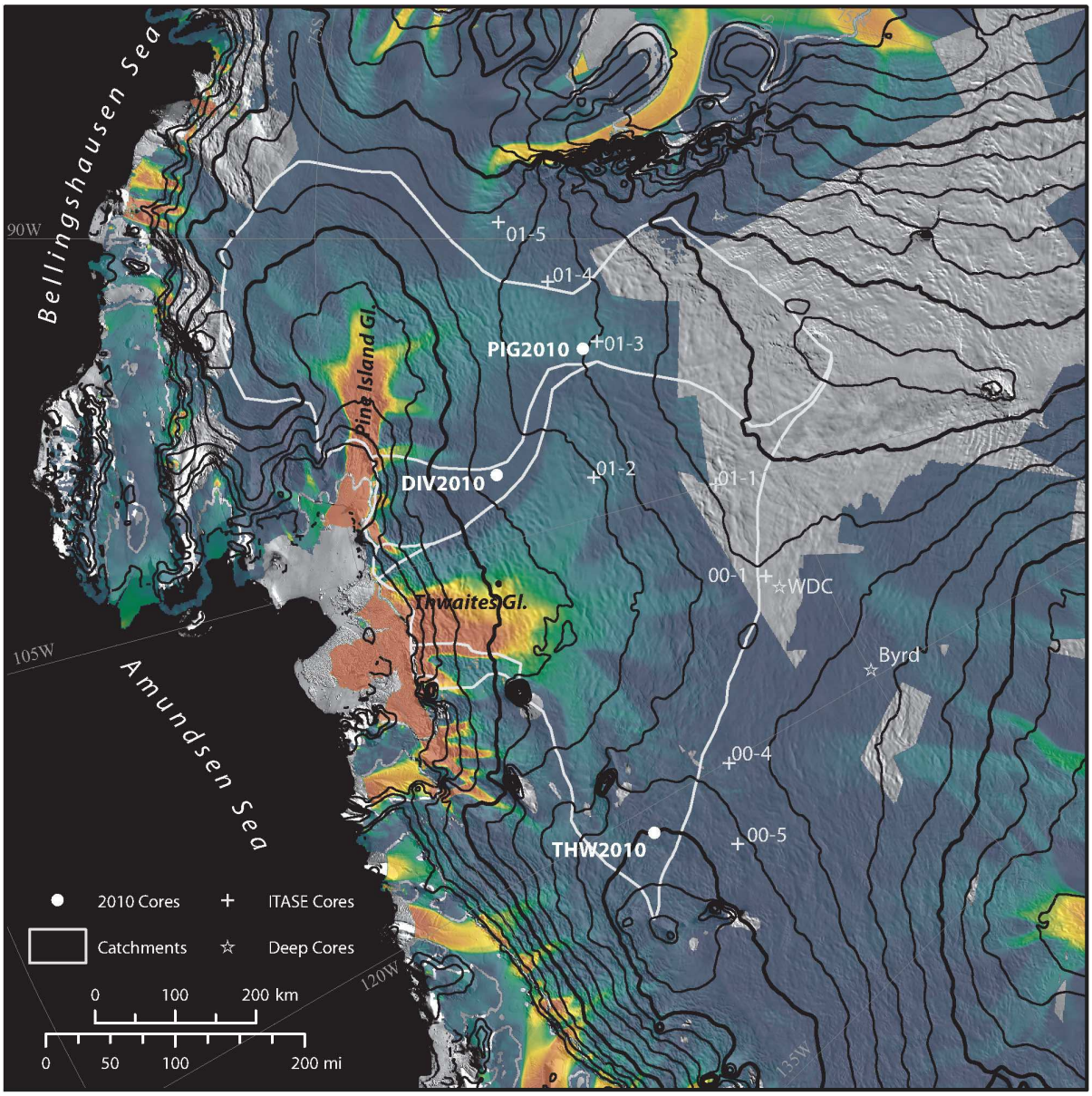
Bellingshausen Sea
Amundsen Sea
90W
105W
120W
135W
75S
01-5
01-4
01-3
01-2
01-1
00-1
00-4
00-5
PIG2010
DIV2010
THW2010
Pine Island Gl.
Thwaites Gl.
WDC
Byrd
2010 Cores
ITASE Cores
Catchments
Deep Cores
0
100
200 km
0
50
100
200 mi

Figure 4.1 – The locations of the 2010 cores (circles), ITASE cores (+), and deep cores (stars) in and around the Pine Island-Thwaites drainage system overlaid on the MODIS mosaic and surface velocities. Elevation is contoured every 200 m with bolded contours every 1000 m.

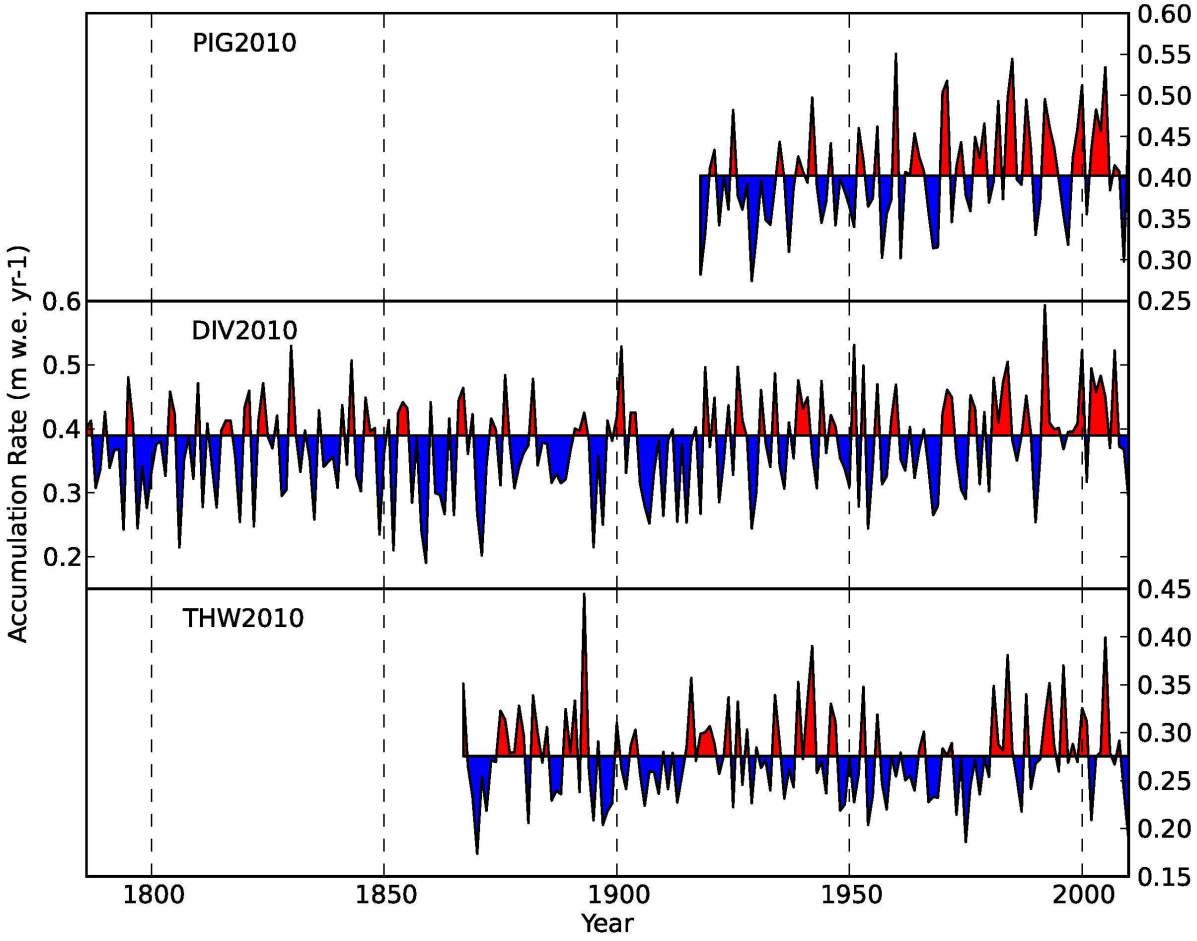

Figure 4.2 – The annual accumulation records for the PIG2010 (top), DIV2010 (middle), and THW2010 (bottom) records. Areas shaded red (blue) indicate years when the accumulation rate was greater (less) than the 1918–2010 mean accumulation rate, which is the time interval common to all three records.

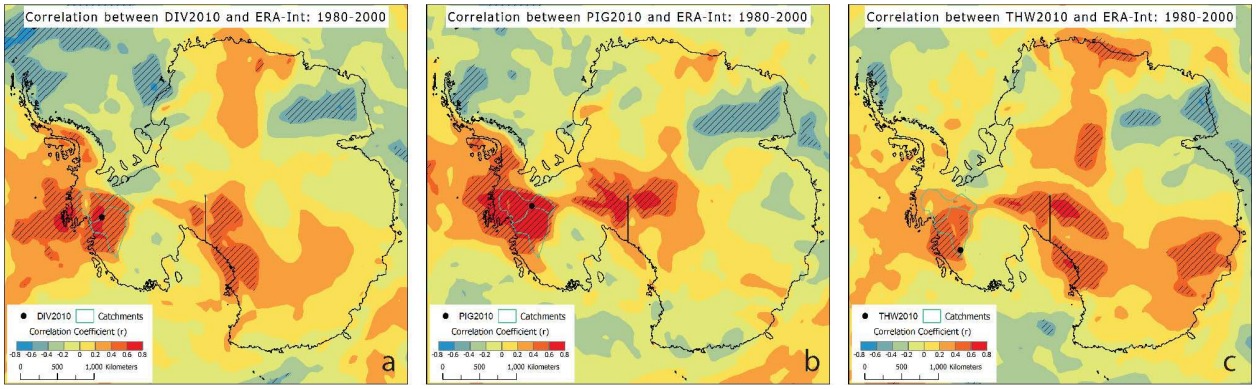

Figure 4.3 – Spatial correlation of the DIV2010 (left), PIG2010 (middle), and THW2010 (right) accumulation record with the ERA-Interim *P-S* product. Increasing red (blue) intensity is indicative of more positive (negative) correlations. Hatch marks represent areas that are statistically significant at the 90% confidence level.

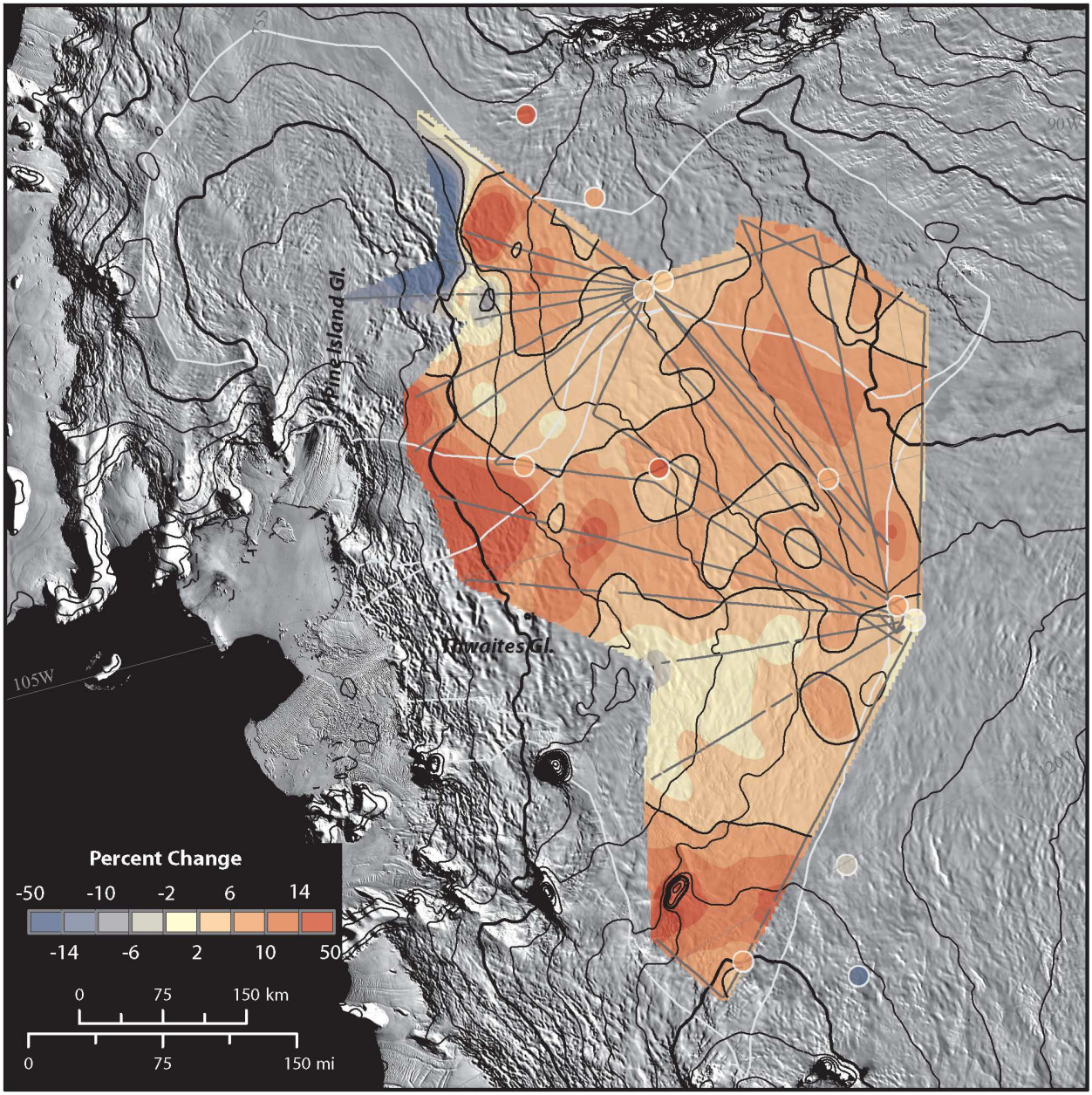

Figure 4.4 – The percent change in accumulation rate between 1944–1984 and 1985–2009 overlaid on the MODIS mosaic. Increasing red (blue) intensity is indicative of more positive (negative) accumulation increases. The grey lines show the accumulation measurements used to generate the gridded accumulation rates. The filled circles show the 1944–1984 to 1985–2009 percent change from various ice-core records.

Table 4.1 – Summary of ice-core accumulation records

Name	Latitude (°)	Longitude (°)	Elevation (m)	Velocity (m / yr)	Bottom Depth (m)	Time Interval	Accumulation Rate (m w.e. / yr)[a]		
							Entire Record	1944–1984	1985-2009
PIG2010	-77.96	-95.96	1590	27.5	59.4	1917–2010	0.403 ± 0.062	0.402 ± 0.061	0.424 ± 0.066
DIV2010	-76.77	-101.74	1330	4.6	111.7	1786–2010	0.372 ± 0.075	0.383 ± 0.075	0.412 ± 0.072
THW2010	-76.95	-121.22	2020	5.5	61.8	1867–2010	0.274 ± 0.045	0.265 ± 0.041	0.286 ± 0.045

[a]Values represent the $\mu \pm 1\ \sigma$

Table 4.2 – Change in accumulation between 1944–1984 and 1985–2009, cores sorted by longitude

	Acc. Rate (m w.e. yr^{-1})		
Core[a]	1944−1984	1985−2009[b]	% Change
ITASE 01-5	*0.321*	*0.382*	*18.9*
ITASE 01-4	*0.324*	*0.346*	*6.8*
ITASE 01-3	0.338	0.346	2.4
PIG2010	0.402	0.424	5.5
DIV2010	0.383	0.412	7.7
ITASE 01-2	0.425	0.488	14.9
ITASE 01-1	*0.333*	*0.361*	*8.6*
ITASE 00-1	0.224	0.244	9.2
WDC05Q	*0.200*	*0.199*	*-0.2*
WDC05A	*0.200*	*0.202*	*1.2*
ITASE 00-4	*0.194*	*0.189*	*-2.5*
THW2010	0.265	0.286	8.2
ITASE 00-5	*0.137*	*0.123*	*-10.4*

[a]Italicized cores are located outside of the Pine Island-Thwaites drainage system

[b]The interval for the ITASE cores is 1985−2000/1 and for the WDC cores is 1985−2004

Chapter 5: Insights from Radar-Derived Accumulation

Airborne radar mapping of near-surface internal horizons has revealed spatial and temporal variations in accumulation previously unmeasured over Pine Island and Thwaites glaciers. Deriving accumulation rates using radar-tracked horizons is a more appropriate method of calculating catchment-wide accumulation than traditional methods (i.e., ice cores, stake farms) because it requires minimal field work and the data are easily collected over large areas. From the radar-derived measurements presented, we determined the recent mass balance history of Pine Island and Thwaites glaciers and also investigated long-term accumulation changes. Because few spatiotemporal measurements at the regional scale exist, our measurements provide a unique means with which to test the skill of various atmospheric models, which is essential considering many studies are using model output in place of measurements.

5.1 Future accumulation radar studies

Because airborne radar systems provide excellent spatial coverage, they will likely provide the accumulation measurements for future mass balance studies elsewhere in Antarctica and Greenland. Additionally, flying multiple systems that operate over different frequency ranges (i.e., the accumulation and snow radars) at the same time will provide accumulation rates at varied temporal resolution and coverage, which is important when considering both recent and long-term changes. A system with coarser vertical resolution (such as the accumulation radar) will require independent depth-age information, yet will provide a longer record of accumulation. We found that the finer vertical resolution system (the snow radar) imaged annual horizons, eliminating the need for independent age information. While several factors influence whether the radar will find annual horizons

elsewhere, because the system is flown as part of NASA's Operation IceBridge mission, I hope to investigate the use of this radar system in both Greenland and Antarctica. The finer vertical resolution means the accumulation record will be relatively short but possibly annual. There is also potential to use the depth-age scale derived from the snow radar system to date horizons imaged by the accumulation radar, further minimizing the need for independent field data collection. At the same time, the accumulation calculations still rely on density measurements, which could potentially limit our ability to use this radar method elsewhere where field measurements are few. Therefore, we find that although ice-core records are still valuable because they provide the age tiepoints for the radar horizons and the density information, future mass balance studies will greatly benefit from radar-derived accumulation measurements, especially from airborne systems.

5.2 The recent mass balance of Pine Island and Thwaites glaciers

We found that while ice discharge from Pine Island and Thwaites has increased substantially over the past two decades, snow accumulation has not experienced a significant trend. This result confirms that snow accumulation has not been compensating the increased ice discharge from this region, which indicates an increasing contribution to sea-level rise. Because accumulation showed no trend over the past few decades, using the 1985–2009 mean accumulation rate map should provide a good approximation of annual catchment-wide accumulation, especially when integrated. Combining the radar-derived accumulation map and flux-gate discharge estimates, we find that these glaciers have contributed ~3 mm to sea level over the past two decades. The rate of contribution tripled from 0.09 ± 0.04 mm yr^{-1} in the mid-90s to 0.27 ± 0.04 mm yr^{-1} by 2010. These values match well with prior studies [*Rignot,* 2008] , however, the uncertainty has been greatly reduced.

5.3 Implications of long-term accumulation change

While no recent trend in accumulation exists, a longer-term increase was found in both the ice-core and radar-derived accumulation records. Specifically, an increase of 6% to 10% was found over much of Thwaites and part of Pine Island between 1944–1984 and 1985–2009. Based on the ice-core records, we determined that accumulation likely jumped (rather than trended) towards a higher mean around 1980. This accumulation jump suggests: (1) these glaciers might have been out of balance earlier than originally thought, (2) an increase in driving stress, resulting in increased velocities and discharge, and (3) a potential thickening of the firn column. The latter effect could mean that firn column thickening might hide any underlying dynamic thinning from this region and therefore, should be considered in interpretations of surface elevation change.

5.4 Assessment of atmospheric model skill

The accumulation measurements presented provide the means with which to test the ability of various atmospheric models in reproducing the spatial and temporal variability in snow accumulation. The observation-constrained global reanalyses reproduce the temporal variability with high fidelity, whereas the high-resolution regional climate model (RACMO2) more accurately reproduces the spatial variability. We also found that the catchment-wide accumulation rates from RACMO2 show little bias, whereas the reanalyses underestimate the total magnitude to varying degrees. Based on these findings, interpretations of glacier mass balance from surface elevation change would most appropriately account for fluctuations due to accumulation variability from the reanalysis products. When using the mass-budget method to determine mass balance, RACMO2 provides the most accurate spatial mean.

Additional regional studies of radar-derived accumulation rates elsewhere will provide more insight into these model's strengths and weaknesses.

5.5 Summary

Studies of the spatiotemporal accumulation rate provide important information needed to precisely determine glacier mass balance using the mass-budget method as well as from interpretation of surface elevation and gravity changes. Accumulation measurements derived from airborne radar provide the spatial and temporal coverage necessary to generate an accurate spatial mean and to also investigate recent and long-term accumulation variability and trends. Based on the measurements presented here, we found that: (1) the accumulation rate is not keeping pace with the accelerated ice discharge from Pine Island and Thwaites as no accumulation increase was found over the past three decades; (2) the 1985–2009 mean accumulation is larger than the 1944–1984 mean, which might indicate these glaciers were out of balance earlier than previously thought; (3) the mass loss from these glaciers has tripled over ~15 years, resulting in a current sea-level contribution of 0.27 mm yr^{-1}; and (4) atmospheric models are decent replacements for actual accumulation measurements in areas where few measurements exist. Because of the copious amount of radar data collected using both the snow and accumulation radars, the methodologies here should be easily applied elsewhere to further our understanding of ice-sheet accumulation rates and mass balance in both Antarctica and Greenland.

REFERENCES

Agosta, C., V. Favier, C. Genthon, H. Gallee, G. Krinner, J. T. M. Lenaerts, and van den Broeke, M. R. (2012), A 40-year accumulation dataset for Adelie Land, Antarctica and its application for model validation, *Clim. Dyn., 38*(1-2), 75-86, doi: 10.1007/s00382-011-1103-4.

Allen, C. (2010, updated 2013), IceBridge MCoRDS L2 Ice Thickness, *Boulder, Colorado USA: NASA DAAC at the National Snow and Ice Data Center*.

Alley, R. B., P. U. Clark, P. Huybrechts, and I. Joughin (2005), Ice-Sheet and Sea-Level Changes, *Science, 310*(5747), 456-460, doi: 10.1126/science.1114613.

Anschutz, H., O. Eisen, H. Oerter, D. Steinhage, and M. Scheinert (2007), Investigating small-scale variations of the recent accumulation rate in coastal Dronning Maud Land, East Antarctica, *Ann. Glaciol., 46*, 14-21, doi: 10.3189/172756407782871756.

Anschutz, H., D. Steinhage, O. Eisen, H. Oerter, M. Horwath, and U. Ruth (2008), Small-scale spatio-temporal characteristics of accumulation rates in western Dronning Maud Land, Antarctica, *J. Glaciol., 54*(185), 315-323, doi: 10.3189/002214308784886243.

Arcone, S. A., V. B. Spikes, G. S. Hamilton, and P. A. Mayewski (2004), Stratigraphic continuity in 400 MHz short-pulse radar profiles of firn in West Antarctica, *Ann. Glaciol., 39*(1), 195-200, doi: 10.3189/172756404781813925.

Arcone, S. A., V. B. Spikes, and G. S. Hamilton (2005a), Phase structure of radar stratigraphic horizons within Antarctic firn, *Ann. Glaciol., 41*(1), 10-16, doi: 10.3189/172756405781813267.

Arcone, S. A., V. B. Spikes, and G. S. Hamilton (2005b), Stratigraphic variation within polar firn caused by differential accumulation and ice flow: interpretation of a 400 MHz short-pulse radar profile from West Antarctica, *J. Glaciol., 51*(174), 407-422, doi: 10.3189/172756505781829151.

Arthern, R. J. and D. J. Wingham (1998), The Natural Fluctuations of Firn Densification and Their Effect on the Geodetic Determination of Ice Sheet Mass Balance, *Clim. Change, 40*(3-4), 605-624, doi: 10.1023/A:1005320713306.

Arthern, R. J., D. P. Winebrenner, and D. G. Vaughan (2006), Antarctic snow accumulation mapped using polarization of 4.3-cm wavelength microwave emission, *J. Geophys. Res., 111*, D06107, doi: 10.1029/2004JD005667.

Bamber, J. L., J. Gomez-Dans, and J. A. Griggs (2009), A new 1 km digital elevation model of the Antarctic derived from combined satellite radar and laser data. Part 1: Data and methods, *Cryosphere, 3*(1), 101-111, doi: 10.5194/tc-3-101-2009.

Banta, J. R., J. R. McConnell, M. M. Frey, R. C. Bales, and K. Taylor (2008), Spatial and temporal variability in snow accumulation at the West Antarctic Ice Sheet Divide over recent centuries, *J. Geophys. Res., 113,* 23102, doi: 10.1029/2008JD010235.

Blair, J. B. and M. Hofton (2010, updated 2012), IceBridge LVISL2 Geologcated Surface Elevation Product, *Boulder, Colorado USA: NASA DAAC at the National Snow and Ice Data Center*.

Bromwich, D. H. (1988), Snowfall in high southern latitudes, *Rev. Geophys., 26*(1), 149-168.

Bromwich, D. H., J. P. Nicolas, and A. J. Monaghan (2011), An Assessment of Precipitation Changes over Antarctica and the Southern Ocean since 1989 in Contemporary Global Reanalyses, *J. Clim., 24*(16), 4189-4209, doi: 10.1175/2011JCLI4074.1.

Bromwich, D. H., J. P. Nicolas, A. J. Monaghan, M. A. Lazzara, L. M. Keller, G. A. Weidner, and A. B. Wilson (2013), Central West Antarctica among the most rapidly warming regions on Earth, *Nat. Geosci., 6*(2), 139-145.

Burgener, L. et al. (2013), An observed negative trend in West Antarctic accumulation rates from 1975 to 2010: Evidence from new observed and simulated records, *J. Geophys. Res., 118*(10), 4205-4216, doi: 10.1002/jgrd.50362.

Comiso, J. C. (2000), Variability and Trends in Antarctic Surface Temperatures from In Situ and Satellite Infrared Measurements, *J. Clim., 13*(10), 1674-1696, doi: 10.1175/1520-0442(2000)013<1674:VATIAS>2.0.CO;2.

Dansgaard, W. and S. Johnsen (1969), A flow model and a time scale for the ice core from Camp Century, Greenland, *J. Glaciol., 8,* 215-223.

Dee, D. P. et al. (2011), The ERA-Interim reanalysis: configuration and performance of the data assimilation system, *Q. J. R. Meteorol. Soc., 137*(656), 553-597, doi: 10.1002/qj.828.

Eisen, O., W. Rack, U. Nixdorf, and F. Wilhelms (2005), Characteristics of accumulation around the EPICA deep-drilling site in Dronning Maud Land, Antarctica, *Ann. Glaciol., 41,* 41-46, doi: 10.3189/172756405781813276.

Fretwell, P. et al. (2013), Bedmap2: improved ice bed, surface and thickness datasets for Antarctica, *Cryosphere, 7*(1), 375-393, doi: 10.5194/tc-7-375-2013.

Frezzotti, M. et al. (2005), Spatial and temporal variability of snow accumulation in East Antarctica from traverse data, *J. Glaciol., 51*(172), 113-124, doi: 10.3189/172756505781829502.

Frezzotti, M., S. Urbini, M. Proposito, C. Scarchilli, and S. Gandolfi (2007), Spatial and temporal variability of surface mass balance near Talos Dome, East Antarctica, *J. Geophys. Res., 112*(F11), F02032, doi: 10.1029/2006JF000638.

Genthon, C., G. Krinner, and H. Castebrunet (2009), Antarctic precipitation and climate-change predictions: horizontal resolution and margin vs plateau issues, *Ann. Glaciol., 50*(50), 55-60, doi: 10.3189/172756409787769681.

Gladstone, R. M., V. Lee, J. Rougier, A. J. Payne, H. Hellmer, A. Le Brocq, A. Shepherd, T. L. Edwards, J. Gregory, and S. L. Cornford (2012), Calibrated prediction of Pine Island Glacier retreat during the 21st and 22nd centuries with a coupled flowline model, *Earth Planet. Sci. Lett., 333–334*(0), 191-199, doi: 10.1016/j.epsl.2012.04.022.

Haran, T., T. Bohlander, T. Scambos, T. Painter, and M. A. Fahnestock (2005, updated 2006), MODIS mosaic of Antarctica (MOA) image map, *Boulder, Colorado USA: NASA DAAC at the National Snow and Ice Data Center*.

Herron M.M. and C. C. Langway Jr. (1980), Firn densification: an empirical model, *J. Glaciol., 25*, 373-385.

Holt, J. W., D. D. Blankenship, D. L. Morse, D. A. Young, M. E. Peters, S. D. Kempf, T. G. Richter, D. G. Vaughan, and H. F. J. Corr (2006), New boundary conditions for the West Antarctic Ice Sheet: Subglacial topography of the Thwaites and Smith glacier catchments, *Geophys. Res. Lett., 33*(9), - L09502, doi: 10.1029/2005GL025561.

Huybrechts, P., O. Rybak, D. Steinhage, and F. Pattyn (2009), Past and present accumulation rate reconstruction along the Dome FujiKohnen radio-echo sounding profile, Dronning Maud Land, East Antarctica, *Ann. Glaciol., 50*(51), 112-120, doi: 10.3189/172756409789097513.

Joughin, I. and S. Tulaczyk (2002), Positive mass balance of the Ross ice streams, West Antarctica, *Science, 295*(5554), 476-480.

Joughin, I. (2002), Ice-sheet velocity mapping: a combined interferometric and speckle-tracking approach, *Ann. Glaciol., 34*(1), 195-201, doi: 10.3189/172756402781817978.

Joughin, I., R. B. Alley, and D. M. Holland (2012), Ice-Sheet Response to Oceanic Forcing, *Science, 338*(6111), 1172-1176, doi: 10.1126/science.1226481.

Joughin, I., E. Rignot, C. E. Rosanova, B. K. Lucchitta, and J. Bohlander (2003), Timing of Recent Accelerations of Pine Island Glacier, Antarctica, *Geophys. Res. Lett., 30*(13), - 1706, doi: 10.1029/2003GL017609.

Joughin, I., B. E. Smith, and D. M. Holland (2010), Sensitivity of 21st century sea level to ocean-induced thinning of Pine Island Glacier, Antarctica, *Geophys. Res. Lett., 37*(20), - L20502, doi: 10.1029/2010GL044819.

Kameda, T., H. Motoyama, S. Fujita, and S. Takahashi (2008), Temporal and spatial variability of surface mass balance at Dome Fuji, East Antarctica, by the stake method from 1995 to 2006, *J. Glaciol., 54*(184), 107-116, doi: 10.3189/002214308784409062.

Kanagaratnam, P., S. P. Gogineni, V. Ramasami, and D. Braaten (2004), A wideband radar for high-resolution mapping of near-surface internal layers in glacial ice, *IEEE Trans. Geosci. Remote Sens.*, *42*(3), 483-490.

Kaspari, S., P. A. Mayewski, D. A. Dixon, V. B. Spikes, S. B. Sneed, M. J. Handley, and G. S. Hamilton (2004), Climate variability in West Antarctica derived from annual accumulation-rate records from ITASE firn/ice cores, *Ann. Glaciol.*, *39*(1), 585-594, doi: 10.3189/172756404781814447.

Krabill, W. B. (2010, updated 2013), IceBridge ATML1B Qfit Elevation and Return Strength, *Boulder, Colorado USA: NASA DAAC at the National Snow and Ice Data Center*.

Lenaerts, J. T. M., van den Broeke, M. R.., van de Berg, W. J., E. van Meijgaard, and P. Kuipers Munneke (2012), A new, high-resolution surface mass balance map of Antarctica (1979–2010) based on regional atmospheric climate modeling, *Geophys. Res. Lett.*, *39*(4), L04501, doi: 10.1029/2011GL050713.

Leuangthong, O., K. D. Khan, and C. V. Deutsch (2011), *Solved Problems in Geostatistics*, John Wiley & Sons.

Leuschen, C. (2010, updated 2011), IceBridge Snow Radar L1B Geolocated Radar Echo Strength Profiles, October 18, 2009, November 19, 2010, November 9 & 12, 2011, *Boulder, Colorado USA: NASA DAAC at the National Snow and Ice Data Center*.

Lewis, C. (2010), Airborne UHF Radar for Fine Resolution Mapping of Near-Surface Accumulation Layers in Greenland and West Antarctica (Master's Thesis). Retrieved from KU ScholarWorks.

Liston, G. E. and J. Winther (2005), Antarctic Surface and Subsurface Snow and Ice Melt Fluxes, *J. Clim.*, *18*(10), 1469-1481, doi: 10.1175/JCLI3344.1.

Looyenga, H. (1965), Dielectric constants of heterogeneous mixtures, *Physica*, *31*(3), 401-406, doi: 10.1016/0031-8914(65)90045-5.

MacGregor, J. A., K. Matsuoka, M. R. Koutnik, E. D. Waddington, M. Studinger, and D. P. Winebrenner (2009), Millennially averaged accumulation rates for the Vostok Subglacial Lake region inferred from deep internal layers, *Ann. Glaciol.*, *50*(51), 25-34, doi: 10.3189/172756409789097441.

Maselli, O., D. Fritzche, L. Layman, J. McConnell, and H. Meyer (2013), Comparison of water isotope ratio determinations using two cavity ring-down instruments and classical mass spectrometry in continuous ice-core analysis, *Isot. Environ. Health Stud., In Press*.

McConnell, J. R., R. Edwards, G. L. Kok, M. G. Flanner, C. S. Zender, E. S. Saltzman, J. R. Banta, D. R. Pasteris, M. M. Carter, and J. D. W. Kahl (2007), 20th-Century Industrial Black

Carbon Emissions Altered Arctic Climate Forcing, *Science, 317*(5843), 1381-1384, doi: 10.1126/science.1144856.

McConnell, J. R., G. W. Lamorey, S. W. Lambert, and K. C. Taylor (2002), Continuous Ice-Core Chemical Analyses Using Inductively Coupled Plasma Mass Spectrometry, *Environ. Sci. Technol., 36*(1), 7-11, doi: 10.1021/es011088z.

Medley, B. et al. (2013), Airborne-radar and ice-core observations of annual snow accumulation over Thwaites Glacier, West Antarctica confirm the spatiotemporal variability of global and regional atmospheric models, *Geophys. Res. Lett., 40*(14), 3649-3654, doi: 10.1002/grl.50706.

Meier, M. F., M. B. Dyurgerov, U. K. Rick, S. O'Neel, W. T. Pfeffer, R. S. Anderson, S. P. Anderson, and A. F. Glazovsky (2007), Glaciers Dominate Eustatic Sea-Level Rise in the 21st Century, *Science, 317*(5841), 1064-1067, doi: 10.1126/science.1143906.

Monaghan, A. J., D. H. Bromwich, and S. Wang (2006), Recent trends in Antarctic snow accumulation from Polar MM5 simulations, *Philos. Trans. R. Soc. A, 364*(1844), 1683-1708, doi: 10.1098/rsta.2006.1795.

Nereson, N. A., C. F. Raymond, R. W. Jacobel, and E. D. Waddington (2000), The accumulation pattern across Siple Dome, West Antarctica, inferred from radar-detected internal layers, *J. Glaciol., 46*(152), 75-87, doi: 10.3189/172756500781833449.

Nicolas, J. P. and D. H. Bromwich (2011), Climate of West Antarctica and Influence of Marine Air Intrusions, *J. Climate, 24*(1), 49-67, doi: 10.1175/2010JCLI3522.1.

Orsi, A. J., B. D. Cornuelle, and J. P. Severinghaus (2012), Little Ice Age cold interval in West Antarctica: Evidence from borehole temperature at the West Antarctic Ice Sheet (WAIS) Divide, *Geophys. Res. Lett., 39*(9), L09710, doi: 10.1029/2012GL051260.

Panzer, B., C. Leuschen, A. Patel, T. Markus, and S. Gogineni (2010), Ultra-wideband radar measurements of snow thickness over sea ice, 2010 Int. IEEE Geosci. Remote Sens. Symp. (IGARSS): 3130-3133, doi: 10.1109/IGARSS.2010.5654342.

Panzer, B., D. Gomez-Garcia, C. Leuschen, J. Paden, F. Rodriguez-Morales, A. Patel, T. Markus, B. Holt, and S. Gogineni (2013), An ultra-wideband, microwave radar for measuring snow thickness on sea ice and mapping near-surface internal layers in polar firn, *J. Glaciol*., 59 (214), 244-254, doi: 10.3189/2013JoG12J128.

Pritchard, H. D., S. R. M. Ligtenberg, H. A. Fricker, D. G. Vaughan, d. B. van, and L. Padman (2012), Antarctic ice-sheet loss driven by basal melting of ice shelves, *Nature, 484*(7395), 502-505.

Pritchard, H. D., R. J. Arthern, D. G. Vaughan, and L. A. Edwards (2009), Extensive dynamic thinning on the margins of the Greenland and Antarctic ice sheets, *Nature, 461*(7266), 971-975.

Ramillien, G., A. Lombard, A. Cazenave, E. Ivins, M. Llubes, F. Remy, and R. Biancale (2006), Interannual variations of the mass balance of the Antarctica and Greenland ice sheets from GRACE, *Global Planet. Change, 53*(3), 198-208.

Richardson, C., E. Aarholt, S. Hamran, P. Holmlund, and E. Isaksson (1997), Spatial distribution of snow in western Dronning Maud Land, East Antarctica, mapped by a ground-based snow radar, *J. Geophys. Res., 102*(B9), 20343-20353, doi: 10.1029/97JB01441.

Rienecker, M. M. et al. (2011), MERRA: NASA's Modern-Era Retrospective Analysis for Research and Applications, *J. Clim., 24*(14), 3624-3648, doi: 10.1175/JCLI-D-11-00015.1.

Rignot, E., I. Velicogna, van den Broeke, Michiel R., A. J. Monaghan, and J. Lenaerts (2011), Acceleration of the contribution of the Greenland and Antarctic ice sheets to sea level rise, *Geophys. Res. Lett., 38*, L05503, doi: 10.1029/2011GL046583.

Rignot, E. (1998), Fast recession of a West Antarctic glacier, *Science, 281*(5376), 549-551.

Rignot, E. (2001), Evidence for rapid retreat and mass loss of Thwaites Glacier, West Antarctica, *J. Glaciol., 47*(157), 213-222, doi: 10.3189/172756501781832340.

Rignot, E. (2008), Changes in West Antarctic ice stream dynamics observed with ALOS PALSAR data, *Geophys. Res. Lett., 35*(12), - L12505, doi: 10.1029/2008GL033365.

Rignot, E., J. L. Bamber, van den Broeke, Michiel R., C. Davis, Y. Li, van de Berg, Willem Jan, and E. van Meijgaard (2008), Recent Antarctic ice mass loss from radar interferometry and regional climate modelling, *Nat. Geosci., 1*(2), 106-110.

Rignot, E. and R. H. Thomas (2002), Mass Balance of Polar Ice Sheets, *Science, 297*(5586), 1502-1506, doi: 10.1126/science.1073888.

Rignot, E., D. G. Vaughan, M. Schmeltz, T. Dupont, and D. MacAyeal (2002), Acceleration of Pine Island and Thwaites Glaciers, West Antarctica, *Ann. Glaciol., 34*(1), 189-194, doi:10.3189/172756402781817950.

Rodriguez-Morales, F. et al. (2013), Advanced Multifrequency Radar Instrumentation for Polar Research, *IEEE Trans. Geosci. Remote Sens., PP*(99), 1-19, doi: 10.1109/TGRS.2013.2266415.

Rotschky, G., O. Eisen, F. Wilhelms, U. Nixdorf, and H. Oerter (2004), Spatial distribution of surface mass balance on Amundsenisen plateau, Antarctica, derived from ice-penetrating radar studies, *Ann. Glaciol., 39*, 265-270, doi: 10.3189/172756404781814618.

Saha, S. et al. (2010), The NCEP Climate Forecast System Reanalysis, *Bull. Amer. Meteor. Soc., 91*(8), 1015-1057, doi: 10.1175/2010BAMS3001.1.

Shepherd, A. et al. (2012), A Reconciled Estimate of Ice-Sheet Mass Balance, *Science, 338*(6111), 1183-1189, doi: 10.1126/science.1228102.

Shepherd, A. and D. Wingham (2007), Recent Sea-Level Contributions of the Antarctic and Greenland Ice Sheets, *Science, 315*(5818), 1529-1532, doi: 10.1126/science.1136776.

Shepherd, A., D. J. Wingham, J. A. D. Mansley, and H. F. J. Corr (2001), Inland Thinning of Pine Island Glacier, West Antarctica, *Science, 291*(5505), 862-864, doi: 10.1126/science.291.5505.862.

Shepherd, A., D. Wingham, and E. Rignot (2004), Warm ocean is eroding West Antarctic Ice Sheet, *Geophys. Res. Lett., 31*(23), - L23402, doi: 10.1029/2004GL021106.

Siegert, M. J. and A. J. Payne (2004), Past rates of accumulation in central West Antarctica, *Geophys. Res. Lett., 31*, L12403, doi: 10.1029/2004GL020290.

Sinisalo, A., A. Grinsted, J. C. Moore, E. Karkas, and R. Pettersson (2003), Snow-accumulation studies in Antarctica with ground-penetrating radar using 50,100 and 800 MHz antenna frequencies, *Ann. Glaciol., 37*, 194-198, doi: 10.3189/172756403781815825.

Spikes, V. B., G. S. Hamilton, S. A. Arcone, S. Kaspari, and P. A. Mayewski (2004), Variability in accumulation rates from GPR profiling on the West Antarctic plateau, *Ann. Glaciol., 39*, 238-244, doi: 10.3189/172756404781814393.

Steig, E. J., D. P. Schneider, S. D. Rutherford, M. E. Mann, J. C. Comiso, and D. T. Shindell (2009), Warming of the Antarctic ice-sheet surface since the 1957 International Geophysical Year, *Nature, 457*(7228), 459-462.

Thomas, E. R., G. J. Marshall, and J. R. McConnell (2008), A doubling in snow accumulation in the western Antarctic Peninsula since 1850, *Geophys. Res. Lett., 35*, L01706, doi: 10.1029/2007GL032529.

Thomas, R. et al. (2004), Accelerated Sea-Level Rise from West Antarctica, *Science, 306*(5694), 255-258, doi: 10.1126/science.1099650.

Urbini, S., M. Frezzotti, S. Gandolfi, C. Vincent, C. Scarchilli, L. Vittuari, and M. Fily (2008), Historical behaviour of Dome C and Talos Dome (East Antarctica) as investigated by snow accumulation and ice velocity measurements, *Global Planet. Change, 60*(3-4), 576-588, doi: 10.1016/j.gloplacha.2007.08.002.

van de Berg, W. J., M. R. Van den Broeke, C. H. Reijmer, and E. Van Meijgaard (2005), Characteristics of the Antarctic surface mass balance, 19582002, using a regional

atmospheric climate model, *Ann. Glaciol.*, *41*(1), 97-104, doi:10.3189/172756405781813302.

van den Broeke, M. R. (2008), Depth and Density of the Antarctic Firn Layer, *Arct. Antarct. Alp. Res.*, *40*(2), 432-438.

van den Broeke, M. R., W. J. van de Berg, and E. van Meijgaard (2006), Snowfall in coastal West Antarctica much greater than previously assumed, *Geophys. Res. Lett.*, *33*, L02505, doi: 10.1029/2005GL025239.

Vaughan, D. G., J. L. Bamber, M. Giovinetto, J. Russell, and A. P. Cooper (1999), Reassessment of Net Surface Mass Balance in Antarctica, *J. Clim.*, *12*(4), 933-946, doi: 10.1175/1520-0442(1999)012<0933:RONSMB>2.0.CO;2.

Vaughan, D. G., H. F. J. Corr, F. Ferraccioli, N. Frearson, A. O'Hare, D. Mach, J. W. Holt, D. D. Blankenship, D. L. Morse, and D. A. Young (2006), New boundary conditions for the West Antarctic ice sheet: Subglacial topography beneath Pine Island Glacier, *Geophys. Res. Lett.*, *33*(9), - L09501, doi: 10.1029/2005GL025588.

Velicogna, I. (2009), Increasing rates of ice mass loss from the Greenland and Antarctic ice sheets revealed by GRACE, *Geophys. Res. Lett.*, *36*(19).

Velicogna, I. and J. Wahr (2006), Measurements of time-variable gravity show mass loss in Antarctica, *Science*, *311*(5768), 1754-1756.

Waddington, E. D., T. A. Neumann, M. R. Koutnik, H. Marshall, and D. L. Morse (2007), Inference of accumulation-rate patterns from deep layers in glaciers and ice sheets, *J. Glaciol.*, *53*(183), 694-712, doi: 10.3189/002214307784409351.

Wingham, D., D. Wallis, and A. Shepherd (2009), Spatial and temporal evolution of Pine Island Glacier thinning, 1995–2006, *Geophys. Res. Lett.*, *36*(17), L17501.

Wingham, D. J., A. Shepherd, A. Muir, and G. J. Marshall (2006), Mass balance of the Antarctic ice sheet, *Philos. Trans. R. Soc. A*, *364*(1844), 1627-1635, doi: 10.1098/rsta.2006.1792.

Zwally, H. J., D. Schutz, D. Hancock, and J. Dimarzio (2012), GLAS/ICESatL2 Antarctic and Greenland Ice Sheet Altimetry Data (HDF5). Version 33, *Boulder, Colorado USA: NASA DAAC at the National Snow and Ice Data Center*.

Appendix A

A.1 Error Analysis

Radar-derived accumulation rate measurement errors stem from the error in the time separation between each horizon and the variation in the depth-density profile. Horizons are assumed to be annually spaced, $\Delta t = 1$ year, but in reality Δt likely varies between horizons. The radar signal is reflecting off dielectric contrasts generated by low density hoar layers and ice crusts that typically form in the summer/autumn. To account for variability in the time of horizon creation, we use an error in Δt of $\pm$ 1 month that is assumed constant with depth. This error is independent of the error in the density profile and translates directly into an ~8.3% error in the accumulation rate. This is the largest source of error in our accumulation estimates.

We account for the impact of spatial variation in the density profile on the conversion between twtt and depth as well as the cumulative mass profile, which is dependent on the former. We take the mean of several depth-density profiles in the region and fit a simple densification model to the mean (Figure A.1). This model-fit profile is used for all accumulation calculations. It is clear from Figure A.1 that there is some spatial variation in the depth-density profile, which must be accounted for in our accumulation rate errors. The maximum variation ($\pm$ 12%) in the density profile occurs near the surface and rapidly declines to $\pm$4% at just over 7 m depth. The small variation in density profiles at greater depths indicates that this component of our error estimates will be less significant than the horizon time interval at depth. We determine the accumulation rate error resulting from regional density variation by accounting for variation in the conversion between twtt and depth, the variation in the cumulative mass profile, and digitization error. Unlike the error in

Δt, these errors are depth-dependent and thus dependent on location because horizon depth varies spatially. Therefore, we use radar-derived accumulation rate calculations at the PIG2010 site as an example.

Figure A.2 shows the relative errors resulting from the error in time horizon interval and propagating the variation in density through our radar-derived accumulation rate estimates at the PIG2010 core site. Beginning with the error in Δt, we see that the 8.3% error is constant with depth. Large regional density variation dominates the accumulation rate error near the surface. The density variation diminishes quickly with depth, and the variation in the time horizon interval dominates at just above 4 m depth. Most accumulation rate errors are less than 10% at a site, and are mainly the function of the error in Δt.

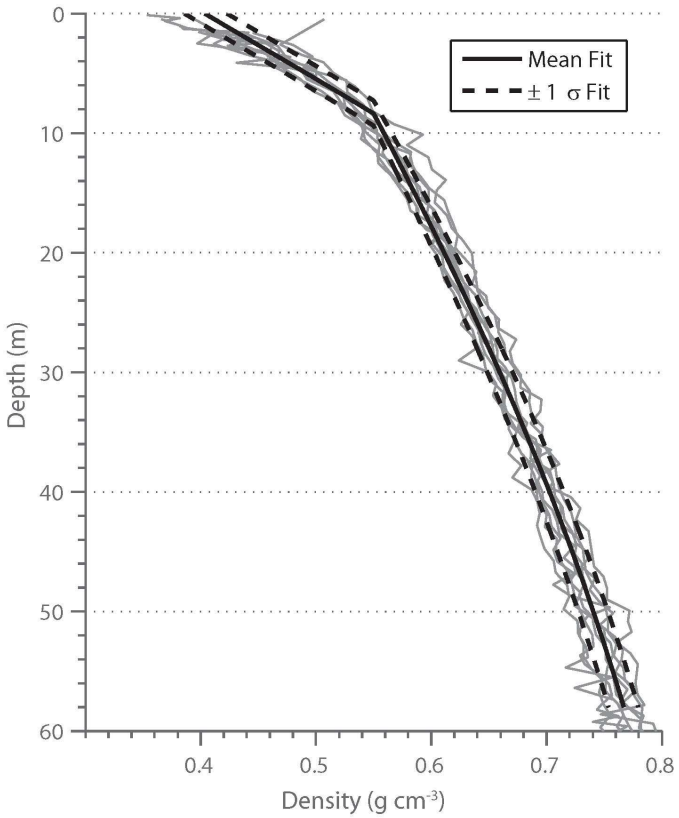

Figure A.1 – Model fit to nine depth-density profiles in the region. The grey lines are the actual raw (no smoothing applied) observations of density. The solid black line is the model fit to the mean of the profiles. The dashed black lines show the model fit to ± 1σ from the mean profile, which are used to estimate the errors in our accumulation measurements. The cores used include the PIG2010, DIV2010, and THW2010 (density samples typically spaced just under 1 m apart), and the WDC05A and ITASE cores 00-2, 00-3, 01-1, 01-2, and 01-4 (density samples typically spaced about 1 m apart). Cores were selected based on length (> 50m) and spatial distribution.

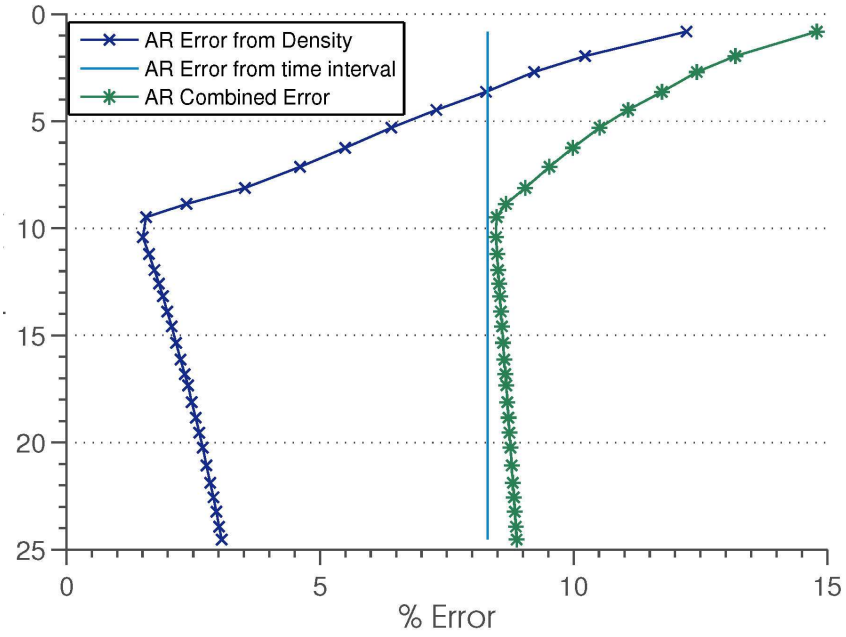

Figure A.2 – Components of the accumulation rate error based on horizon depth at the PIG2010 site. The accumulation error resulting from variation in the time interval between horizons is shown by a pale blue line and is constant with depth. The accumulation error resulting from the variation in the density profile is shown by a dark blue line with x markers at each of the horizons at the PIG2010 site. The impact of density variation declines rapidly with depth and is greater than 5% for only the most recent 7 years of the record (or above 7 m depth). The green line with asterisks is the total error combining the independent errors resulting from density variations and variation in horizon time intervals. Above 4 m depth, density variability is large enough to make it the dominant source of error in the accumulation rate estimates. Below, the variation in the horizon time interval dominates. Total accumulation errors are less than 10% for much of the record.